

**DOSE ASSESSMENT OF NATURAL RADIOACTIVITY IN FLY ASH AND  
ENVIRONMENTAL MATERIALS FROM MORUPULE A COAL-FIRED  
POWER STATION IN BOTSWANA**

**BY**

**JOHN MUDIWA, 10435641**

**BSc BIOMEDICAL ENGINEERING, 2003**

**A THESIS SUBMITTED TO THE DEPARTMENT OF MEDICAL PHYSICS,  
UNIVERSITY OF GHANA, GRADUATE SCHOOL OF NUCLEAR AND ALLIED  
SCIENCES**

**IN PARTIAL FULFILLMENT OF THE REQUIREMENTS FOR THE AWARD  
OF**

**MASTER OF PHILOSOPHY (MPhil)**

**IN**

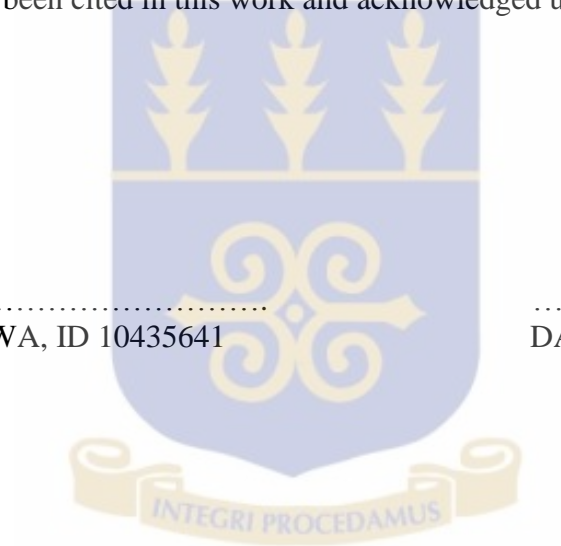
**NUCLEAR SCIENCE AND TECHNOLOGY PROGRAM**

**JULY, 2015**

## DECLARATION

I hereby declare that this thesis submission is a result of research work undertaken by John Mudiwa under the Department of Medical Physics, Graduate School of Nuclear and Allied Sciences, University of Ghana, under the awesome supervision of Prof. Emmanuel Ofori Darko and Dr. Augustine Faanu.

This work has never been submitted in whole or in part anywhere else for any sort of award. In parts of this submission where other sources of information have been used, such sources have been cited in this work and acknowledged under references.



.....  
JOHN MUDIWA, ID 10435641  
(STUDENT)

.....  
DATE

.....  
PROF. EMMANUEL OFORI DARKO  
(PRINCIPAL SUPERVISOR)

.....  
DATE

.....  
DR. AUGUSTINE FAANU  
(CO-SUPERVISOR)

.....  
DATE

## **DEDICATION**

First and foremost, I dedicate this work to my Lord and personal savior, Jesus Christ. I dedicate this research work to my father Mr. Ben Buyen Barnabas Mudiwa and especially my wife Neo Daphne Mudiwa for her wonderful support, encouragement and positive attitude towards my life.



## ACKNOWLEDGEMENT

I would like to show gratitude for God's blessings and favour upon my life that have enabled me to complete this thesis work. I earnestly show my deepest appreciation to my supervisors Prof. Emmanuel Ofori Darko (Deputy Director, Radiation Protection Institute, GAEC) and Dr. Augustine Faanu (Head of Department at NSS, University of Ghana).

I am extremely grateful to the Director of the Radiation Protection Institute (RPI), Prof. G. Emi-Reynolds and the Director of the Graduate School of Nuclear and Allied Sciences (SNAS) at the University of Ghana, Prof. Yaw Serfor-Armah. My deep gratitudes also go to the former and current supervisors of international students at SNAS, being Rev. Dr. A. Bamford and Dr. D. K. Adotey respectively. I am extremely thankful to all my lecturers at SNAS, including Prof. C. Schandorf, Prof. Akaho, Prof. J. Fletcher, Prof. Nana Ayensu, Dr. J. K. Amoako, Dr. J. Yeboah and Dr. Joseph Tandoh for all the knowledge they have equipped me with in preparation for this work. My heartfelt appreciation also goes to the GAEC Radiation Protection Institute laboratory staff who gave me so much support especially during sample preparation and analysis. I also sincerely give thanks to the technical staff and officials of Morupule Coal-Fired Power Station for all the assistance they offered me in availing samples and other useful information used in this study.

I am grateful to my father Mr. Ben Buyen Barnabas Mudiwa and my wife Neo Daphne Mudiwa for their encouragement before and during my thesis work. I am also giving my heartfelt appreciation to the International Atomic Energy Agency for awarding me a full sponsorship to undertake the MPhil in Nuclear Science and Technology Program as well as this research work.

## TABLE OF CONTENTS

DECLARATION .....	i
DEDICATION .....	ii
ACKNOWLEDGEMENT .....	iii
TABLE OF CONTENTS.....	iv
LIST OF TABLES .....	vii
LIST OF FIGURES .....	ix
LIST OF PLATES .....	xi
ABBREVIATIONS .....	xii
ABSTRACT.....	1
CHAPTER ONE: INTRODUCTION.....	3
1.1 BACKGROUND TO THE STUDY .....	3
1.2 STATEMENT OF PROBLEM .....	5
1.3 OBJECTIVES OF THE STUDY .....	6
1.4 RELEVANCE AND JUSTIFICATION .....	6
1.5 SCOPE AND LIMITATION .....	8
1.6 THESIS STRUCTURE.....	9
CHAPTER TWO: LITERATURE REVIEW.....	11
2.1 IONIZING RADIATION EXPOSURE DUE TO NATURAL SOURCES .....	11
2.1.1 COSMIC RADIATION.....	12
2.1.2 TERRESTRIAL RADIATION.....	14
2.1.3 RADIOACTIVITY IN SOIL, COAL, WATER AND FLY ASH.....	18
2.2 EXPOSURE PATHWAYS .....	21
2.3 DOSE RECONSTRUCTION .....	22
2.3.1 DOSE RECONSTRUCTION TECHNIQUES .....	24
2.4 INSTRUMENTATION TO MEASURE NATURAL RADIOACTIVITY .....	26
2.4.1 RESOLUTION AND EFFICIENCY.....	28
CHAPTER THREE: MATERIALS AND METHODS .....	30
3.1 MATERIALS .....	30
3.2 DESCRIPTION OF STUDY AREA .....	30

3.2.1 METEOROLOGY OF THE STUDY AREA .....	36
3.2.2 GEOLOGY AND SOILS .....	36
3.2.3 HYDROGEOLOGY .....	37
3.2.4 VEGETATION .....	38
3.3 METHOD.....	39
3.3.1 SAMPLES COLLECTION .....	39
3.3.1.1 SOIL/COAL/FLY ASH SAMPLING .....	39
3.3.1.2 WATER SAMPLING.....	40
3.3.2 SAMPLE PREPARATION FOR DIRECT GAMMA SPECTROMETRY .....	40
3.3.2.1 SOIL/COAL/FLY ASH SAMPLE PRAPARATION .....	40
3.3.2.2 WATER SAMPLE PREPARATION .....	41
3.3.3 SAMPLE ANALYSIS USING DIRECT GAMMA SPECTROMETRY .....	42
3.3.3.1 ENERGY CALIBRATION .....	42
3.3.3.2 EFFICIENCY CALIBRATION .....	44
3.3.3.3 MINIMUM DETECTABLE ACTIVITY .....	45
3.3.3.4 CALCULATION OF ANNUAL EFFECTIVE DOSE DUE TO THE RADIOACTIVITY IN SAMPLES.....	46
3.3.3.5 ANNUAL EFFECTIVE DOSE CALCULATIONS FROM EXTERNAL GAMMA DOSE RATE MEASUREMENTS .....	48
3.3.4 RADIOLOGICAL HAZARD ASSESSMENT .....	48
3.3.5 DOSE RECONSTRUCTION .....	50
3.3.5.1 TAYLOR SERIES METHOD FOR NUMERICAL SOLUTIONS IN DOSE RECONSTRUCTION .....	52
CHAPTER FOUR: RESULTS AND DISCUSSION .....	55
4.1 ENERGY AND EFFICIENCY CALIBRATION.....	55
4.2 MINIMUM DETECTABLE ACTIVITY .....	57
4.3 ACTIVITY CONCENTRATIONS, ABSORBED DOSE RATES AND ANNUAL EFFECTIVE DOSES IN THE STUDY AREA .....	57
4.3.1 FLY ASH.....	57
4.3.2 COAL.....	61
4.3.3 SOIL.....	64

4.3.4 WATER .....	67
4.4 COMPARISON OF ACTIVITY CONCENTRATION, GAMMA DOSE RATE AND ANNUAL EFFECTIVE DOSE TO SAMPLE TYPE.....	70
4.5 RADIUM EQUIVALENT ACTIVITY, REPRESENTATIVE LEVEL INDEX, EXTERNAL AND INTERNAL HAZARD INDICES.....	73
4.6 RECONSTRUCTED DOSES FROM THE STUDY AREA.....	80
4.7 ANNUAL EFFECTIVE DOSE MODEL OF THE FLY ASH STORAGE AREA	88
4.8 ANNUAL EFFECTIVE DOSE MODEL OF THE COAL STORAGE AREA .....	89
4.9 ANNUAL EFFECTIVE DOSE MODEL FOR SOIL SAMPLES FROM THE STUDY AREA.....	90
4.10 ANNUAL EFFECTIVE DOSE MODEL FOR WATER SAMPLES FROM THE FLY ASH PONDS .....	91
CHAPTER FIVE: CONCLUSION AND RECOMMENDATIONS .....	97
5.1 CONCLUSION .....	97
5.2 RECOMMENDATIONS .....	100
5.2.1 MANAGEMENT OF MORUPULE A COAL-FIRED POWER STATION.....	100
5.2.2 WORKERS OF MORUPULE A COAL-FIRED POWER STATION .....	100
5.2.3 MEMBERS OF THE PUBLIC .....	101
5.2.4 THE REGULATORY AUTHORITY OF BOTSWANA.....	101
5.2.5 RESEARCH SCIENTISTS .....	102
REFERENCES .....	103
APPENDICES .....	110

## LIST OF TABLES

Table 2-1:	Typical cosmogenic radionuclides
Table 2-2:	Thorium (4n) series
Table 2-3:	Neptunium (4n+1) series
Table 2-4:	Uranium (4n+2) series
Table 2-5:	Actinium (4n+3) series
Table 2-6:	Worldwide natural radionuclide concentration of coal
Table 2-7:	Natural radionuclide activity concentrations from fly ash and soil samples around Orji River Thermal Power Station
Table 2-8:	Radionuclide content of 20 fly ash samples from French coal-fired power stations
Table 2-9:	Average world activity concentration of $^{40}\text{K}$ , $^{238}\text{U}$ , $^{232}\text{Th}$ and $^{226}\text{Ra}$ in fly ash and coal in Bq/kg
Table 3-1	Standard radionuclides used for the energy and efficiency calibration
Table 4-1	Minimum detectable activities of K-40, Th-232 and U-238
Table 4-2	Experimental results for the average activity concentrations, absorbed dose rates and annual effective doses due to natural radionuclides in fly ash from the study area
Table 4-3	Activity concentrations, absorbed dose rates and annual effective doses due to natural radionuclides in coal from the study area
Table 4-4	Activity concentrations, absorbed dose rates and annual effective doses due to natural radionuclides in soil from the study area
Table 4-5	Activity concentrations, absorbed dose rates and annual effective doses due to natural radionuclides in water from the fly ash ponds
Table 4-6	Dose rate, annual effective dose, representative level index ( $I_{\gamma r}$ ), radium equivalent activity ( $Ra_{eq}$ ), external hazard index ( $H_{ext}$ ) and internal hazard index ( $H_{int}$ ) for fly ash samples



Table 4-7      Dose rate, annual effective dose, representative level index ( $I_{\gamma r}$ ), radium equivalent activity ( $Ra_{eq}$ ), external hazard index ( $H_{ext}$ ) and internal hazard index ( $H_{int}$ ) for coal samples

Table 4-8      Dose rate, annual effective dose, representative level index ( $I_{\gamma r}$ ), radium equivalent activity ( $Ra_{eq}$ ), external hazard index ( $H_{ext}$ ) and internal hazard index ( $H_{int}$ ) for soil samples

Table 4-9      Dose rate, annual effective dose, representative level index ( $I_{\gamma r}$ ), radium equivalent activity ( $Ra_{eq}$ ), external hazard index ( $H_{ext}$ ) and internal hazard index ( $H_{int}$ ) for water samples from the fly ash ponds

Table 4-10     Reconstructed annual effective doses for fly ash samples

Table 4-11     Reconstructed annual effective doses for coal samples

Table 4-12     Reconstructed annual effective doses for soil samples

Table 4-13     Reconstructed annual effective doses for water samples

## LIST OF FIGURES

- Fig. 2-1      Worldwide exposure to natural radiation sources
- Fig. 2-2      Setup of the HPGe detector
- Fig. 3-1      General location of Morupule Coal-Fired Power Station in Botswana
- Fig. 3-2      Detailed location of Morupule Coal-Fired Power Station in Botswana
- Fig. 3-3      Aerial view showing part of the study area
- Fig. 3-4      Layout of Morupule Coal-Fired Power Station showing sampling points
- Fig. 3-5      3-D Satellite image showing positions of Lotsane and Morupule rivers
- Fig. 4-1      Energy calibration curve using mixed radionuclides standard
- Fig. 4-2      Efficiency calibration curve using mixed radionuclides standard
- Fig. 4-3      Plot of activity concentration for natural radionuclides Th-232, U-238 and K-40 in fly ash samples from the study area
- Fig. 4-4      Plot of activity concentration for natural radionuclides Th-232, U-238 and K-40 in coal samples from the study area
- Fig. 4-5      Plot of activity concentration for natural radionuclides Th-232, U-238 and K-40 in soil samples from the study area
- Fig. 4-6      Plot of activity concentration for natural radionuclides Th-232, U-238 and K-40 in water samples from the fly ash ponds
- Fig. 4-7      Activity concentration comparison for samples in the study area
- Fig. 4-8      Gamma dose rates comparison for samples in the study area
- Fig. 4-9      Annual effective dose comparison for samples in the study area
- Fig. 4-10      Comparison of hazard indices and radium equivalent values for all samples
- Fig. 4-11      Actual reconstructed annual effective dose for fly ash storage area
- Fig. 4-12      Actual reconstructed annual effective dose for coal storage area
- Fig. 4-13      Actual reconstructed annual effective dose for soil

- Fig. 4-14      Actual reconstructed annual effective dose for water
- Fig. 4-15      Graphical representation of the fly ash storage area model
- Fig. 4-16      Graphical representation of the coal storage area model
- Fig. 4-17      Graphical representation of the soil model for the study area
- Fig. 4-18      Graphical representation of the water model for the fly ash ponds

**LIST OF PLATES**

- |           |   |
|-----------|---|
| Plate 1-1 | Schematic of a Coal-Fired Power Station |
| Plate 3-1 | Two fly ash storage tanks               |
| Plate 3-2 | Coal Storage Area                       |

**ABBREVIATIONS**

<b>ALARA</b>	As low as reasonably achievable
@	At
$\lambda$	Decay constant for the specific radionuclide
<b>1L</b>	1 liter
$\mu\text{s}$	Microsecond
<b>1M HNO<sub>3</sub></b>	1 Molar nitric acid
$\sigma$	Standard deviation
<b>3-D</b>	Three dimensional
<b>Ac-228</b>	Actinium-228
$A_i$	Initial radionuclide activity
$A_{iu}$	Initial radionuclide activity
$Amount_i$	Total activity limit
<b>ANSI</b>	American National Standards Institute
<b><sup>7</sup>Be</b>	Berillium-7
<b>Bi-214</b>	Bismuth-214
<b>Bq</b>	Becquerel
<b>Bq/kg</b>	Becquerel per kilogram
<b>Bq/l</b>	Becquerel per liter
<b>BSS</b>	Basic Safety Standards
<b>C</b>	Activity concentration for radionuclide at any time t
<b><sup>14</sup>C</b>	Carbon-14
$C_{iu}$	Initial activity concentration for radionuclide i
<b>Co-60</b>	Cobalt-60

$C_o$	Initial activity concentration
$Conc_i$	Activity concentration limit for radionuclide i
dc	Direct current
$Dose_i$	Total dose due to the initial radionuclide activity
$Dose_{lim}$	Relevant dose limit in Sv/y
$Dose_{iu}$	Dose due to the initial activity of radionuclide i
EC	Electron capture
Ecosurv	Environmental consultancy company in Botswana
eV	Electron volt
EIA	Environmental Impact Assessment
FWHM	Full Width at Half Maximum
FWTM	Full Width at Tenth of Maximum
g/kg	Gram per kilogram
GAEC	Ghana Atomic Energy Commission
GPS	Global Positioning System
$^3\text{H}$	Tritium
HPGe	High Purity Germanium Detector
IAEA	International Atomic Energy Agency
ICRP	International Commission on Radiological Protection
IEEE	Institute of Electrical and Electronics Engineers
ILO	International Labor Organization
$^{39}\text{K}$	Potassium-39
$\text{K-40}$	Potassium-40
$^{41}\text{K}$	Potassium-41

<b>K</b>	Kelvin
<b>keV</b>	Kiloelectrovolt
<b>mg/L</b>	Milligram per liter
<b>mm</b>	Millimeter
<b>mm/year</b>	Millimeter per year
<b>m/s</b>	Meter per second
<b>MCA</b>	Multi channel analyser
<b>MDA</b>	Minimum detectable activity
<b>MeV</b>	Megaelectronvolt
<b>mSv</b>	Milli Sievert
<b>nA</b>	Nano-Amperes
<b><sup>22</sup>Na</b>	Sodium-22
<b>nGy/h</b>	Nano gray per hour
<b>NORM</b>	Naturally Occuring Radioactive Material
<b><sup>237</sup>Np</b>	Neptunium-237
<b>NSS</b>	Nuclear Safety and Security
<b>ODE</b>	Ordinary Differential Equations
<b>Pb-214</b>	Lead-214
<b>ppm</b>	Parts per million
<b><math>\rho_{bd}</math></b>	Dry bulk density of the material
<b><math>Q</math></b>	Actual activity of radionuclide i
<b><math>Q_{i,l}</math></b>	Activity limit for radionuclide i
<b>Ra<sub>eq</sub></b>	Radium equivalent activity concentration
<b>Ra-226</b>	Radium-226

<b>RPI</b>	Radiation Protection Institute
<b>SNAS</b>	Graduate School of Nuclear and Allied Sciences
<b>STD</b>	Standard
<b>Sv</b>	Sievert
<b>Sv/y</b>	Sieverts per year
<b>Th-232</b>	Thorium-232
<b>Tl-208</b>	Thallium-208
<b>TLD</b>	Thermoluminescence detector
<b>U-234</b>	Uranium-234
<b>U-235</b>	Uranium-235
<b>U-238</b>	Uranium-238
<b>UN</b>	United Nations
<b>UNSCEAR</b>	UN Scientific Committee on the Effects of Atomic Radiation
<b>UPS</b>	Uninterrupted Power Supply (UPS)
<b>USEPA</b>	United States Environmental Protection Agency
<b>USGS</b>	United States Geological Survey
<b>V</b>	Volt
<b><math>V_w</math></b>	Volume of material that has a radiological impact in the scenario
<b>z</b>	z-score value



## ABSTRACT

This study has been undertaken to estimate the occupational and public radiation doses due to natural radioactivity at Morupule A Coal-Fired Power Station and its environs. The radiation doses were reconstructed to include 60 year period from 1985 to 2045. Direct gamma ray spectroscopy was used to determine the natural radionuclides Th-232, U-238, and K-40 both qualitatively and quantitatively for fly ash, coal, soil and water (from the fly ash ponds) samples. The average activity concentrations for Th-232, U-238, and K-40 in fly ash samples were 64.54 Bq/kg, 49.37 Bq/kg and 40.08 Bq/kg respectively. In the case of coal, the corresponding average activity concentrations for Th-232, U-238, and K-40 were 27.43 Bq/kg, 18.10 Bq/kg and 17.38 Bq/kg respectively. For soil samples, the average activity concentrations for Th-232, U-238, and K-40 were 10.11 Bq/kg, 6.76 Bq/kg and 118.03 Bq/kg respectively. In water samples, the average activity concentrations for Th-232, U-238, and K-40 were 0.79 Bq/l, 0.32 Bq/l and 1.01 Bq/l respectively. These average activity concentrations were generally comparable to the average world activity concentrations in the case of coal samples, but were generally lower than the average world activity concentrations in the case of fly ash, soil and water samples. The average annual effective doses for the study area were estimated as 0.320 mSv, 0.126 mSv, 0.069 mSv and 0.003 mSv for fly ash, coal, soil and water samples respectively. Dose reconstruction modelling estimated the average fly ash annual effective doses for the years 1985, 1995, 2005, 2015, 2025, 2035 and 2045 to be 0.182 mSv, 0.459 mSv, 0.756 mSv, 0.320 mSv, 0.183 mSv, 0.137 mSv and 0.124 mSv respectively. The reconstructed average coal annual effective doses for similar years were 0.070 mSv, 0.182 mSv, 0.303 mSv, 0.126 mSv, 0.070 mSv, 0.060 mSv and 0.046 mSv respectively. The dose reconstruction modelling also

estimated the average soil annual effective doses for the same years as above to be 0.048 mSv, 0.091 mSv, 0.136 mSv, 0.070 mSv, 0.048 mSv, 0.041 mSv and 0.039 mSv respectively. Likewise, the reconstructed average annual effective doses for water were 0.0016 mSv, 0.0049 mSv, 0.0083 mSv, 0.0033 mSv, 0.0016 mSv, 0.0011 mSv and 0.0010 mSv respectively. All estimated and reconstructed average annual effective doses are within the recommended public and occupational dose limits of 1 mSv and 20 mSv respectively. The radium equivalent activity, representative level index, external and internal hazard indices for all samples are within recommended international values for their safe use as building materials. Results from this study reveal that there is no significant radiological impact to both the workers and the public within Morupule A Coal-Fired Power Station and its environs.

## **CHAPTER ONE: INTRODUCTION**

The main aim of this chapter is to give a brief but rich introduction to the dose assessment of natural radioactivity from Morupule A Coal-Fired Power Station. This chapter includes a brief background to this study as well as the associated problem statement. The chapter also gives insight on the objectives, relevance and justification of this study.

### **1.1 BACKGROUND TO THE STUDY**

NORM is mostly used in referring to all naturally occurring radioactive materials where the activities of humans have increased potential for radiation exposure. Natural radioactivity released into the environment in the generation of electricity from coal-fired power stations by coal combustion has been stated as possible causes of health, environmental, and technological problems associated with the use of coal [U.S. Geological Survey Fact Sheet FS-163-97, 1997].

Coal-fired power stations basically generate electricity through coal (a fossil fuel) combustion. The heat generated is used to create steam from water. This steam turns a turbine that is connected to a generator and the generator creates an electric current. The conditioned output current will then be sent out to the main electrical power grid. Plate 1-1 below is a schematic of a typical coal-fired power station.

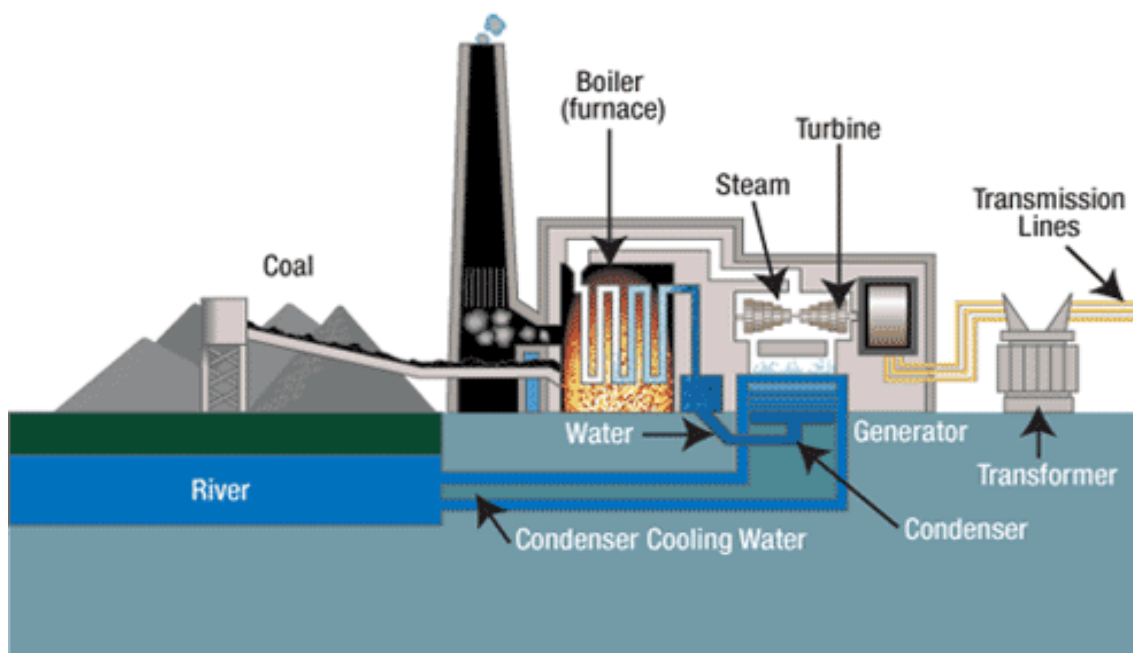


**Plate 1-1: Schematic of a Coal-Fired Power Station [en.wikipedia.org]**

Coal combustion takes place in the coal-fired power station and gaseous products are emitted through the stack gas pipe. Coal used in the combustion will contain some trace quantities of long-lived radionuclides giving rise to natural radioactivity such as U-238, K-40, Th-232 and decay products like Ra-226 or Rn-222. During coal combustion, some mechanisms will enhance the concentrations of these long-lived radionuclides. By combusting coal, most non-combustible material remains in the fly-ash formed. This essentially means that most of the NORM will be transferred to the fly ash produced while some will leave through the stack gas pipe into the atmosphere. The fly ash has to be stored securely to prevent contamination of larger areas and this fly ash could be better utilized in making other products such as cement.

The type of coal used and plant design has a very major effect on the activity discharged into the environment. Morupule A Coal-Fired Station uses the bituminous type of coal. Coal is grouped into four major categories being anthracite, bituminous, subbituminous

and lignite. This categorization depends mainly on its percentage composition of carbon. The percentage compositions of carbon for anthracite, bituminous, subbituminous and lignite coal are 86%-97% C, 45%-86% C, 35%-45% C and 25%-35% C respectively [USEIA, 2010]. This research focuses on the dose assessment of natural radioactivity in fly ash and environmental materials from Morupule A Coal-Fired Power Station. Results obtained from this research were compared with the recommended IAEA and BSS values of natural radionuclide concentrations.

## **1.2 STATEMENT OF PROBLEM**

Generally, stochastic and deterministic health effects due to NORM exposure from coal-fired power stations is usually considered to be negligible. Natural radioactivity release by human activities such as coal combustion in coal-fired power stations into the environment is a major global issue. Fly ash waste generated through the coal combustion contains NORM and may release even more natural radioactivity into the environment [USEPA, 2006].

A NORM Environmental Impact Assessment was never performed prior to the commissioning of Morupule A Coal-Fired Power Station, which has been operating for almost 30 years now. The accumulated radiation doses and reference levels in the coal-fired power station and its surroundings due to these natural radionuclides are thus unknown. This implies that the NORM exposure to the coal-fired power station workers and members of the public in the vicinity is also unknown. There is therefore the need to establish natural radioactivity reference (baseline) data. There is generally lack of

knowledge and awareness on natural radioactivity levels in the study area to both Morupule A Coal-Fired Power Station workers and surrounding public.

### **1.3 OBJECTIVES OF THE STUDY**

The main objective of this study is to assess the natural radioactivity impact of Morupule A Coal-Fired Power Station to both workers and the public living in the vicinity of the power station.

This research has the following specific objectives:

- (a) To establish the activity concentration of the natural radionuclides U-238, Th-232 and K-40 in coal, fly ash, soil and water samples by gamma spectroscopy with the aid of high purity germanium detector (HPGe).
- (b) To estimate baseline data for these natural radionuclides through mathematical dose reconstruction modelling.
- (c) To provide suitable radiation protection recommendations to the regulatory authority, Morupule A Coal-Fired Power Station management and all other relevant stakeholders.

### **1.4 RELEVANCE AND JUSTIFICATION**

Electricity is very vital in our daily lives. It boosts the economy, vital life-saving equipment in hospitals and investor confidence. At the same time there is need to ensure the safety and protection of Morupule A Coal-Fired Power Station workers against the harmful effects of ionizing radiation. In so many countries worldwide inclusive of Botswana, NORMS from raw materials are not under adequate regulatory control. Documented

information on natural radionuclide concentrations in raw materials and public exposures are minimal [Darko et al, 2005].

In this study, the annual effective dose from Morupule A Coal-Fired Power Station will be compared to the occupational annual effective worker dose limit of 20 mSv and the public effective annual dose limit of 1 mSv. This is meant to ensure compliance with ILO (International Labor Organization) and BSS (Basic Safety Standards). This study allows analysis of how much natural radionuclides the coal-fired power station releases into the environment. This work is justified because research on the NORM release from Morupule A Coal-Fired Power Station to the environment has never been carried out before.

Scrubbers/ filters reduce the amount of radionuclides eventually emitted from the stack gas pipe into the atmosphere. These scrubbers/filters are normally a major component of the emission reduction technologies generally used in coal-fired power stations. The outcomes of this particular work will show the effectiveness of any emission reduction technology currently in place at Morupule A Coal-Fired Power Station.

Study results will give an indication on the extent of radiological contamination around the power station due to the combustion of coal in the power station. Recommendations for improvement have been made based on the results. Results of this research may also unearth new ideas concerning natural radioactivity release from coal-fired power stations and may trigger other related research in years to come. The results will also contribute to preserve the environment and its natural resources like grasslands and vegetation for future

generations. This work and other similar research will aid in the formulation of NORM regulations for Botswana. Of the overall importance is protection of the worker, environment and members of the public against the harmful effects of ionizing radiation.

### **1.5 SCOPE AND LIMITATION**

This research covered the following steps:

- (a) The meteorological, vegetation, geological and hydrogeological data of the proposed study area were collected from relevant bodies such as the Ministry of Environment in Botswana. Meteorological data included factors such as precipitation, wind speed and wind direction. Online tools such as Google Earth were used to preview an aerial view of the study area and assess possible sampling points.
- (b) Fly ash, coal, soil and water samples were collected from the study area in the month of July, 2014.
- (c) Samples were analyzed by gamma spectroscopy at the Radiation Protection Institute laboratories of the Ghana Atomic Energy Commission in the period September 2014 to March 2015, after which the annual effective doses due to all the study area samples were estimated. MATLAB software was used to reconstruct the annual effective doses of the study area to include the sixty-year period  $1985 \leq \text{Year} \leq 2045$ .
- (d) Due to thesis submission deadlines as well as expensive airline tickets constraints, sampling was done only during the winter season, which is also the driest season in Botswana. Sampling should have also been done in the wet/rainy season so as to cater for the seasonal variations of the results obtained.



## **1.6 THESIS STRUCTURE**

This thesis consists of six major chapters as follows:

### **(a) Chapter One**

This chapter gives a general introduction and background to the study. An important aspect of this chapter is that it clarifies the importance of this work as well as its relevance to a coal-fired power station.

### **(b) Chapter Two**

This chapter gives an insight on what has so far been done on this topic from past and related work. It also shows the gaps in knowledge that need to be addressed, possibly through this research. Available theoretical approaches relevant to the dose assessment of natural radioactivity from coal-fired power stations are also discussed in this chapter.

### **(c) Chapter Three**

Chapter three discusses the materials, equipment and methods used in this study as well as the calculations relevant to the research study.

### **(d) Chapter Four**

Chapter four gives the results from this study in a clear and logical manner, aided by the use of tables or figures as required. The chapter also gives a discussion of results from the research study. It also emphasizes the significance of the results obtained. Any limitations of the experimental design of this research are elaborated in this chapter.

**(e) Chapter Five**

Chapter five concludes the study and gives an overall summary of the research, recommendations, lessons learned and any other relevant aspects based on the findings from this work.

## **CHAPTER TWO: LITERATURE REVIEW**

The main aim of this chapter is to give an insight to the natural radioactivity sources as well as occupational and public exposure to these sources. It also focuses on natural radioactivity in samples of various matrices from Morupule A Coal-Fired Power Station and its surroundings. The detector resolution, detector efficiency, radiation exposure pathways, dose reconstruction and instrumentation used for measuring natural radioactivity are some key components of this section.

### **2.1 IONIZING RADIATION EXPOSURE DUE TO NATURAL SOURCES**

There is a continuous exposure of all living organisms to ionizing radiation emanating from natural sources [UNSCEAR, 2000]. The levels of such exposures differ with respect to altitude and location. Irradiation coming externally from radionuclides that are present naturally within the environment or anthropogenic practices is an important aspect when dealing with human populations. Estimates by the United Nations Scientific Committee on the Effects of Atomic Radiation (UNSCEAR) have revealed that exposure due to natural sources accounts for over 98% of the total radiation dose on the population, excluding medical exposure [UNSCEAR, 2000]. The major sources of exposure due to natural radiation are:

- i.** Cosmic rays from outer space
- ii.** Terrestrial radionuclides

Figure 2-1 is a graphical illustration of worldwide exposure to natural radiation sources. These sources include cosmic rays, indoor/outdoor gamma ray exposure as well as radon gas.

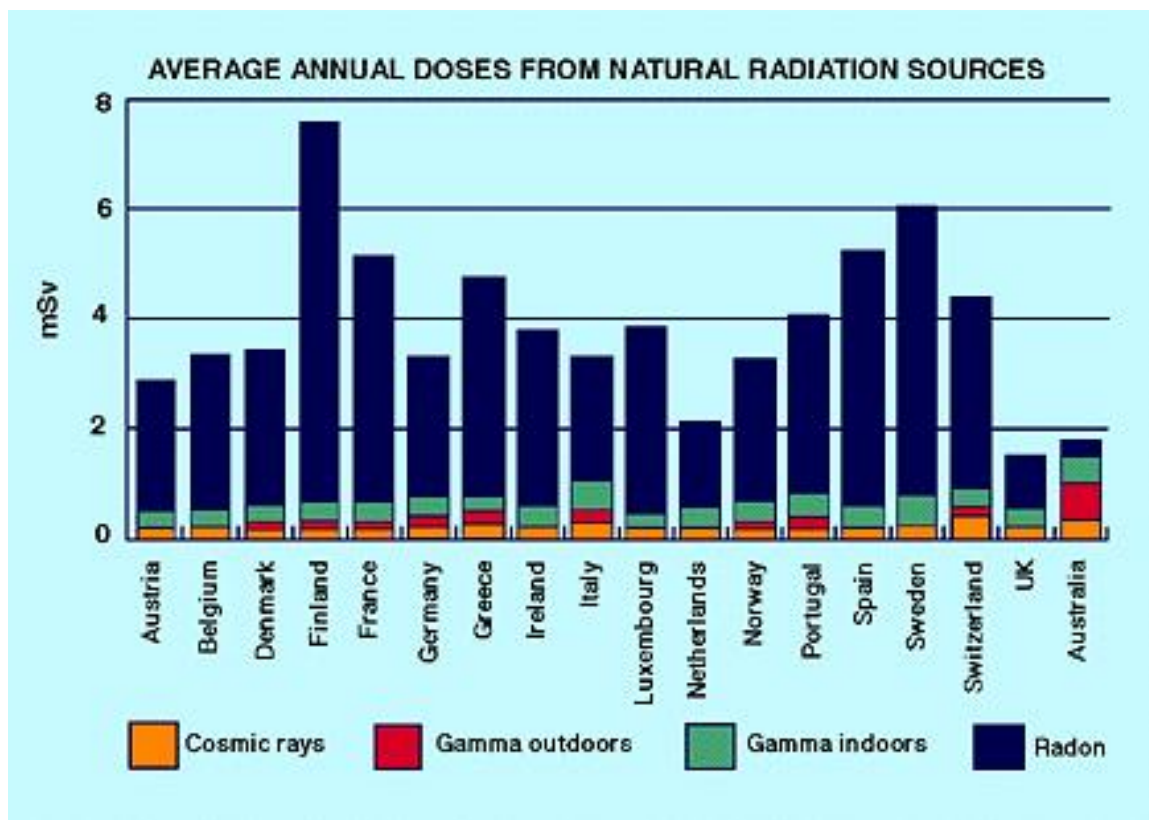


**Fig. 2-1: Worldwide exposure to natural radiation sources [world-nuclear.org]**

### 2.1.1 COSMIC RADIATION

The primary cosmic radiation sources are outer space galaxies, while the sun is the secondary source. Cosmic radiation sources from outer space are normally referred to as galactic cosmic radiation. Galactic cosmic radiation comprises of about 2% electrons and 98% baryons [Reitz, 1993]. Protons constitute about 87% of the baryons. They are particles with very high energy. The Austrian physicist Victor Hess received a Nobel Prize for his discovery of cosmic rays in 1936 [Cember, 2009]. The continuous interaction between cosmic rays with atmospheric nitrogen results in cosmic radiation. The resulting radionuclides are referred to as cosmogenic radionuclides. Cosmogenic radionuclides include  $^3\text{H}$ ,  $^{14}\text{C}$ ,  $^{22}\text{Na}$  and  $^7\text{Be}$  as depicted in Table 2-1.

**Table 2-1: Typical cosmogenic radionuclides [Cooper, Randle and Sochi, 2003]**

<b>Radionuclide</b>	<b>Half life (years)</b>	<b>Mode of decay</b>
$^3\text{H}$	12.26	Beta
$^7\text{Be}$	0.15	EC
$^{10}\text{Be}$	1.6E6	Beta
$^{14}\text{C}$	5.73E3	Beta
$^{22}\text{Na}$	2.6	EC
$^{26}\text{Al}$	7.4E5	EC
$^{32}\text{Si}$	280	Beta
$^{32}\text{P}$	0.04	Beta
$^{33}\text{P}$	0.07	Beta
$^{35}\text{S}$	0.24	Beta
$^{36}\text{Cl}$	3.01E5	Beta
$^{39}\text{Ar}$	269	Beta
$^{81}\text{Kr}$	2.29E5	EC

With the exception of  $^{14}\text{C}$ ,  $^3\text{H}$  and  $^{22}\text{Na}$ , the three of which have human body metabolic functions, cosmogenic radionuclides generally have a minimal contribution to radiation doses [UNSCEAR, 2000]. Most shielding from cosmic radiation is provided by the atmosphere of the earth. Therefore at lower altitudes, the additional shielding provided by the atmosphere of the earth reduces cosmic radiation dose. In general, the exposure to cosmic radiation mostly depends on altitude and has a weak dependence on latitude. Cosmic radiation adds to the earth's background radiation.

### 2.1.2 TERRESTRIAL RADIATION

Primordial radionuclides are those naturally occurring radionuclides originating on earth such that their half lives are comparable to planet earth's age [UNSCEAR, 2008]. The primordial radionuclides are found in almost all environmental materials, the human body inclusive. Examples of primordial radionuclides are  $^{232}\text{Th}$ ,  $^{40}\text{K}$ ,  $^{235}\text{U}$ ,  $^{238}\text{U}$  and  $^{87}\text{Rb}$  with half lives of  $1.41 \times 10^{10}$  years,  $1.28 \times 10^9$  years,  $7.04 \times 10^8$  years,  $4.47 \times 10^9$  years and  $4.70 \times 10^{10}$  years respectively. Natural uranium is a mixture of three isotopes being 99.3%  $^{238}\text{U}$ , 0.7%  $^{235}\text{U}$  and 0.005%  $^{234}\text{U}$ .  $^{234}\text{U}$  and  $^{238}\text{U}$  isotopes are part of a decay series known as the uranium series ( $4n+2$ ). The  $^{235}\text{U}$  isotope is part of the actinium series ( $4n + 3$ ).  $^{232}\text{Th}$  is part of a decay series known as the thorium series ( $4n$ ).  $^{232}\text{Th}$  is actually the most abundant of these naturally occurring primordial radionuclides.  $^{237}\text{Np}$  is part of the neptunium series ( $4n+1$ ). In all the four above-mentioned radioactive decay series, the first radionuclide in the decay series is long lived. The terminal radionuclides for the  $4n$ ,  $4n+1$ ,  $4n+2$  and  $4n+3$  series are  $^{208}\text{Th}$ ,  $^{209}\text{Bi}$ ,  $^{206}\text{Pb}$  and  $^{207}\text{Pb}$  respectively [Cember, 2009]. Tables 2-2 to 2-5 show the  $4n$ ,  $4n+1$ ,  $4n+2$  and  $4n+3$  series respectively.

**Table 2-2: Thorium (4n) series [Cember, 2009]**

NUCLIDE	HALF-LIFE	ENERGY (MeV)		
		ALPHA <sup>a</sup>	BETA	GAMMA (PHOTONS/ TRANS.) <sup>b</sup>
<sup>232</sup> Th <sub>90</sub>	1.39 10 <sup>10</sup> yrs	3.98		
<sup>228</sup> Ra (MsTh1) <sub>88</sub>	6.7 yrs		0.01	
<sup>228</sup> Ac (MsTh2) <sub>89</sub>	6.13 h		Complex decay scheme Most intense beta group is 1.11 MeV	1.59 (n.v.) 0.966 (0.2) 0.908 (0.25)
<sup>228</sup> Th (RdTh) <sub>90</sub>	1.91 yrs	5.421		0.084 (0.016)
<sup>224</sup> Ra (ThX) <sub>88</sub>	3.64 d	5.681		0.241 (0.038)
<sup>220</sup> Rn (Tn) <sub>86</sub>	52 s	6.278		0.542 (0.0002)
<sup>216</sup> Po (ThA) <sub>82</sub>	0.158 s	6.774		
<sup>212</sup> Pb (ThB) <sub>82</sub>	10.64 h		0.35, 0.59	0.239 (0.40)
<sup>212</sup> Bi (ThC) <sub>83</sub>	60.5 min	6.086 (33.7%) <sup>c</sup>	2.25 (66.3%) <sup>c</sup>	0.04 (0.034 branch)
<sup>212</sup> Po (ThC') <sub>84</sub>	3.04 × 10 <sup>-7</sup> s	8.776		
<sup>208</sup> Tl (ThC'') <sub>81</sub>	3.1 min		1.80, 1.29, 1.52	2.615 (0.997)
<sup>208</sup> Pb (ThD) <sub>82</sub>	Stable			

**Table 2-3: Neptunium (4n+1) series [Cember, 2009]**

NUCLIDE	HALF-LIFE	ENERGY (MeV)		
		ALPHA <sup>b</sup>	BETA	GAMMA (PHOTONS/ TRANS.) <sup>c</sup>
<sup>241</sup> Pu <sub>94</sub>	13.2 yrs		0.02	
<sup>241</sup> Am <sub>95</sub>	462 yrs	5.496		0.060 (0.4)
<sup>237</sup> Np <sub>93</sub>	2.2 × 10 <sup>6</sup> yrs	4.77		
<sup>233</sup> Pa <sub>91</sub>	27.4 d		0.26, 0.15, 0.57	0.31 (very strong) <sup>c</sup>
<sup>233</sup> U <sub>92</sub>	1.62 × 10 <sup>5</sup> yrs	4.823		0.09 (0.02) 0.056 (0.02) 0.042 (0.15)
<sup>229</sup> Th <sub>90</sub>	7.34 × 10 <sup>3</sup> yrs	5.02		
<sup>225</sup> Ra <sub>88</sub>	14.8 d		0.32	
<sup>225</sup> Ac <sub>89</sub>	10.0 d	5.80		
<sup>221</sup> Fr <sub>87</sub>	4.8 min	6.30		0.216 (1)
<sup>217</sup> At <sub>85</sub>	0.018 s	7.02		
<sup>213</sup> Bi <sub>83</sub>	47 min	5.86 (2%) <sup>d</sup>	1.39 (98%) <sup>d</sup>	
<sup>213</sup> Po <sub>84</sub>	4.2 × 10 <sup>-6</sup> s	8.336		
<sup>209</sup> Tl <sub>81</sub>	2.2 min		2.3	0.12 (weak) <sup>c</sup>
<sup>209</sup> Pb <sub>82</sub>	3.32 h		0.635	
<sup>209</sup> Bi <sub>83</sub>	Stable			

**Table 2-4: Uranium (4n+2) series [Cember, 2009]**

NUCLIDE	HALF-LIFE	ENERGY (MeV)		
		ALPHA <sup>a</sup>	BETA	GAMMA (PHOTONS/ TRANS.) <sup>b</sup>
<sup>238</sup> <sub>92</sub> U	4.51 × 10 <sup>9</sup> yrs	4.18		
<sup>234</sup> <sub>90</sub> Th (U X <sub>1</sub> )	24.10 d		0.193, 0.103	0.092 (0.04) 0.063 (0.03)
<sup>234m</sup> <sub>91</sub> Pa (U X <sub>2</sub> )	1.175 min		2.31	1.0 (0.015) 0.76 (0.0063), I.T.
<sup>234</sup> <sub>91</sub> Pa (UZ)	6.66 h		0.5	Many (weak)
<sup>234</sup> <sub>92</sub> U (UII)	2.48 × 10 <sup>5</sup> yrs	4.763		
<sup>230</sup> <sub>90</sub> Th (Io)	8.0 × 10 <sup>4</sup> yrs	4.685		0.068 (0.0059)
<sup>230</sup> <sub>90</sub> Ra	1,622 yrs	4.777		
<sup>222</sup> <sub>86</sub> Em (Rn)	3.825 d	5.486		0.51 (very weak)
<sup>218</sup> <sub>84</sub> Po (RaA)	3.05 min	5.998 (99.978%) <sup>c</sup>	Energy not known (0.022%) <sup>c</sup>	0.186 (0.030)
<sup>218</sup> <sub>85</sub> At (RaA')	2 s	6.63 (99.9%) <sup>c</sup>	Energy not known (0.1%) <sup>c</sup>	
<sup>218</sup> <sub>86</sub> Em (RaA'')	0.019 s	7.127		
<sup>214</sup> <sub>82</sub> Pb (RaB)	26.8 min		0.65	0.352 (0.036) 0.295 (0.020) 0.242 (0.07)
<sup>214</sup> <sub>83</sub> Bi (RaC)	19.7 min	5.505 (0.04%) <sup>c</sup>	1.65, 3.7 (99.96%) <sup>c</sup>	0.609 (0.295) 1.12 (0.131)
<sup>214</sup> <sub>84</sub> Po (RaC')	1.64 × 10 <sup>-4</sup> s	7.680		
<sup>210</sup> <sub>81</sub> Tl (RaC'')	1.32 min		1.96	2.36 (I) 0.783 (I) 0.297 (I)
<sup>210</sup> <sub>82</sub> Pb (RaD)	19.4 yrs		0.017	0.0467 (0.045)
<sup>210</sup> <sub>83</sub> Bi (RaE)	5.00 d		1.17	
<sup>210</sup> <sub>84</sub> Po (RaF)	138.40 d	5.298		0.802 (0.000012)
<sup>206</sup> <sub>82</sub> Pb (RaG)	Stable			



**Table 2-5: Actinium (4n+3) series [Cember, 2009]**

NUCLIDE	HALF-LIFE	ENERGY (MeV)		
		ALPHA <sup>a</sup>	BETA	GAMMA (PHOTONS/ TRANS.) <sup>b</sup>
<sup>235</sup> U	7.13 × 10 <sup>8</sup> yrs	4.39		0.18 (0.7)
<sup>231</sup> Th (UY)	25.64 h		0.094, 0.302, 0.216	0.022 (0.7) 0.0085 (0.4) 0.061 (0.16)
<sup>231</sup> Pa	3.43 × 10 <sup>4</sup> yrs	5.049		0.33 (0.05) 0.027 (0.05) 0.012 (0.01)
<sup>227</sup> Ac	21.8 yrs	4.94 (1.2%) <sup>a</sup>	0.0455 (98.8%) <sup>c</sup>	
<sup>227</sup> Th (RdAc)	18.4 d	6.03		0.24 (0.2) 0.05 (0.15)
<sup>223</sup> Fr (AcK)	21 min		1.15	0.05 (0.40) 0.08 (0.24)
<sup>223</sup> Ra (AcX)	11.68 d	5.750		0.270 (0.10) 0.155 (0.055)
<sup>219</sup> Em (An)	3.92 s	6.824		0.267 (0.086) 0.392 (0.048)
<sup>215</sup> Po (AcA)	1.83 × 10 <sup>-3</sup> s	7.635		
<sup>211</sup> Pb (AcB)	36.1 min		1.14, 0.5	Complex spectrum, 0.065–0.829 MeV
<sup>211</sup> Bi (AcC)	2.16 min	6.619 (99.68%) <sup>c</sup>	Energy not known (0.32%) <sup>c</sup>	0.35 (0.14)
<sup>211</sup> Po (AcC')	0.52 s	7.434		0.88 (0.005) 0.56 (0.005)
<sup>207</sup> Tl (AcC'')	4.78 min		1.47	0.87 (0.005)
<sup>207</sup> Pb	Stable			

<sup>40</sup>K is a naturally occurring radionuclide with a low atomic number and widespread environmental distribution. Crystal rocks, oceans, plants and animals have been found to contain an average <sup>40</sup>K concentration of 27 g/kg, 380 mg/L, 1.7 g/kg and 1.7 g/kg respectively [Cember, 2009]. Potassium in nature comprises of the three isotopes <sup>39</sup>K, <sup>40</sup>K and <sup>41</sup>K such that <sup>40</sup>K is the only radioactive of the three. The natural isotopic abundance of <sup>40</sup>K is 0.0118%. Potassium is also found in rocks and is soluble, therefore it dissolves in wet conditions [Xhixha, 2012]. Homeostatis control normally keeps the <sup>40</sup>K concentration at a constant level in the body, therefore environmental concentration changes of <sup>40</sup>K do

not normally significantly affect the total  $^{40}\text{K}$  dose that is delivered to humans [IAEA, 2007].

### **2.1.3 RADIOACTIVITY IN SOIL, COAL, WATER AND FLY ASH**

As mentioned in Section 2.1.2 above, primordial radionuclides are found in almost all environmental materials. Such environmental materials include soil, coal and the fly ash generated in the combustion of coal. In coal-fired power stations, the fly ash is collected by means of an electronic precipitator as a dry powder or it may be discharged into the fly ash pond as slurry in a semi-wet condition [Shamshad, Fulekar and Bhawana, 2012]. The fly ash slurry may be transported to the open fly ash pond or disposal site using either the open or closed water cycle systems [Paschoa and Steinhausler, 2010]. Thus, the fly ash water from the fly ash disposal sites or the fly ash ponds also constitutes these environmental materials. Radionuclides released into the environment will undergo radioactive decay, or they may undergo wet or dry deposition [UNSCEAR, 2000]. Previous work done on natural radioactivity from certain coal-fired power stations around the world is available. Table 2-6 shows natural radionuclide concentrations in coal from various parts of the world.

**Table 2-6: Worldwide natural radionuclide concentration of coal [Uslu and Gökmeşe, 2010]**

State	Region	Calorific Value (kcal/kg)	Ash content	Concentration		
				<sup>238</sup> U (ppm)	<sup>232</sup> Th (ppm)	<sup>40</sup> K (%)
Australia	DT	7070	9.6	0.80	2.1	0.097
	UL	6500	17.6	0.95	3.0	0.60
	BR	6330	18.4	1.8	6.5	0.15
Canada	CV	6360	9.2	1.1	2.0	0.66
China	FS	6390	21.4	1.7	5.5	0.16
Japan	HO	6420	20	0.96	3.9	0.45
	TH	6320	12.5	0.78	2.2	0.13
	HN	6280	20.8	0.53	1.9	0.17
	TS	5940	24.4	0.99	3.5	0.31
	ND	4420	40.5	0.93	3.8	0.42
S. Africa	EM	6510	13.7	1.7	4.8	0.87
	WB	6350	18.0	1.9	7.3	0.10
U.S.A.	CO	6430	14.3	0.31	0.49	0.0066

Table 2-6 shows that the concentrations of natural radionuclides vary with different types of coal and generally depend on the ash content and caloric value [Uslu and Gökmeşe, 2010]. Human activities like mining and the combustion of natural resources like coal may result in enhancing of NORMS such that they may cause elevated natural radioactivity exposure to humans as well as the environment [UNSCEAR, 2000]. Table 2-7 shows the natural radionuclide activity concentrations from fly ash and soil samples around Orji River Coal-Fired Thermal Power Station in Nigeria [Ademola and Onyema, 2014].

**Table 2-7: Natural radionuclide activity concentrations from fly ash and soil samples around Orji River Thermal Power Station [Ademola and Onyema, 2014]**

Sample	No.	<sup>226</sup> Ra (Bq/kg)		<sup>232</sup> Th (Bq/kg)		<sup>40</sup> K (Bq/kg)	
		Mean± $\sigma$	Range	Mean± $\sigma$	Range	Mean± $\sigma$	Range
Fly ash	10	28.2±8.3	18.1-38.8	37.6±5.0	31.6-44.7	335±32	287-385
Soil (10m)	10	32.7±4.3	26.3-38.4	40.0±4.2	32.1-46.6	298±15	278-324
Soil (100m)	10	39.1±11.2	14.6-52.4	34.1±5.2	25.2-40.2	257±19	223-286

Fly ash radioactivity is mostly due to <sup>40</sup>K, <sup>238</sup>U and <sup>232</sup>Th decay series [Degrange, Lepicard; 2004]. A study was conducted on the radionuclide content of 20 samples from French coal-fired power stations and the results are shown in Table 2-8.

**Table 2-8: Radionuclide content of 20 fly ash samples from French coal-fired power stations [Degrange and Lepicard, 2004]**

Radionuclide	Low-level Bq.kg <sup>-1</sup>	High-level Bq.kg <sup>-1</sup>	Mean-level Bq.kg <sup>-1</sup>	Standard deviation
U-238	54	246	133,9	59,1
Th-234	54	246	133,9	59,1
Pa-234m	54	360	160,3	90,8
Pa-234	0,2	1,2	0,5	0,3
U-234	54	246	133,9	59,1
Th-230	38	246	118,3	60
Ra-226	44	260	138	75,6
Po-218	44	260	138	75,6
At-218	44	260	138	75,6
Pb-214	47	231	117,5	58,8
Bi-214	45	231	112,2	57
Po-214	47	231	117,5	58,8
Pb-210	29	274	116,8	64,8
Bi-210	29	274	116,8	64,8
Po-210	29	274	116,8	64,8
Th-232	66	173	119,3	39,2
Ra-228	66	173	119,3	39,2
Ac-228	66	173	119,3	39,2
Th-228	66	190	123,6	42,4
Ra-224	66	190	123,6	42,4
Po-216	66	190	123,6	42,4
Pb-212	65	180	128,2	39,7
Bi-212	73	200	133,5	42,6
Po-212	42	122	79,2	27,2
Tl-208	23	62,3	44,7	14,4
K-40	170	1703	955,6	481,7

Average world activity concentration shows that the NORM content of coal is less than that of fly ash as depicted in Table 2-9 [UNSCEAR, 1982].

**Table 2-9: Average world activity concentration of  $^{40}\text{K}$ ,  $^{238}\text{U}$ ,  $^{232}\text{Th}$  and  $^{226}\text{Ra}$  in fly ash and coal in Bq/kg [UNSCEAR, 1982]**

Nuclides	Coal	Fly Ash
$^{40}\text{K}$	50	265
$^{238}\text{U}$	20	200
$^{226}\text{Ra}$	20	240
$^{232}\text{Th}$	20	70

## 2.2 EXPOSURE PATHWAYS

Exposure pathways are the various ways through which individuals may be exposed to ionizing radiation. Therefore the following are all the relevant and applicable exposure pathways in this natural radioactivity research:

- (a) External exposure to gamma rays
- (b) Internal exposure by inhalation
- (c) Internal exposure by ingestion
- (d) Contamination of the skin by radioactive material directly deposited on the skin

Close and prolonged contact of workers with material containing NORMs results in occupational exposure. Inhalation of radioactive dust as a result of work also results in occupational exposure. The most common exposure pathway for natural radionuclides is external gamma radiation [IAEA, 2005]. Due to the low specific activity of NORM material, skin contamination is normally considered irrelevant in NORM dose assessments.

Public exposure may result due to products from an industrial process such as liquid or atmospheric discharges of radionuclides. The use of industrial products such as fly ash for making cement or concrete will also result in public exposure. The most significant radiation exposure pathways for the public are normally external gamma rays, ingestion and inhalation [European Commission, 2001].

### **2.3 DOSE RECONSTRUCTION**

Assessment of likely radiological doses to members of the public are to be done with reference to the critical group. The critical group is the individuals being exposed to the highest radiation dose. In cases where radiation exposure mechanisms result in future doses, the critical group concept may not be ideal since there is a possibility of significant human habitat change over a small time period [IAEA, 2003]. Radiation from environmental radionuclides could be calculated from radionuclide deposition on plants or soil during a liquid or atmospheric release. It could also be calculated from a residual radionuclides exposure in the environment some time after the end of this release. The calculated radiation doses are actually accumulated radiation doses due to continuous chronic exposure. The committed effective dose for the first year is also calculated. Another important aspect is the calculation of an integrated dose for a specified number of years. Internal radiation doses are calculated using equations from the International Commission on Radiological Protection (ICRP). Calculations for doses due to external exposure from contaminated water and soil are based on the assumption that the contaminated medium is big enough to be treated like an infinite plane or volume with respect to the range of radiation released [Napier, Kennedy Jr. and Soldat, 1980].

Normal exposure refers to radiation exposure which would be reasonably expected to occur, with a probability of unity [ICRP, 1993]. In case of normal exposures, individual doses are expressed as annual effective doses due to external radiation. Annual effective committed dose is used in the case of radionuclides intake. The sum of external annual effective dose and annual effective committed dose is normally compared with the established dose constraint.

Potential exposures should be included in the overall safety analysis of a facility. A potential exposure is one that is not certain to happen, but has the potential to happen [IAEA, 2003]. Risk control due to potential exposure is attained by increasing protection to reduce the probability of occurrence of events. This risk control is also attained by mitigation, which simply means increasing protection such that the consequences will be reduced. Protection against potential exposures must have similar objective levels as protection against normal exposure since both normal and potential exposure have a similar risk of health effects [ICRP, 1997].

Dose reconstruction is necessary for defining dose levels in public exposures. Doses due to external and internal radiation sources can be reconstructed for internal organs and tissue. In dose reconstruction, organ doses may be used for evaluating the stochastic detriment and defining radiation threshold values in order to prevent deterministic effects [IAEA, 2004].

The Basic Safety Standards contains some dose limits and dose constraints for workers and the public [IAEA, 2003]. According to the Basic Safety Standards, the occupational exposure limits for all workers are:

(a) 20 mSv effective dose per year, averaged over a consecutive 5 year period, or [IAEA, 2003].

(b) 50 mSv total effective dose in any single year [IAEA, 2003].

The Basic Safety Standards further states that dose limits to members of the public are:

(c) 1 mSv effective dose in a year [IAEA, 2003].

### **2.3.1 DOSE RECONSTRUCTION TECHNIQUES**

Theoretical models may be used for generating radiation doses to public members within the critical group. A mathematical model may be used in the form of algebraic and differential equations. The solutions to these mathematical models can be analytical or numerical and can be simulated by means of a computer programming language. Analytical methods are restricted to solving simple mathematical problems, while numerical methods can solve even the more complicated polynomials of order five and above [Stroud, 2003]. Field measurements will normally provide the relevant input parameters for the computer programming used. An analytical solution is generally an exact solution to a mathematical equation, while, a numerical solution is an approximation [Ye Zhang, 2011]. The activity concentration,  $C$ , for a radionuclide at any time  $t$  is calculated by Equation 2.4:

$$C = C_o e^{-\lambda t} \quad (2.4)$$

Where,  $C_o$  represents the initial activity concentration and  $\lambda$  represents the decay constant for the specific radionuclide [IAEA, 2003]. The actual activity concentration limit for a



given radionuclide is computed through Equation 2.5 below:

$$Conc_i = \frac{Dose_{lim} \cdot C_{iu}}{Dose_{iu}} \quad (2.5)$$

Where,  $Conc_i$  represents the activity concentration limit (Bq/kg) for radionuclide  $i$  in the scenario,  $Dose_{lim}$  represents the scenario relevant dose limit in Sv/y,  $C_{iu}$  represents the initial activity concentration (Bq/kg) for radionuclide  $i$  that has a radiological impact in the area, while  $Dose_{iu}$  represents the dose due to the initial activity of radionuclide  $i$  in Sv/y [IAEA, 2003].  $C_{iu}$  represents the initial activity concentration (Bq/kg) for radionuclide  $i$  that has a radiological impact in the scenario and is defined by Equation 2.6:

$$C_{iu} = \frac{A_{iu}}{\rho_{bd} V_w} \quad (2.6)$$

Where,  $A_{iu}$  represents the initial radionuclide activity (Bq) that has a radiological impact in the scenario,  $\rho_{bd}$  represents the dry bulk density of the material in  $\text{kg/m}^3$  and  $V_w$  represents the volume ( $\text{m}^3$ ) of material that has a radiological impact in the scenario [IAEA, 2003]. For each radionuclide in the material, the total activity limit (Bq) is given by Equation 2.7:

$$Amount_i = \frac{Dose_{lim} \cdot A_i}{Dose_i} \quad (2.7)$$

Where,  $Dose_{lim}$  represents the applicable dose limit in Sv/y,  $A_i$  represents the initial radionuclide activity (Bq) in the total amount of material and  $Dose_i$  represents the total dose (Sv/y) due to the initial radionuclide activity [IAEA, 2003]. As soon as the required radionuclide activity limits are established in the material, it should be ensured that the combined doses from all radionuclides remain below the relevant public or worker dose limit. This can be attained by the summation rule from Equation 2.8:

$$\sum_i \frac{Q}{Q_{i,l}} \leq 1 \quad (2.8)$$

Where,  $Q$  represents the actual activity (Bq or Bq/kg) of radionuclide  $i$  that will be disposed and  $Q_{i,l}$  represents the activity limit (Bq or Bq/kg) for radionuclide  $i$  from the available samples, based on the assumption that only radionuclide  $i$  will be disposed [IAEA, 2003].

Our calculation end points are the radionuclide activity concentration limits as well as the total activity limit that corresponds to an annual effective dose limit of 1 mSv/y and 20 mSv/y to members of the public and occupationally exposed workers respectively.

## 2.4 INSTRUMENTATION TO MEASURE NATURAL RADIOACTIVITY

Various instruments can be used to measure the ionizing radiation emitted by samples. Typical instruments used are scintillation counters, gas filled detectors and solid state detectors. Examples of scintillation counters are the liquid scintillation counter [Abdellah, 2013]. Ionization chambers, proportional counters and Geiger-Muller counters are examples of gas filled detectors that are widely used [Faanu, 2011]. Solid state detectors are basically semiconductor detectors [Saha, 2006]. The basic requirement for each of these instruments is that the incoming ionizing radiation should interact with the detector such that the magnitude of the response of the instrument is proportional to the radiation effect that is being measured [Cember, 2009; Faanu, 2011]. To get a response from the detector, the radiation should have undergone either the Photoelectric Effect, Compton Scattering or Pair Production.

The result of interaction in a detector is the appearance of a given amount of electric charge within the detector's active volume [Cember, 2009; Faanu, 2011]. Ionizing gamma rays

interact with atoms in the sensitive detector volume and this produces electrons by the ionization process. Collection of these electrons results in an output pulse. Figure 2-2 below shows the basic HPGe experimental setup required to achieve the output pulse.

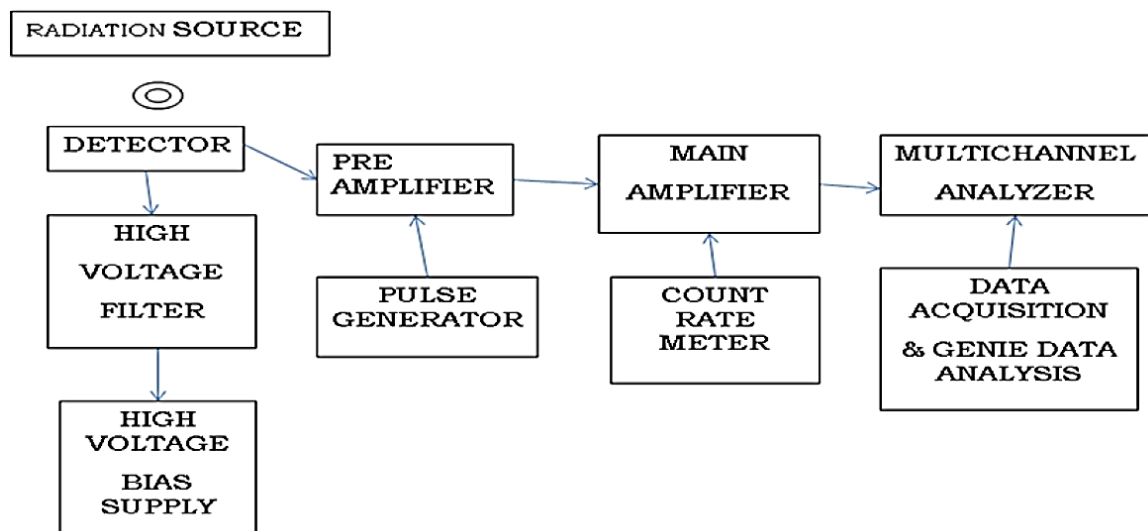


**Fig. 2-2: Setup of the HPGe detector [Hossain, Sharip and Viswanathan, 2011]**

The energy required to produce ionization event in semi conductor detectors is 3.5 eV in contrast to the gas filled detectors which require mean high energy of 30-35 eV [Cember, 2009; Faanu, 2011]. Being neither good insulators nor conductors, semiconductors have electrical conduction properties midway between insulators and conductors, such that the most widely used semiconductors are germanium and silicon [Winn, 2010]. Semiconductors are members of group IV in the periodic table. Each member of this group has four valence electrons and will form a crystal lattice of covalently bonded atoms. These covalent bonds could be disrupted by the absorption of energy. An energy of 1.12 eV is needed for knocking out one valence electron from silicon. This would then result in a free electron and “hole” in the position that was previously occupied by the valence electron [Faanu, 2011]. The resulting hole and free electron are able to move about in the lattice

structure. An electron that is adjacent to the hole can jump into the hole, thus leaving another hole behind. This property of semiconductors implies that current will flow through them if they are connected in a closed electrical circuit [Cember, 2009]. Therefore, the operation of a semiconductor detector is dependent on the excess holes or excess electrons present. An n-type semiconductor has excess electrons, while the p-type semiconductor has excess holes [Winn, 2010].

#### 2.4.1 RESOLUTION AND EFFICIENCY

Resolution refers to the ability of the detector to distinguish between two energy peaks that are very close to each other. This implies that two sharp energy peaks must be produced by the detector in order for them to be clearly distinguished. The resolution is given by Equation 2.9 below:

$$Resolution = \frac{FWHM}{Energy} \quad (2.9)$$

Where, Full Width at Half Maximum is represented by 'FWHM'. Resolution decreases with energy. Detector efficiency is the quotient that relates the source activity to the number of counts observed. Various types of efficiency such as Absolute efficiency, Intrinsic efficiency and Full energy photo peak efficiency may be used for gamma-ray detectors [Akkurt, Gunoglu and Arda, 2014]. Absolute efficiency is the ratio of counts recorded on the detector to the number of gamma rays emitted. The detector's absolute efficiency is necessary in radioactivity measurements and is given by Equation 2.10 below:

$$\epsilon_{abs} = \frac{N_c}{N_s} \quad (2.10)$$

Where,  $\epsilon_{abs}$  is the absolute efficiency of the detector,  $N_C$  is the number of counts the detector records and  $N_S$  is the number of gamma rays the source emits. Intrinsic efficiency is the ratio of the total number of pulses recorded on the detector to the number of gamma-rays arriving at the detector. Full energy photo peak efficiency refers to the efficiency for making only the full energy peaks [Akkurt, Gunoglu and Arda, 2014].

### **CHAPTER THREE: MATERIALS AND METHODS**

This chapter gives insight on the geology as well as the location of the study area. The type of samples collected, sampling procedure, sample preparation and analysis method are also described in this section. Mathematical functions or details to be used for natural radionuclide activity concentration calculations are also explained. Sampling was conducted in the study area from 01/07/2014 to 18/07/2014. Details pertaining to the radiation dose reconstruction are thoroughly presented.

#### **3.1 MATERIALS**

Several materials and equipment were used to successfully carry out this research. Polythene bags, clean 1L polythene containers, 0.45  $\mu\text{m}$  filter paper and 1M  $\text{HNO}_3$  are some of the materials that were crucial for this study. A gamma spectroscopy system that comprised of Genie 2000 software, a High Purity Germanium Detector (HPGe) and multi channel analyzer (MCA) were very important for this research. 1 liter Marinelli beakers, analytical balance, gloves, sample drying trays, sample grinder, sample drying oven, 500  $\mu\text{m}$  sample wire mesh sieve and Global Positioning System device (GPS) with model number 6195us, serial number 584037-001 and version 001 were excellent resources for the success of this study. MATLAB R2011b and Microsoft Excel software were also used for this project.

#### **3.2 DESCRIPTION OF STUDY AREA**

The study area is Morupule A Coal-Fired Power Station, located in Morupule (Botswana) at GPS coordinates 22.520°S 27.037°E and comprising of four turbo generators, each with an output of 33 MW. The power station uses 560, 000 to 630, 000 tonnes of bituminous coal each year and has been in operation since 1986. Basically, Morupule A Coal-fired

Power Station was the first major power station built in Botswana. The coal-fired power station is located 300 km to the north of Botswana's capital city, Gaborone. Road networks giving access to the power station are the A14 (connecting Palapye village and Serowe village) and the A1 (connecting Francistown city to Gaborone city via Palapye). Figure 3-1 is a map of Botswana showing the general positional location (C) of Morupule A Coal-Fired Power Station. Figure 3-2 is another map showing the location (C) Morupule A Coal-Fired Station in Botswana with more details like nearby urban or rural locations.



**Fig. 3-1: General location of Morupule A Coal-Fired Power Station in Botswana**



**Fig. 3-2: Detailed location of Morupule Coal-Fired Power Station in Botswana**

A small primary school (Kgaswe Primary School) is located approximately adjacent to the A14 road described above and about 800m to the south of Morupule Coal-Fired Power Station. The GPS coordinates of the school are 22.530°S 27.038°E. Palapye village is the nearest village and is located approximately 6 km to the east of Morupule A Coal-Fired Power Station. The land surrounding Morupule A Coal-Fired Power Station is mostly used as a communal grazing area for livestock such as cattle, sheep and goats. The fly-ash storage is just adjacent to the electrical power generation units, outside of the main building. There is a vast expanse of open space around the power station with vegetation such as trees and grass. Figure 3-3 shows an aerial view representing part of the study area. It shows the positions of the two fly ash storage tanks that are adjacent to the electrical



power generation units (turbo generators), the coal storage area, the fly ash pond, the main power station gate, Kgaswe Primary School and all other features are shown. Figure 3-4 shows the points where samples were collected in and around Morupule A Coal-Fired Power Station, including those sampling points from just outside of Palapye village and at the new Bus Rank in Palapye. Plates 3-1 to 3-2 are actual on-site photographs that show some of the points where sampling was done within Morupule A Coal-Fired Power Station and its surroundings.



**Fig. 3-3: Aerial view showing part of the study area [Google Earth]**

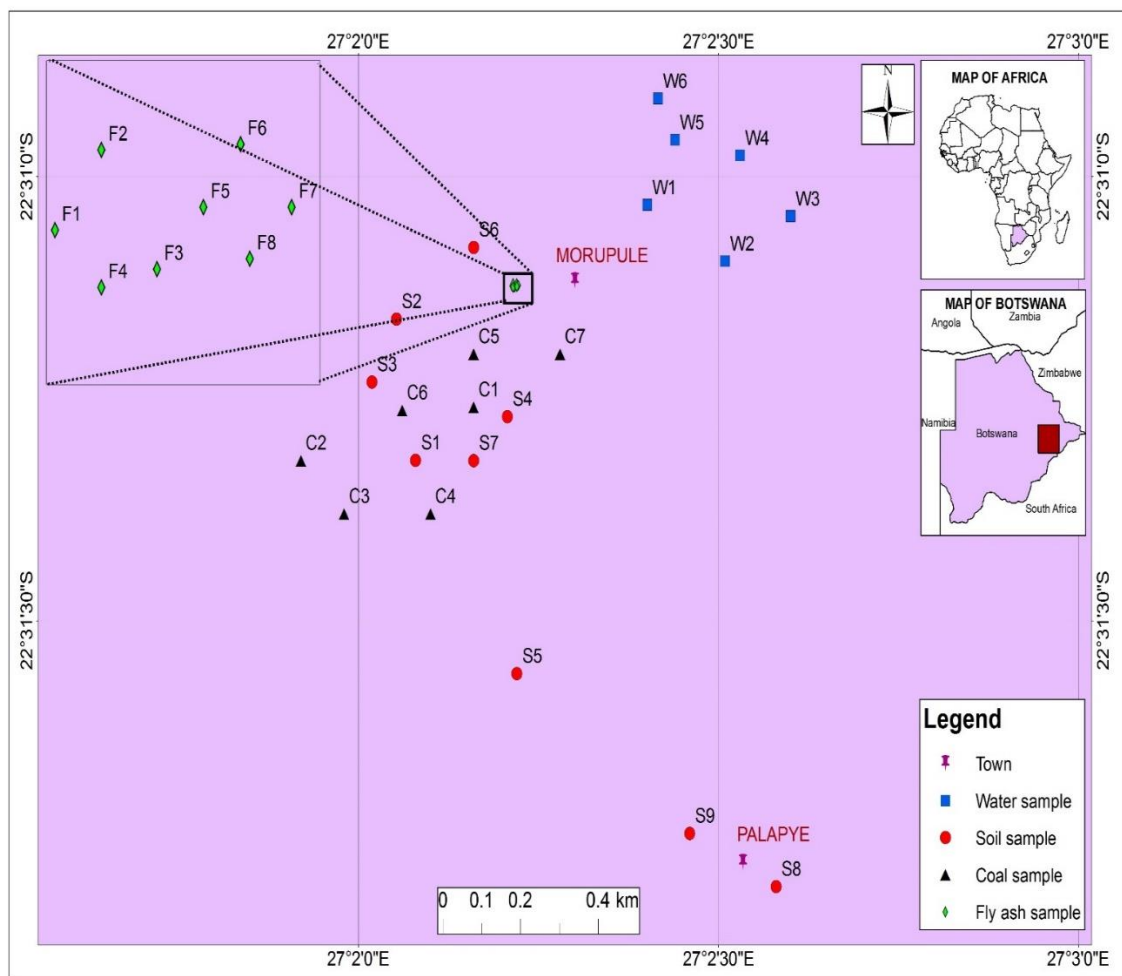


**Fig. 3-4: Layout of Morupule Coal-Fired Power Station showing sampling points**



**Plate 3-1: Two fly ash storage tanks**



**Plate 3-2: Coal Storage Area**



### **3.2.1 METEOROLOGY OF THE STUDY AREA**

Botswana generally has a predominantly subtropical climate that makes the whole country to be mostly semi-arid to arid. This therefore applies to the climate of Morupule. The rainy season lies in the summer months between October to March. January normally presents the peak of the rainy season. The winter season normally lies between the months of May to August. Winter is usually dry with peak winds in August. The transition months are usually April and September. The Morupule area has a potential evapotranspiration rate of 900 mm/year to 1200 mm/year, receives a mean annual precipitation of 371 mm and has average annual temperatures that lie between 30°C and 14°C [Ecosurv Environmental Consultants, 2008]. The north easterly winds are dominant in the area and have an average wind speed of 3 m/s. The evapotranspiration rate is thus about two or three times the average annual rainfall [Ecosurv Environmental Consultants, 2008].

### **3.2.2 GEOLOGY AND SOILS**

The location of the area is on the Karoo Supergroup and the Palapye Group [Ecosurv Environmental Consultants, 2008]. Assemblages on the lower main seam Karoo at Morupule in Botswana are similar to the *Striatopodocarpites fusus* Biozone in the Collie Basin of Western Australia and to the 3a Microfloral Biozone in the Northern Karoo Basin of South Africa. An Aktastinian age for the Morupule strata is indicated by this [Stephenson and McLean, 2004]. Geology of the area comprises of mudstones and shales (Lotsane formation) covered by relatively thin Kalahari Beds. Tswapong formation fractured quartzites are found outcropping the western slope on the Tswapong Hills while black shales consisting of the Karoo Supergroup sediment siltstones and mudstones are

found covering the Lotsane formation [Ecosurv Environmental Consultants and GIBB Botswana, 2007]. The eastern edge is made up of these rocks, as well as successive shales, sandstones and conglomerates. The coal seams providing fuel for Morupule A Coal-Fired Power Station are found within all these sequences [Ecosurv Environmental Consultants and GIBB Botswana, 2007].

The study area has soils that are of orange color, sandy silt loam texture and fine grain size. The soils are wind blown, and were formed by the weathering of the Ntane Sandstone Formation that outcrops the Serowe escarpment. Ferralic Arenosols is the main soil type in the Morupule A Coal-Fired Power Station Area, whereas Calcaric Cambisols and Orthic Luvisols soil types predominate southwards, while clay soil is found in the lower soil profile [Ecosurv Environmental Consultants and GIBB Botswana, 2007].

### **3.2.3 HYDROGEOLOGY**

The area is approximately 950 m above the mean sea level and there generally is a gentle slope falling away towards the south east of the area. Lotsane and Morupule rivers are each located within 10 km of Morupule A Coal-Fired Power Station and are both ephemeral, meaning that they only flow at certain times during the year. Morupule river runs north-southwards and actually pours into Lotsane river, which in turn flows eastwards towards Palapye. Figure 3-5 shows the locations of Lotsane and Morupule rivers in relation to Morupule A Coal-Fired Power Station and other nearby topographical features [Water Surveys Botswana, 2007], all in 3-D (three dimensions).

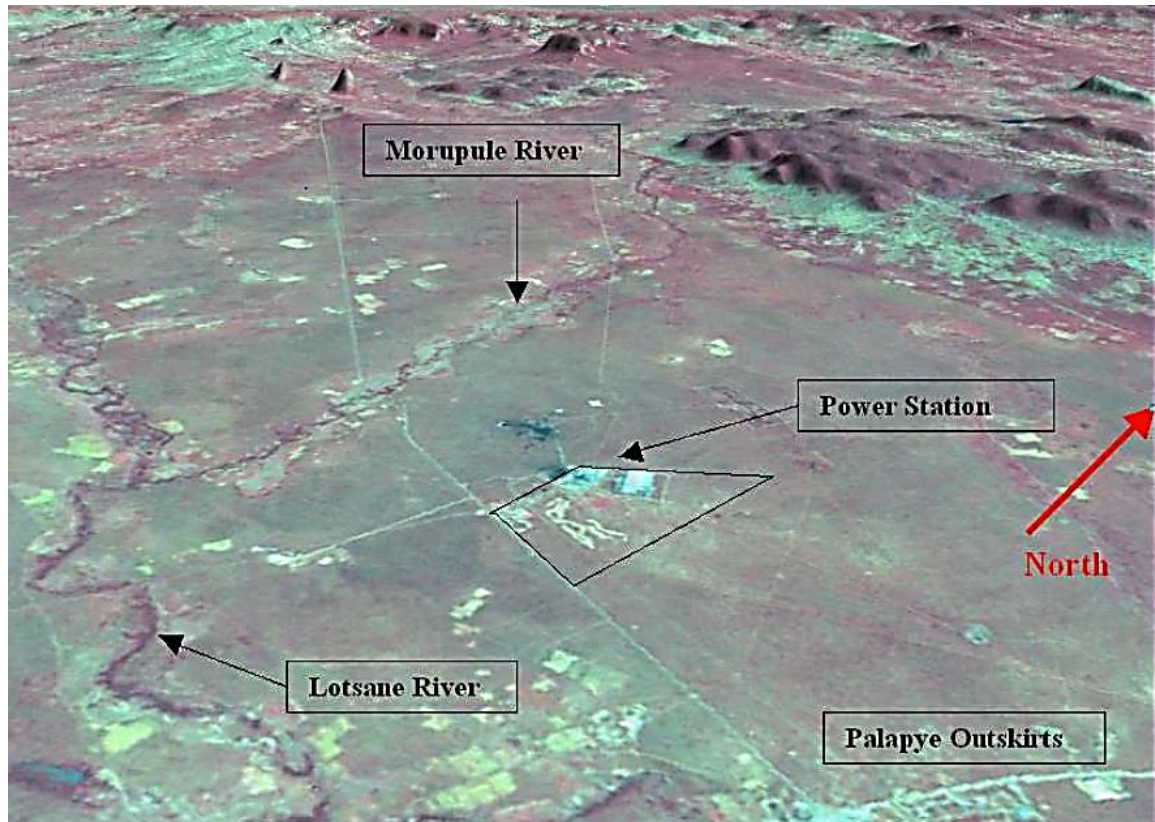


**Fig. 3-5: 3-D Satellite image showing positions of Lotsane and Morupule rivers**

Lotsane river then feeds the Limpopo river at the Botswana-South Africa border. Below the Lotsane formation mentioned in Section 3.1.3 above lies the Palapye fractured quartzitic which may be considered to be a very minor aquifer. The Lotsane formation as well as the shales and mudstones from the Karoo sequence mentioned in Section 3.1.3 above do not have usable groundwater quantities [Ecosurv Environmental Consultants and GIBB Botswana, 2007].

### **3.2.4 VEGETATION**

Acacia/Burkea/Ochna Savannah and Acacia Savannah are the two main vegetation types that are found in the area. The rocky hill outcrops is an additional vegetation type that is also found within the area. Invasive species of *Argemone Mexicana* and *Dichrostachys*

cineria also exist in this area [Ecosurv Environmental Consultants, 2008]. *Nicotiana* sp is the most common bushy plant species that is found on the walls of the fly ash ponds [Ecosurv Environmental Consultants and GIBB Botswana, 2007].

### **3.3 METHOD**

#### **3.3.1 SAMPLES COLLECTION**

Thirty (30) samples of various matrices were collected in and around Morupule A Coal-Fired Power Station. These comprised of:

- (a) Nine (9) soil samples from the power station, its surroundings and the nearby village of Palapye (about 5 km away).
- (b) Seven (7) bituminous coal samples from within the power station.
- (c) Eight (8) fly ash samples from the fly ash storage area.
- (d) Six (6) water samples from the fly ash ponds.

Random sampling was performed over a large area to ensure that each sample was a true representative of the whole and suitable to use in the study. All sample collection equipment, sample preparation areas and containers were kept clean to avoid contamination. Any sample with relatively high levels of activity was kept separated from other samples to avoid cross contamination.

##### **3.3.1.1 SOIL/COAL/FLY ASH SAMPLING**

Soil samples from different and undisturbed areas were collected to a depth of 25-50 cm with a coring tool into clearly labelled polythene bags. Bituminous coal and fly ash samples from different locations were collected by means of a scooping tool into clearly labelled polythene bags. Visible objects like grass and roots were removed manually from the soil and bituminous coal samples. All labelled samples were tightly sealed in their polythene

bags. The labelled samples were then transferred to GAEC laboratory to be prepared for analysis. As a precaution for ensuring that representative samples were collected for analysis from the area, a survey was first done with the sole aim of determining the sampling points. All soil sampling points were marked by means of a Global Positioning System device (GPS) with model 6195us, serial number 584037-001 and version 001. Appendix 3 shows all soil sampling points within Morupule A Coal-Fired Power Station and its surroundings. Appendices 4 and 5 show all fly ash and bituminous coal sampling points respectively within Morupule A Coal-Fired Power Station.

### **3.3.1.2 WATER SAMPLING**

Clean and clearly labelled 1L polythene containers were used to collect water samples from regions of interest within the fly ash pond. Visible coarse material or suspended sediments were first removed by filtering the water samples using 0.45  $\mu\text{m}$  filter paper, after which the collected water samples were immediately spiked with 1M  $\text{HNO}_3$  before the respective container lids were sealed in place. The 1M  $\text{HNO}_3$  was meant to prevent the adsorption of radionuclides onto the internal surface of the polythene container walls [Martin, Hancock; 1992]. All water sampling points were marked by means of a Global Positioning System device (GPS) with model 6195us, serial number 584037-001 and version 001. All labelled and sealed water samples were then transferred to GAEC laboratory to be prepared for analysis. Appendix 6 shows all water sampling points from the fly ash ponds.

### **3.3.2 SAMPLE PREPARATION FOR DIRECT GAMMA SPECTROMETRY**

#### **3.3.2.1 SOIL/COAL/FLY ASH SAMPLE PRAPARATION**

At GAEC laboratory, the soil, bituminous coal and fly ash samples were spread onto clean aluminium trays and air dried in the laboratory for several days as required. They were then



dried to a constant weight in an oven for 3 hours at 105 °C [Faanu, 2011]. The soil and coal samples were crushed into a fine powdery state by means of a grinder, after which they were sieved into previously weighed 1 liter marinelli beakers using a 500 µm wire mesh sieve. The dry fly ash samples were added into previously weighed 1 liter marinelli beakers without first being crushed since they were already in a fine powder state. All these marinelli beakers with samples were then tightly sealed with their respective lids and paper tape, after which the sealed marinelli beakers were weighed again to obtain the actual weight of the samples. The tightly sealed 1 liter marinelli beakers were then kept for 30 days to achieve secular equilibrium between the parent and daughter radionuclide of the enclosed contents [Faanu, 2011; Agalga, Darko and Schandorf, 2013; Ademola and Onyema, 2014]. After this period of 30 days, the contents of the sealed marineli beakers underwent radionuclide detection and measurement by a gamma spectrometry system using HPGe detector (High Purity Germanium Detector) for 10 hours. The resulting radionuclide activity concentrations were in the units Bq/kg [Faanu, 2011].

### **3.3.2.2 WATER SAMPLE PREPARATION**

The collected 1 liter water samples were filtered into their respective previously weighed 1 liter Marinelli beakers. The respective Marinelli beakers with samples were then tightly sealed with their respective lids and paper tape, after which the sealed marinelli beakers were weighed again to obtain the actual weight of the water samples. The sealed Marineli beakers then underwent radionuclide detection and measurement by a gamma spectrometry system using HPGe detector (High Purity Germanium Detector) for 10 hours. The resulting radionuclide activity concentrations were in the units Bq/l [Faanu, 2011].

### **3.3.3 SAMPLE ANALYSIS USING DIRECT GAMMA SPECTROMETRY**

A computerized gamma ray spectrometry system was used for this study. The system comprises of n-type High Purity Germanium Detector (HPGe) coupled with a Multi Channel Analyzer (MCA) [Faanu, Ephraim and Darko, 2010]. The computer system used is loaded with the software Genie 2000. Liquid nitrogen is used for cooling the HPGe detector to a temperature of 77 K [Reguigui, 2006]. The computerized gamma spectrometry system is powered by an uninterrupted power supply (UPS) unit. HPGe detector relative efficiency is 25% and its energy resolution is 1.8 keV at a Co-60 gamma energy of 1332 keV [Faanu et al., 2013]. Qualitative identification of radionuclides was done with the aid of their photopeak energies, while their quantification was done using the software Genie 2000.

HPGe detector energy and efficiency calibrations were performed before analysis of the collected samples. The energy and efficiency calibrations were performed to allow the qualitative identification and quantification of the natural radionuclides of interest. HPGe detector calibration was performed by means of a reference standard solution. The reference standard solution was measured into a 1 liter marinelli beaker and counted for 10 hours.

#### **3.3.3.1 ENERGY CALIBRATION**

The HPGe detector energy daily calibration was performed through the matching of gamma energy peaks in the spectrum of the reference standard to the spectrometer channel number [Çetiner, 2008]. The centroid channels and corresponding radionuclide energy peaks were recorded and used to make a calibration curve of Energy vs. Channel Number.

A least square curve fitting was done to obtain the calibration curve in polynomial form, represented by Equation 3.1 below:

$$E_i = \sum_0^N a_n C_i^n \quad (3.1)$$

Where,  $E_i$  is the calibration energy for the  $i^{\text{th}}$  channel number,  $C_i$  is the  $i^{\text{th}}$  channel number, the summation is from  $n = 0$  to  $n = N$ , while  $a_n$  gives the calibration constant [Çetiner, 2008]. The calibration was performed through the counting of standard radionuclides with known activities and gamma energy peaks from 60 keV to 2000 keV [Faanu, 2011]. The HPGe detector was used to count the standard for 10 hours. Table 3-1 gives the standard radionuclides used in the energy calibration as well as their activities, emission rates and gamma energies.

**Table 3-1: Standard radionuclides used for the energy and efficiency calibration**

Radionuclide	Gamma Energy (keV)	Activity (Bq)	Emission Rate
Americium-241	60	4.694E03	0.359
Cadmium-109	88	1.454E+04	0.036
Cerium-139	166	1.355E+03	0.800
Cobalt-57	122	1.156E+03	0.856
Cobalt-57	136	1.156E+03	0.107
Cobalt-60	1173	2.697E+03	0.999
Cobalt-60	1332	2.697E+03	0.999
Caesium-137	662	2.689E+03	0.851
Tin-113	255	4.000E+03	0.018
Tin-113	392	4.000E+03	0.640
Strontium-85	514	4.570E+03	0.960
Yttrium-88	1836	5.323E+03	0.992

### 3.3.3.2 EFFICIENCY CALIBRATION

Detector efficiency was defined earlier in Section 2.4.1. Efficiency calibration of the system was performed accurately to ensure proper quantification of the radionuclides that were present in the samples [Faanu, 2011]. During efficiency calibration, the peak search algorithm was necessary to locate as well as quantify peaks before associating them with decay-corrected emission rates for each line. Thus, an efficiency curve and equation were determined in the process, such that the efficiency curve may go to as high as the 9<sup>th</sup> order polynomial [Çetiner, 2008]. For this particular work, a 4<sup>th</sup> order polynomial was used. It is imperative that all detector system adjustments and settings be carried out prior to determining the efficiencies and this should be maintained until a new calibration is undertaken [Faanu, 2011; IAEA, 1989]. The efficiency calibration of the HPGe detector generally shows that efficiency decreases as the energy increases [Rahman, Naher, Ghosh and Islam, 2014].

The same mixed radionuclides standard was used for both the energy and efficiency calibration of the HPGe detector, with the standard being counted for 10 hours at a number of calibration points between 60 keV to 2000 keV [Faanu, 2011]. To determine efficiencies, Equation 3.2 was used [Darko et al., 2007; Faanu, 2011]:

$$\eta(E) = \frac{N_T - N_B}{P_E \cdot A_{STD} T_{STD}} \quad (3.2)$$

Where,  $N_T$  represents the total counts under a photopeak,  $N_B$  denotes the background count,  $P_E$  is the gamma ray yield,  $A_{STD}$  represents the activity of calibration standard during the time of measurement in Becquerels (Bq), while  $T_{STD}$  represents the counting time of the

standard. Table 3-1 gives the standard radionuclides used in the efficiency calibration as well as their activities, emission rates and gamma energies.

### 3.3.3.3 MINIMUM DETECTABLE ACTIVITY

The minimum detectable activity (MDA) is the lowest radioactivity quantity that can be measured at specific conditions. Thus, the MDA becomes particularly important for environmental level systems in which the sample count rate is almost similar to the background reading [Faanu, 2011]. The main factor affecting MDA is the background value, such that this background value can be reduced by better resolution. MDA values become lower at better resolution and higher efficiency of the detector [Abraham, Pelled and German, 2002]. In the determination of MDA, the the background is counted with a blank such as a sample holder. For this research, a distilled water-filled 1L Marinelli beaker was counted for 10 hours such that the average background peaks were used to determine the MDA.

In the case of Ra-226, the MDA was determined by utilizing the average peaks of the daughter gamma lines 295.2 keV and 351.9 keV of Pb-214 as well as 609.31 keV and 1764.5 keV of Bi-214. For determining the MDA of Th-232, the daughter gamma lines 238.63 keV of Pb-212, 583.2 keV and 2614.53 keV of Tl-208, 1460.8 keV of K-40, as well as 911.21 keV of Ac-228 were utilized [Faanu, 2011]. Equation 3.3 was used to determine the MDA:

$$MDA = \frac{K_{\alpha}\sqrt{N_B}}{P_E \cdot \eta(E) T_c M} \quad (3.3)$$

Where, MDA denotes the minimum detectable activity in Bq/kg,  $K_{\alpha}$  represents the statistical coverage factor of 1.645 at 95% confidence level,  $N_B$  represents the background

counts in the region of interest for a particular radionuclide,  $P_E$  represents the gamma emission probability,  $T_c$  is the time of counting,  $\eta(E)$  is the photopeak efficiency while  $M$  is the dry weight of the sample [Khandaker et al., 2012].

### 3.3.3.4 CALCULATION OF ANNUAL EFFECTIVE DOSE DUE TO THE RADIOACTIVITY IN SAMPLES

For soil/coal/fly-ash/water samples, the activity concentration of U-238 was calculated from the average peak energies of 295.21 keV and 351.92 keV for Pb-214 and 609.31 keV as well as 1764.49 for Bi-214. In the same way, activity concentration for Th-232 was calculated from the peak Pb-212 energy of 238.63 keV, Ac-228 peak energy of 911.21 keV, as well as the average peak energies for Tl-208 being 583.19 keV and 2614.53 keV. Activity concentration for K-40 was calculated by utilizing its peak energy of 1460.83 keV. Bi-214, with a peak energy of 609.31 keV, was used to determine Ra-226. Activity concentration for soil, coal and fly ash samples are in the units Bq.kg<sup>-1</sup>. Water sample activity concentration is in the units Bq.l<sup>-1</sup>. Equation 3.4 below was used to calculate activity concentrations of K-40, Th-232, U-238 and Ra-226 for the soil, coal, fly ash and water samples in this study:

$$A_{sp} = \frac{N_D e^{\lambda_P t_d}}{p.T_c.\eta(E).m} \quad (3.4)$$

Where,  $N_D$  represents the radionuclide net count in samples,  $\exp(\lambda_P t_d)$  represents the decay correction factor for delay between time of sampling and counting,  $t_d$  represents the time delay between the sampling and counting,  $P$  represents the gamma-ray yield,  $\eta(E)$  represents the detector system's absolute counting efficiency,  $T_c$  represents the counting

time of sample,  $m$  represents the sample mass in kilograms or volume in liters, while  $\lambda_p$  represents the decay constant associated with the parent radionuclide.

At 1.0 m above the ground for soil/coal/water/fly-ash samples, the external gamma dose rate,  $D_\gamma$ , was calculated from the activity concentrations using Equation (3.5) below [Faanu, Ephraim and Darko, 2010; Faanu et al., 2013; Zeevaert, Sweeck and Vanmarcke, 2005]:

$$D_\gamma(nGyh^{-1}) = DCF_K \times A_K + DCF_U \times A_U + DCF_{Th} \times A_{Th} \quad (3.5)$$

Where,  $DCF_K$ ,  $DCF_U$  and  $DCF_{Th}$  are dose conversion factors for K-40, U-238 and Th-232 respectively in  $nSv.h^{-1}/Bqkg$  such that  $A_K$ ,  $A_{Th}$  and  $A_U$  are the activity concentrations for K-40, Th-232 and U -238 and respectively.  $DCF_K$ ,  $DCF_U$  and  $DCF_{Th}$  values are listed below [UNSCEAR, 2000; Faanu, 2011]:

$$\begin{aligned} DCF_K &= 0.0417 \text{ nSv.h}^{-1}.Bq^{-1}kg^{-1} \\ DCF_U &= 0.462 \text{ nSv.h}^{-1}.Bq^{-1}kg^{-1} \\ DCF_{Th} &= 0.604 \text{ nSv.h}^{-1}.Bq^{-1}kg^{-1} \end{aligned}$$

The average annual effective dose was calculated from the absorbed dose rate by using a dose conversion factor of  $0.7 \text{ Sv.Gy}^{-1}$  as well as the outdoor occupancy factor of 0.2 [UNSCEAR, 2000]. Equation 3.6 below was used to calculate the average annual effective dose:

$$E_\gamma = D_\gamma \times 0.2 \times 8760 \times 0.7 \quad (3.6)$$

Where,  $E_\gamma$  represents the average annual effective dose,  $D_\gamma$  represents the absorbed dose rate in air [Faanu, Ephraim and Darko, 2010; UNSCEAR, 2000].

### 3.3.3.5 ANNUAL EFFECTIVE DOSE CALCULATIONS FROM EXTERNAL GAMMA DOSE RATE MEASUREMENTS

At every sampling point, several external gamma dose rate measurements were made at 1m above the ground with a suitable and calibrated Thermo survey meter (serial number 21535 and model FH40G-L10) and the average dose rate was computed. The annual effective dose ( $E_{\gamma,ext}$ ) was then estimated from this measured average external gamma dose rate using Equation 3.7a below:

$$E_{\gamma,ext} = D_{\gamma,ext} \cdot T_{exp} \cdot DCF_{ext} \quad (3.7a)$$

Where,  $D_{\gamma,ext}$  represents the average external (outdoor) gamma dose rate in  $\mu\text{Gy.h}^{-1}$ ,  $T_{exp}$  represents the exposure duration per year of 8760 hours (365 days x 24 hours) and using the outdoor occupancy factor of 0.2,  $DCF_{ext}$  represents the effective dose to absorbed dose conversion factor of  $0.7 \text{ Sv.Gy}^{-1}$  for the environmental exposure to gamma rays [Faanu, Ephraim and Darko, 2010; UNSCEAR, 2000, Faanu, 2011]. For the indoor case, Equation 3.7b was used to estimate the annual effective dose:

$$E_{\gamma,ind} = D_{\gamma,ind} \cdot T_{exp} \cdot DCF_{ind} \quad (3.7b)$$

Where,  $D_{\gamma,ind}$  denotes the calculated dose rate in  $\text{nGy.h}^{-1}$ ,  $T_{exp}$  denotes the indoor occupancy time ( $0.8 \times 24 \text{ h} \times 365 \text{ days} = 7008 \text{ h.y}^{-1}$ ), and  $DCF_{ind}$  is the conversion factor of  $0.7 \text{ Sv.Gy}^{-1}$  [Allam, Ramadan and Taha, 2014].

### 3.3.4 RADIOLOGICAL HAZARD ASSESSMENT

Soil and fly ash from the study area may be used as building materials. Fly ash is an excellent substitute for concrete, cement and clay [Ademola and Onyema, 2014]. The



radium equivalent activity concentration ( $R_{eq}$ ), external hazard ( $H_{ext}$ ) and internal hazard ( $H_{int}$ ) indices were used to assess the radiological hazard due to natural radioactivity from the fly ash, coal, soil and water which may be used as building/construction material. The only natural radionuclides considered in this radiological assessment are  $^{40}\text{K}$ ,  $^{226}\text{Ra}$  and  $^{232}\text{Th}$ . Calculations of  $R_{eq}$ ,  $H_{ext}$  and  $H_{int}$  were done by means of equations (3.8) to (3.10) respectively:

$$R_{eq} = A_{\text{Ra}} + 1.43A_{\text{Th}} + 0.077A_{\text{K}} \quad (3.8)$$

$$H_{ext} = A_{\text{Ra}}/370 + A_{\text{Th}}/259 + A_{\text{K}}/4810 \leq 1 \quad (3.9)$$

$$H_{int} = A_{\text{Ra}}/185 + A_{\text{Th}}/259 + A_{\text{K}}/4810 \leq 1 \quad (3.10)$$

Where,  $A_{\text{Ra}}$ ,  $A_{\text{Th}}$  and  $A_{\text{K}}$  are activity concentrations for the natural radionuclides  $^{226}\text{Ra}$ ,  $^{232}\text{Th}$  and  $^{40}\text{K}$  in Bq/kg respectively.  $R_{eq}$  index basis is on the estimation that the same gamma dose rate is produced by 1 Bq/kg of  $^{226}\text{Ra}$ , 0.7 Bq/kg of  $^{232}\text{Th}$  and 13 Bq/kg of  $^{40}\text{K}$ . In order to ensure that building materials are safe to use with respect to radiation, the maximum  $R_{eq}$  for these materials must not exceed 370 Bq/kg. The maximum allowed values for  $H_{ext}$  and  $H_{int}$  are unity and dimensionless [Ademola and Onyema, 2014]. The representative level index ( $I_{\gamma r}$ ) is a radiation index hazard that is used to estimate the level of  $\gamma$  radiation hazard [Harb et al., 2008; NEA-OECD, 1979] due to natural radionuclides in samples and is represented by Equation 3.11 below:

$$I_{\gamma r} = A_{\text{Ra}}/150 + A_{\text{Th}}/100 + A_{\text{K}}/1500 \quad (3.11)$$

Where,  $A_{\text{Ra}}$ ,  $A_{\text{Th}}$  and  $A_{\text{K}}$  are activity concentrations for natural radionuclides  $^{226}\text{Ra}$ ,  $^{232}\text{Th}$  and  $^{40}\text{K}$  in Bq/kg respectively. In order for the radiation hazard to be negligible, the value of the representative level index  $I_{\gamma r}$  must be less than unity [Harb et al., 2008].

### 3.3.5 DOSE RECONSTRUCTION

Radioactive decay is a random process, therefore we cannot predict if a single nucleus in a sample will undergo radioactive decay in a given time period. What can be predicted is the average decay behaviour for a very large number of similar radionuclides  $N$  in a sample. During a small interval of time  $\Delta t$ ,  $\Delta N$  of the atoms undergo radioactive decay [Shultis and Faw, 2007]. The probability for any radionuclide in the sample to decay in time interval  $\Delta t$  is therefore given by  $\Delta N/N$ . The value of the statistically averaged decay probability per unit time (considering the limit of infinitely small time interval  $\Delta t$ ) approaches  $\lambda$ , which is the decay constant:

$$\lambda = \lim_{\Delta t \rightarrow 0} \left( \frac{\Delta N/N}{\Delta t} \right) \quad (3.12)$$

Every radionuclide has its own unique decay constant. Decay constant is basically the probability that a radionuclide decays in unit time for an infinitesimal interval of time. The radionuclide decays more slowly for smaller values of the decay constant  $\lambda$ . The decay constant is zero ( $\lambda = 0$ ) for stable radionuclides. For radionuclides,  $\lambda$  only depends on nuclear forces and is not dependent on empirical factors like pressure or temperature [Shultis and Faw, 2007].

In the case of a sample consisting of a large number of similar radionuclides ( $N \gg 1$ ), continuous mathematics is used to define an inherently discrete process. Therefore, at time  $t$ ,  $N(t)$  is the average number of radionuclides present in the sample. The probability for any radionuclide in the sample to decay in a time interval  $dt$  is  $\lambda dt$ . Therefore in  $dt$  and at a time  $t$ ,  $\lambda dt N(t)$  decays are expected in the sample. This should equal the decrease  $-dN$  in the number of radionuclides from the sample as shown below:

$$-dN = \lambda N(t) dt \quad (3.13a)$$

The above expression simplifies to Equation 3.13b below:

$$\frac{dN(t)}{dt} = -\lambda N(t) \quad (3.13b)$$

The solution of the differential Equation 3.13b above is given as Equation 3.14 below:

$$N(t) = N_0 e^{-\lambda t} \quad (3.14)$$

Where,  $N_0$  represents the number of radionuclides present in the sample when  $t = 0$ .

Equation 3.14 is thus known as the radioactive decay law, with a unique property known as the half - life [Shultis and Faw, 2007]. The half - life denotes the time required for the activity to reduce to half of its value by a radioactive decay process [McNaught and Wilkinson, 1997]. The half life is a constant represented by  $T_{1/2}$  and is independent of time.

Using the concept of half life and substituting into Equation 3.14 will yield expression 3.15 below:

$$N(T_{1/2}) = \frac{N_0}{2} = N_0 e^{-\lambda T_{1/2}} \quad (3.15)$$

Solving Equation 3.15 gives Equation 3.16 for  $T_{1/2}$  below:

$$T_{1/2} = \frac{\ln 2}{\lambda} \quad (3.16)$$

Some useful averages and probabilities are determined using the exponential decay law.

Considering  $N_0$  similar radionuclides at an initial time  $t = 0$ , it is expected that the number of atoms will be  $N_0 e^{-\lambda t}$  at a later time  $t$ . Equation 3.17 represents the probability  $\bar{P}$  that any one of the atoms does not undergo radioactive decay in the time interval  $t$ :

$$\bar{P}(t) = \frac{N(t)}{N(0)} = e^{-\lambda t} \quad (3.17)$$

Equation 3.18 below represents the probability  $P(t)$  of radionuclide decay in the time interval  $t$  [Mayin, 2014]:

$$P(t) = 1 - \bar{P}(t) = 1 - e^{-\lambda t} \quad (3.18)$$

As  $t$  becomes very small ( $t \rightarrow \Delta t \ll 1$ ), Taylor series approximation shows that:

$$P(\Delta t) = 1 - e^{-\lambda \Delta t} = 1 - [1 - \lambda \Delta t + \frac{1}{2!} (\lambda \Delta t)^2 - \dots] \approx \lambda \Delta t \quad (3.19)$$

### 3.3.5.1 TAYLOR SERIES METHOD FOR NUMERICAL SOLUTIONS IN DOSE RECONSTRUCTION

The Taylor Series method with numerical derivatives was used to approximate numerical solutions to ordinary differential equations. This Taylor Series method was one of the earliest analytic-numeric algorithms used in the approximation of solutions to ordinary differential equations [Miletics and Molnárka, 2014]. The exponential term (decay factor) from the radioactive decay law was first represented by a polynomial of order 4. This is possible since U-238, Th-232 and K-40 have very long half - lives which are  $4.47 \times 10^9$  years,  $1.41 \times 10^{10}$  years and  $1.28 \times 10^9$  years respectively. To approximate the activity concentration of U-238, Bi-214 was used. This was due to the fact that Bi-214 is a daughter product of U-238 and has a relatively short half - life of 19.9 minutes compared to that of U-238 [Loureiro, 1987]. In approximating the activity concentration of Th-232, its daughter product Ac-228 was used. Ac-228 has a relatively short half - life of 6.1 hours as compared to its parent radionuclide Th-232. The radioactivity build up [Ahmed, 2007; Mayin, 2014] of the daughter product  $A$  at any time  $t$  is denoted by Equation 3.20 below:

$$A = A_o(1 - e^{-\lambda t}) \quad (3.20)$$

Where,  $A_o$  represents the initial parent radioactivity,  $\lambda$  is the decay constant and  $t$  is the decay time. The approximation of the decay factor  $e^{-\lambda t}$  to polynomial form is shown below [Mayin, 2014]:

$$P(\lambda t) = P(x) = e^{-\lambda t} \quad (3.21)$$

Where,

$$e^{-\lambda t} = e^{-x} \quad (3.22)$$

A polynomial is simply a function which can be stated in the form below:

$$P(x) = c_0 + c_1x + \dots + c_nx^n \quad (3.23)$$

Where,  $c_0, c_1, \dots, c_n$  are constant coefficients and  $n$  represents the polynomial order for  $c_n \neq 0$  over a finite interval  $[a, b]$  [Conte and de Boor, 1981]. The Taylor series method of numerical approximations was used to model the non-linear relationship between the average annual effective dose of samples with respect to the elapsed time in years [Smyth, 1998]. Transforming the function  $e^{-x}$  to polynomial form made it easier to approximate and minimized the error of approximation. Values of  $P(x)$  within the range  $[a, b]$  were estimated by interpolation while those outside this range were predicted by extrapolation [Smyth, 1998]. Equation 3.24 below is a representation of the Taylor series [Stroud, 2003]:

$$P(x) = f(x+h) = f(x) + hf'(x) + \frac{h^2}{2!}f''(x) + \dots + \frac{h^n}{n!}f^n(x) \quad (3.24)$$

The exponential function  $P(x) = e^{-\lambda t} = e^{-x}$  was approximated about point  $x = 0$  by means of Equation 3.24 to the polynomial form shown in 3.23 by means of the following steps:

$$e^{-x} = P(x) = f(0) + (x-0)f'(0) + \frac{(x-0)^2}{2}f''(0) + \frac{(x-0)^3}{6}f'''(0) + \frac{(x-0)^4}{24}f^{(4)}(0) \quad (3.25)$$

Where,

$$f(0) = 1, f'(0) = -1, f''(0) = 1, f'''(0) = -1, f^{(4)}(0) = 1 \quad (3.26)$$

Substituting the values from Equations 3.26 into 3.24 yields the 4<sup>th</sup> order polynomial approximation of  $e^{-x}$  given by Equation 3.27:

$$e^{-x} = 1 - x + x^2/2 - x^3/6 + x^4/24 = 0.042x^4 - 0.167x^3 + 0.5x^2 - x + 1 \quad (3.27)$$

Appendix 9 shows the MATLAB algorithm that was used for the above computations to generate the 4<sup>th</sup> order Taylor series polynomial of  $e^{-x}$ .

The half - life of Bi-214 at a peak energy of 609.31 keV, was used to calculate  $x = \lambda t$  for U-238. In the case of Th-232, the half - life of Ac-228 was used at a peak energy of 911.21 keV. The results were then evaluated by utilizing the polynomial approximation expression in 3.27 above. The activity concentrations of these radionuclides were then reconstructed by means of the radionuclide decay expression below:

$$A = A_0 \cdot e^{-\lambda t} \quad (3.28)$$

Equation 3.7b was used to calculate the annual effective dose due to the samples. Microsoft Excel was used to work out the above expressions. The approximation from Equation 3.27 was then used in interpolating the growth for the calculated activity concentration of all the samples utilizing the half lives of Bi-214 and Ac-228. The decay was estimated to thirty years before the time of sample analysis. In the same manner, the radioactive decay was estimated on the calculated activity concentration of the analyzed samples. This was achieved by extrapolating the decay for up to thirty years from the time of sample analysis.

## **CHAPTER FOUR: RESULTS AND DISCUSSION**

This chapter presents and discusses the results from this research. The discussion covers the energy and efficiency calibrations of the HPGe system used for the analysis. It also covers the minimum detectable activity, dose rate, annual effective dose, radiological hazard assessment and natural radionuclide activity concentrations as well as the radiation dose reconstruction of the study area. Results from empirical work were used as the main input data to perform the dose reconstruction. The results are compared with similar facilities and other relevant work done elsewhere.

### **4.1 ENERGY AND EFFICIENCY CALIBRATION**

The gamma spectrometry system was calibrated for energy and efficiency using a mixed radionuclides standard in 1L Marinelli beaker. The resulting energy and efficiency calibration curves are shown in Figure 4-1 and Figure 4-2 respectively. In Figure 4-2, the Efficiency was plotted against Energy, giving an exponential curve.

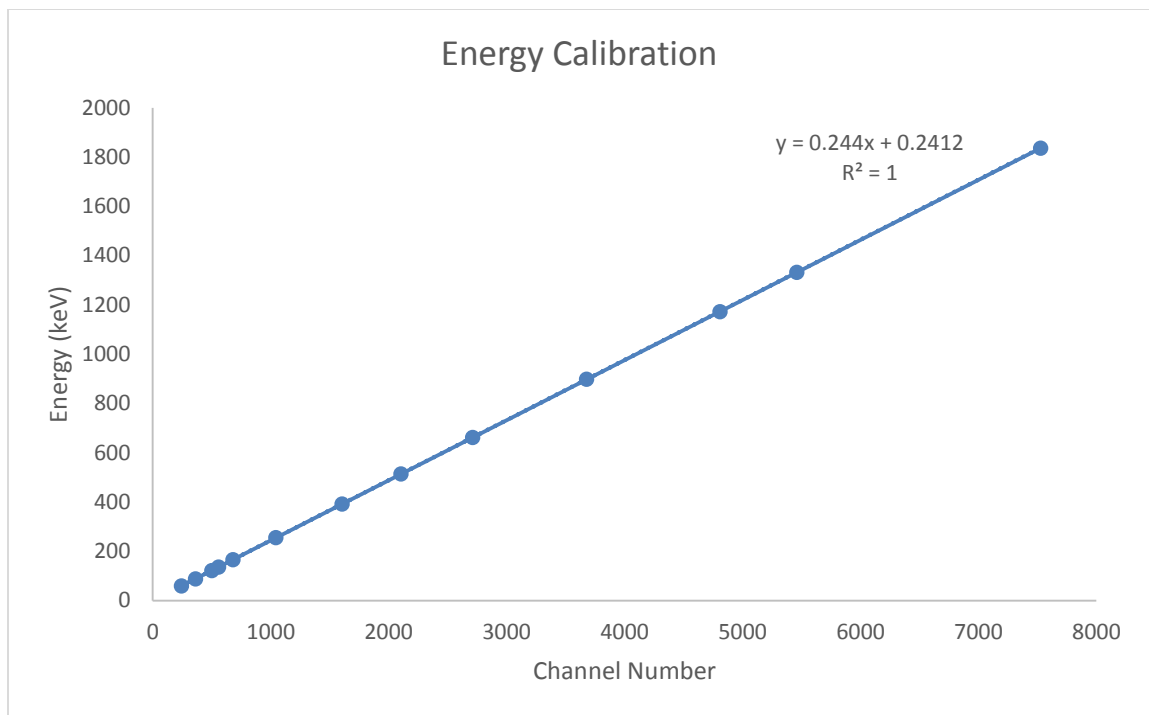


**Fig. 4-1: Energy calibration curve using mixed radionuclides standard**

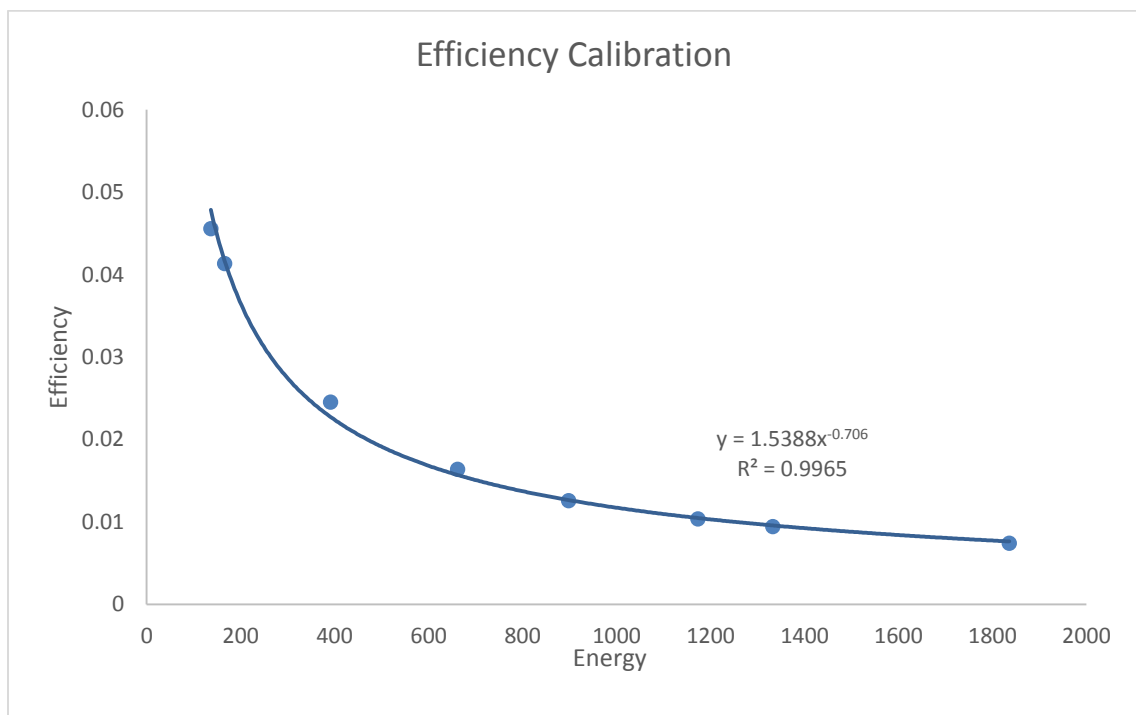


**Fig. 4-2: Efficiency calibration curve using mixed radionuclides standard**



## 4.2 MINIMUM DETECTABLE ACTIVITY

Table 4-1 shows the minimum detectable activities (MDA). The minimum detectable activities were estimated for U-238, Th-232 and K-40. The values obtained were 0.13 Bq/kg, 0.13 Bq/kg and 0.12 Bq/kg respectively. These values indicate the minimum detectable quantities at the 95% confidence level.

**Table 4-1: Minimum detectable activities of K-40, Th-232 and U-238**

Nuclide	Minimum Detectable Activity (Bq/kg)
U-238	0.13
Th-232	0.13
K-40	0.12

## 4.3 ACTIVITY CONCENTRATIONS, ABSORBED DOSE RATES AND ANNUAL EFFECTIVE DOSES IN THE STUDY AREA

The radionuclide activity concentrations, absorbed dose rates and annual effective doses for all sampling points in the study area were determined in separate tables for the fly ash, coal, soil and water samples as shown in sections 4.2.1, 4.2.2, 4.2.3 and 4.2.4 respectively.

### 4.3.1 FLY ASH

Fly Ash samples from the study area were identified with the sample codes ASH-1 to ASH-8. Table 4-2 shows a summary of the results obtained for fly ash samples from the fly ash storage area.

**Table 4-2: Experimental results for the average activity concentrations, absorbed dose rates and annual effective doses due to natural radionuclides in fly ash from the study area**

Sample Code	Activity Concentration (Bq/kg)			Absorbed Dose Rate (nGy/h)	Annual Effective Dose (mSv)
	Th-232	U-238	K-40		
ASH-1	73.00±1.07	52.73±0.90	42.65±1.53	70.24±1.13	0.35±0.01
ASH-2	73.91±1.08	54.42±0.93	42.55±1.50	71.55±1.14	0.35±0.01
ASH-3	71.63±1.05	52.38±0.90	42.54±1.53	69.24±1.11	0.34±0.01
ASH-4	66.10±0.99	48.06±0.84	39.77±1.49	63.79±1.05	0.31±0.01
ASH-5	68.56±1.07	50.65±0.87	41.04±1.50	66.52±1.11	0.33±0.01
ASH-6	67.30±1.07	49.89±0.86	40.88±1.52	65.40±1.11	0.32±0.01
ASH-7	57.50±0.88	39.95±0.71	33.61±1.35	54.59±0.92	0.27±0.01
ASH-8	62.33±0.94	46.87±0.81	37.62±1.44	60.87±1.00	0.30±0.01
Min.	57.50±0.88	39.95±0.71	33.61±1.35	54.59±0.92	0.27±0.01
Max.	73.91±1.08	54.42±0.93	42.65±1.53	71.55±1.14	0.35±0.01
Mean	64.54±1.02	49.37±0.85	40.08±1.48	65.27±1.07	0.32±0.01
Std Dev.	5.58	4.54	3.12	5.57	0.03

Table 4-2 shows the activity concentrations of U-238, Th-232 and K-40 for the eight (8) fly ash samples from the study area, as well as the calculated annual effective doses and absorbed dose rates. The mean activity concentration of Th-232, U-238 and K-40 for the fly ash samples are 64.54±1.02 Bq/kg, 49.37±0.85 Bq/kg and 40.08±1.48 Bq/kg with ranges of 57.50-73.91 Bq/kg, 39.95-54.42 Bq/kg and 33.61-42.65 Bq/kg respectively. Figure 4-3 is a graphical representation of the natural radionuclide activity concentration for Th-232, U-238 and K-40 in fly ash samples from the study area.

The mean fly ash activity concentration values for Th-232, U-238 and K-40 from this study are generally lower than those from average world activity concentrations and French coal-fired power stations as depicted in Table 2-9 [UNSCEAR, 1982] and Table 2-8 [Degrange and Lepicard, 2004] respectively. However, the fly ash activity concentrations of U-238 and Th-232 from this study are almost double in value to those estimated from Orji River Thermal Power Station in Nigeria as shown in Table 2-7 [Ademola and Onyema, 2014]. These variations in activity concentration is expected since fly ash radionuclide concentration depends on the radionuclide concentration of the coal combusted, the type of coal used as well as the power station boiler conditions during the coal combustion [Paschoa and Steinhausler, 2010]. The corresponding standard deviations in the activity concentrations of Th-232, U-238 and K-40 from the fly ash samples are 5.58 Bq/kg, 4.54 Bq/kg and 3.12 Bq/kg respectively.

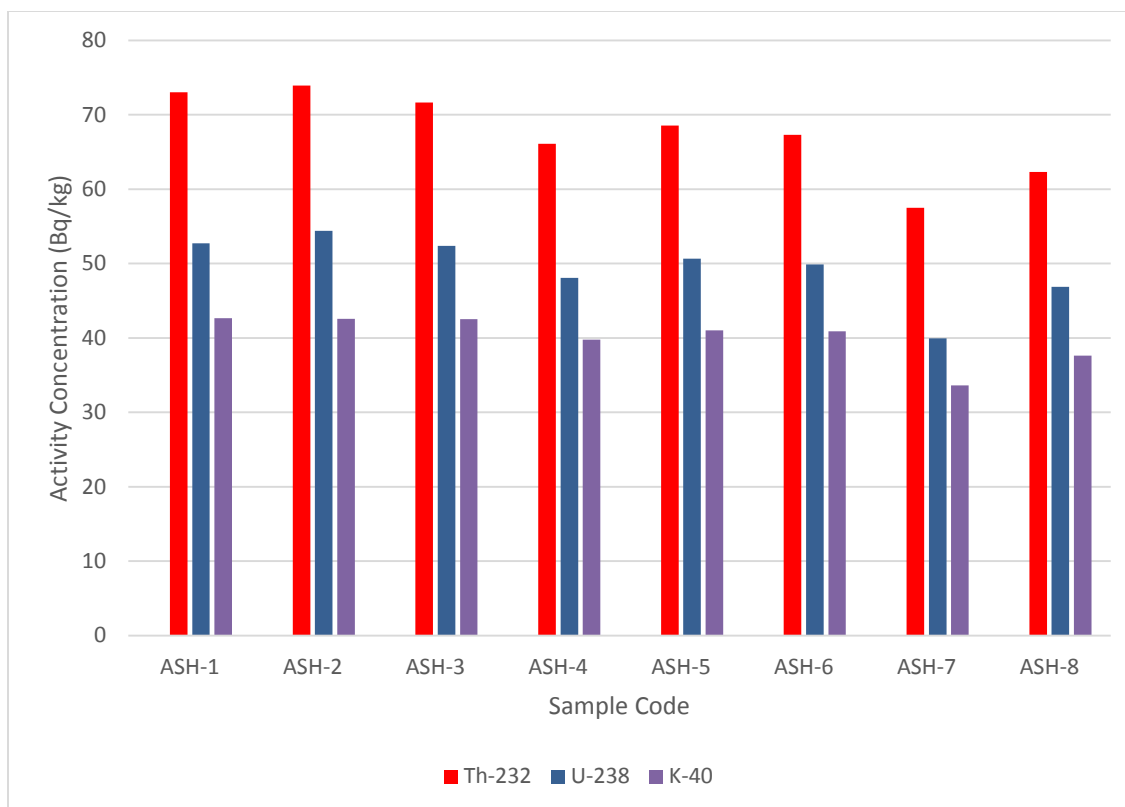


**Figure 4-3: Average activity concentration for natural radionuclides Th-232, U-238 and K-40 in fly ash samples from the study area**

As seen from Table 4-2, the mean gamma dose rate due to terrestrial gamma rays from Th-232, U-238 and K-40 activity concentrations was 65.27 nGy/h, with a range of 54.59-71.55 nGy/h and standard deviation of 5.57 nGy/h respectively. The mean gamma dose rate from this study is slightly higher than the worldwide average value of 60 nGy/h [UNSCEAR, 2000; Faanu, 2011]. The mean gamma dose rate from this study is lower than that obtained from Indian coal-fired thermal power plants whose value is 79.19 nGy/h [Pandit, Sahu and Puranik, 2011]. It is also lower than the average annual external effective dose rate of 0.46 mSv/year [UNSCEAR, 1993; Pandit, Sahu and Puranik, 2011] from terrestrial radionuclides for areas with normal background radiation. As seen in Table 4-2, the mean annual effective dose due to natural radionuclides in the fly ash samples was 0.32 mSv, with a range of 0.27-0.35 mSv and standard deviation of 0.03 mSv. This calculated mean

annual effective dose (0.32 mSv) falls within the public annual effective dose limit of 1 mSv [IAEA, 2003].

#### 4.3.2 COAL

Bituminous coal samples from the study area were identified with the sample codes Coal 1 to Coal 7. Table 4-3 shows a summary of the results associated with coal samples from the study area.

**Table 4-3: Activity concentrations, absorbed dose rates and annual effective doses due to natural radionuclides in coal from the study area**

Sample Code	Activity Concentration (Bq/kg)			Absorbed Dose Rate (nGy/h)	Annual Effective Dose (mSv)
	Th-232	U-238	K-40		
Coal 1	23.10±0.46	15.39±0.33	12.99±0.89	21.61	0.11
Coal 2	24.03±0.47	16.43±0.34	15.63±0.93	22.76	0.11
Coal 3	40.82±0.80	25.61±0.56	25.92±1.54	37.57	0.18
Coal 4	38.91±0.78	24.53±0.54	24.36±1.48	35.85	0.18
Coal 5	21.69±0.48	14.93±0.32	14.58±0.90	20.61	0.10
Coal 6	22.49±0.49	15.67±0.33	15.70±0.91	21.48	0.11
Coal 7	20.97±0.43	14.13±0.31	12.52±0.85	19.71	0.10
Min.	20.97±0.43	14.13±0.31	12.52±0.85	19.71	0.10
Max.	40.82±0.80	25.61±0.56	25.92±1.54	37.57	0.18
Mean	27.43±0.56	18.10±0.39	17.38±1.07	25.65	0.13
Std Dev.	8.57	4.82	5.45	7.63	0.04

Table 4-3 shows the activity concentrations of U-238, Th-232 and K-40 for the seven (7) bituminous coal samples from the study area, as well as the calculated annual effective

doses and absorbed dose rates. The mean activity concentration values of Th-232, U-238 and K-40 for the coal samples are  $27.43 \pm 0.56$  Bq/kg,  $18.10 \pm 0.39$  Bq/kg and  $17.38 \pm 1.07$  Bq/kg with ranges of 20.97-40.82 Bq/kg, 14.13-25.61 Bq/kg and 12.52-25.92 Bq/kg respectively. Figure 4-4 is a graphical representation of the natural radionuclide activity concentration for Th-232, U-238 and K-40 in coal samples from the study area.

The mean coal activity concentrations for U-238 and K-40 from this study are generally slightly lower than those from average world activity concentrations as shown in Table 2-9 [UNSCEAR, 1982]. However, the coal activity concentrations of Th-232 from this study are slightly higher in value to average world coal activity concentrations as shown in Table 2-9 [UNSCEAR, 1982]. Generally, the mean coal activity concentrations for U-238, Th-232 and K-40 in this study are comparable to the average world coal activity concentrations in Table 2-9 [UNSCEAR, 1982]. The corresponding standard deviations in the activity concentrations of Th-232, U-238 and K-40 from the coal samples are 8.57 Bq/kg, 4.82 Bq/kg and 5.45 Bq/kg respectively.

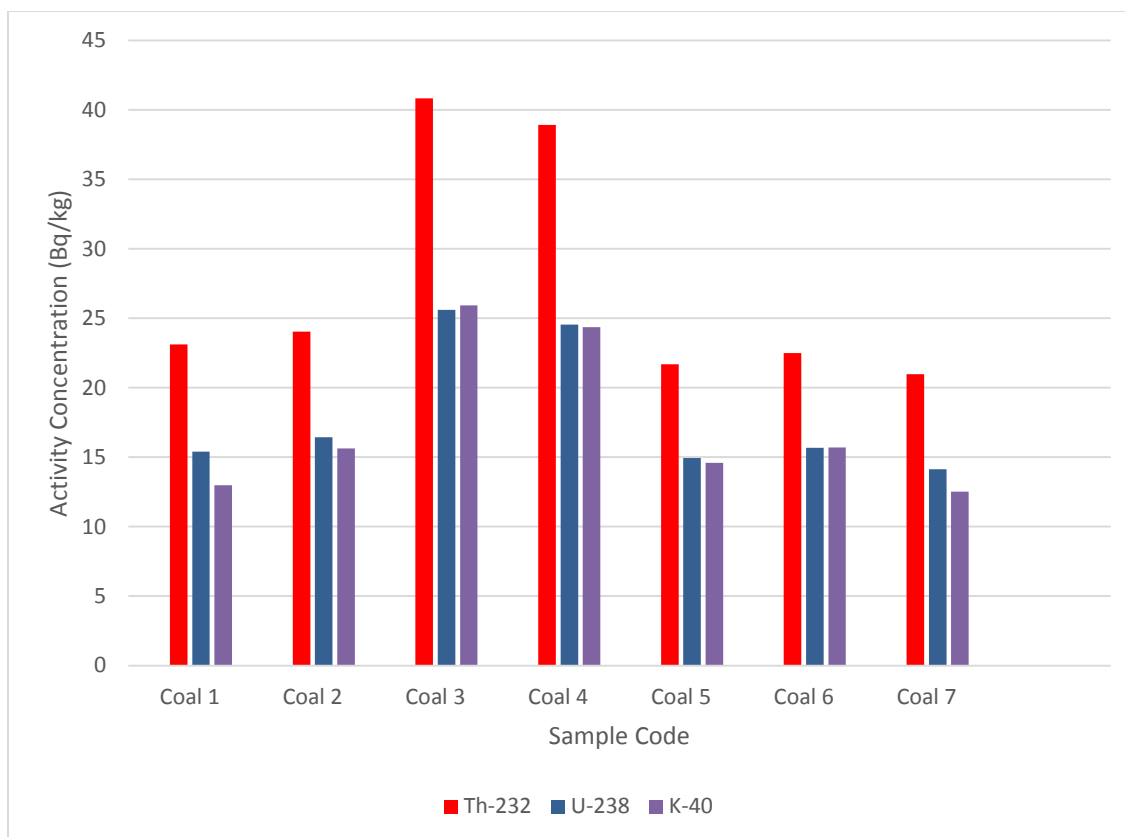


**Figure 4-4: Plot of activity concentration for natural radionuclides Th-232, U-238 and K-40 in coal samples from the study area**

As seen from Table 4-3, the mean gamma dose rate due to terrestrial gamma rays from Th-232, U-238 and K-40 activity concentrations was 25.65 nGy/h, with a range of 19.71-35.57 nGy/h and standard deviation of 7.63 nGy/h respectively. The mean gamma dose rate from this study is lower than the worldwide average value of 60nGy/h [UNSCEAR, 2000; Faanu, 2011]. The mean gamma dose rate from this study (25.65 nGy/h) is lower than that obtained from Indian coal-fired thermal power plants whose value is 79.19 nGy/h [Pandit, Sahu and Puranik, 2011]. It is also lower than the average annual external effective dose rate of 0.46 mSv/year [UNSCEAR, 1993; Pandit, Sahu and Puranik, 2011] from terrestrial radionuclides for areas with normal background radiation. As seen in Table 4-3, the mean annual effective dose due to natural radionuclides in the coal samples was 0.13 mSv, with

a range of 0.10-0.18 mSv and standard deviation of 0.04 mSv. This calculated mean annual effective dose (0.13 mSv) falls within the public annual effective dose limit of 1 mSv [IAEA, 2003].

### 4.3.3 SOIL

Soil samples from the study area were identified with the sample codes Soil 1 to Soil 9.

Table 4-4 shows a summary of the results associated with soil samples from the study area.

**Table 4-4: Activity concentrations, absorbed dose rates and annual effective doses due to natural radionuclides in soil from the study area**

Sample Code	Activity Concentration (Bq/kg)			Absorbed Dose Rate (nGy/h)	Annual Effective Dose (mSv)
	Th-232	U-238	K-40		
Soil 1	8.98±0.31	5.66±0.18	104.68±2.38	12.41	0.06
Soil 2	9.74±0.32	6.96±0.20	111.12±2.50	13.73	0.07
Soil 3	8.60±0.29	5.53±0.17	102.67±2.35	12.03	0.06
Soil 4	13.73±0.37	9.55±0.23	61.15±1.66	15.26	0.08
Soil 5	10.08±0.32	6.04±0.18	99.16±2.29	13.01	0.06
Soil 6	6.07±0.21	4.23±0.15	113.21±2.53	10.34	0.05
Soil 7	14.06±0.39	9.59±0.24	115.13±2.58	17.73	0.09
Soil 8	11.68±0.37	7.55±0.21	197.27±4.00	18.77	0.09
Soil 9	8.01±0.32	5.69±0.18	157.87±3.31	14.05	0.07
Min.	6.07±0.21	4.23±0.15	61.15±1.66	10.34	0.05
Max.	14.06±0.39	9.59±0.24	197.27±4.00	18.77	0.09
Mean	10.11±0.32	6.76±0.19	118.03±2.62	14.15	0.07
Std Dev.	2.64	1.85	38.65	2.71	0.01



Table 4-4 shows the activity concentrations of U-238, Th-232 and K-40 for the nine (9) soil samples from the study area, as well as the calculated annual effective doses and absorbed dose rates. The mean activity concentration values of Th-232, U-238 and K-40 for the soil samples are  $10.11 \pm 0.32$  Bq/kg,  $6.76 \pm 0.19$  Bq/kg and  $118.03 \pm 2.62$  Bq/kg with ranges of 6.07-14.06 Bq/kg, 4.23-9.59 Bq/kg and 61.15-197.27 Bq/kg respectively. Figure 4-5 is a graphical representation of the natural radionuclide activity concentration for Th-232, U-238 and K-40 in soil samples from the study area.

The mean soil activity concentrations for K-40, U-238 and Th-232 from this study are generally lower (by a factor of more than 2.5) than those from Orji River Thermal Power Station [Ademola and Onyema, 2014] in Nigeria as shown in Table 2-7. These mean soil activity concentration values from this study are also lower (by a factor slightly more than 3.5) than the worldwide average soil activity concentrations for U-238, Th-232 and K-40, which are 33 Bq/kg, 45 Bq/kg and 420 Bq/kg respectively [UNSCEAR, 2008]. The corresponding standard deviations in the activity concentrations of Th-232, U-238 and K-40 from the soil samples are 2.64 Bq/kg, 1.85 Bq/kg and 38.65 Bq/kg respectively.

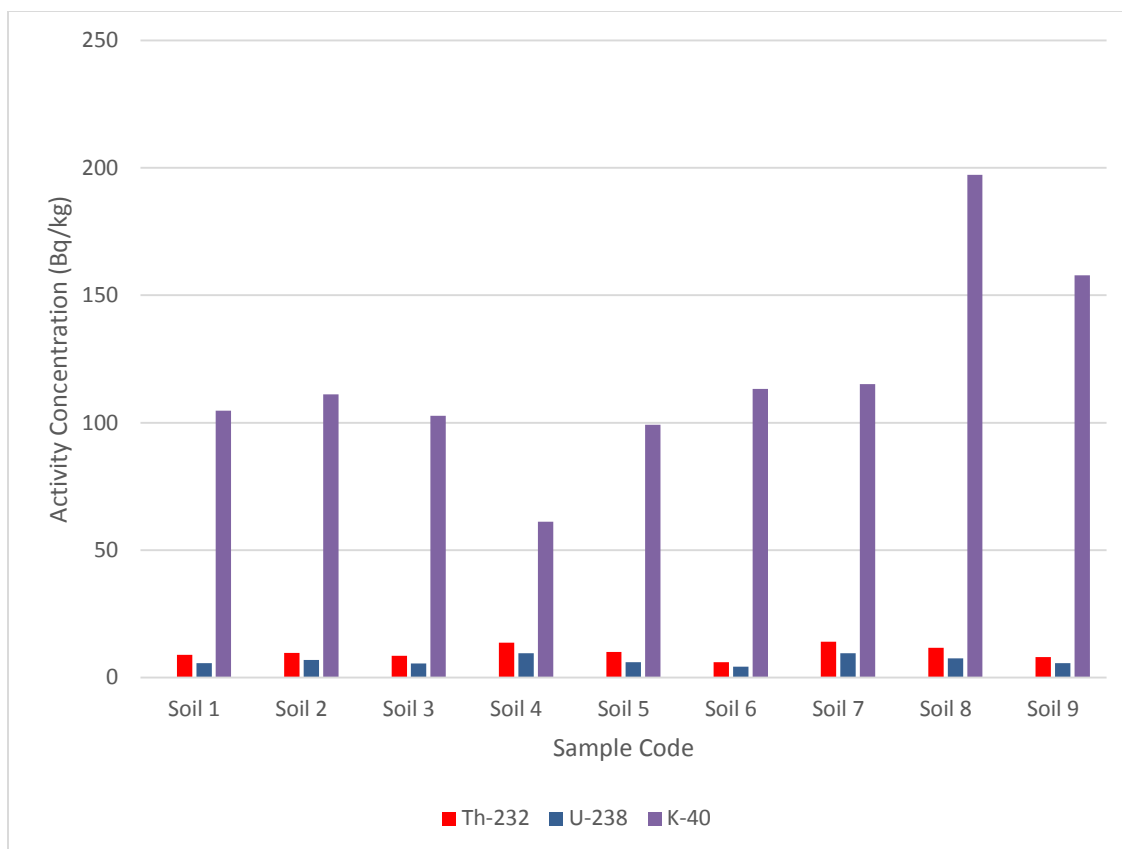


**Figure 4-5: Plot of activity concentration for natural radionuclides Th-232, U-238 and K-40 in soil samples from the study area**

As seen from Table 4-4, the mean soil gamma dose rate due to terrestrial gamma rays from Th-232, U-238 and K-40 activity concentrations was 14.15 nGy/h, with a range of 10.34-18.77 nGy/h and standard deviation of 2.71 nGy/h respectively. The mean soil gamma dose rate from this study is about four (4) times lower than the worldwide average value of 60 nGy/h [UNSCEAR, 2000; Faanu, 2011]. The mean gamma dose rate from this study (14.147 nGy/h) is lower than that obtained from Indian coal-fired thermal power plants whose value is 79.19 nGy/h [Pandit, Sahu and Puranik, 2011]. It is also lower than the average annual external effective dose rate of 0.46 mSv/year [UNSCEAR, 1993; Pandit, Sahu and Puranik, 2011] from terrestrial radionuclides for areas with normal background radiation. These differences in gamma dose rates could be attributed to variations in the

geology and geochemical states of the various sampling sites [Faanu, 2011]. As seen in Table 4-4, the mean annual effective dose due to natural radionuclides in the soil samples was 0.07 mSv, with a range of 0.05-0.09 mSv and standard deviation of 0.01 mSv. This calculated mean annual effective dose (0.07 mSv) falls within the public annual effective dose limit of 1 mSv [IAEA, 2003].

#### 4.3.4 WATER

Water samples from the fly ash ponds were identified with the sample codes Water 1 to Water 6. Table 4-5 shows a summary of the results obtained for the water samples.

**Table 4-5: Activity concentrations, absorbed dose rates and annual effective doses due to natural radionuclides in water from the fly ash ponds**

Sample Code	Activity Concentration (Bq/l)			Absorbed Dose Rate (nGy/h)	Annual Effective Dose (μSv)
	Th-232	U-238	K-40		
Water 1	0.51±0.10	0.21±0.05	0.95±0.50	0.44	2.00
Water 2	0.49±0.07	0.20±0.03	0.86±0.39	0.42	2.00
Water 3	0.66±1.27	0.21±0.06	1.21±0.49	0.55	3.00
Water 4	1.24±0.19	0.93±0.12	1.25±0.53	1.23	6.00
Water 5	0.31±0.07	0.13±0.02	0.80±0.36	0.28	1.00
Water 6	1.51±0.10	0.22±0.05	0.99±0.52	1.05	5.00
Min.	0.31±0.07	0.13±0.02	0.80±0.36	0.28	1.00
Max.	1.51±0.10	0.93±0.12	1.25±0.53	1.23	6.00
Mean	0.79±0.30	0.32±0.06	1.01±0.46	0.66	3.00
Std Dev.	0.48	0.30	0.19	0.39	2.00

Table 4-5 shows the activity concentrations of U-238, Th-232 and K-40 for the six (6) water samples from the fly ash ponds, as well as the calculated annual effective doses and absorbed dose rates. The mean activity concentration values of Th-232, U-238 and K-40 for the water samples are  $0.79 \pm 0.30$  Bq/l,  $0.32 \pm 0.06$  Bq/l and  $1.01 \pm 0.46$  Bq/l with ranges of 0.31-1.51 Bq/l, 0.13-0.93 Bq/l and 0.80-1.25 Bq/l respectively. Figure 4-6 is a graphical representation of the natural radionuclide activity concentration for Th-232, U-238 and K-40 in water samples from the study area.

The mean water activity concentrations from this study are much lower than the worldwide average activity concentrations for U-238, Th-232 and K-40, which are 33 Bq/kg, 45 Bq/kg and 420 Bq/kg respectively [UNSCEAR, 2008]. The corresponding standard deviations in the activity concentrations of Th-232, U-238 and K-40 from the water samples are 0.48 Bq/l, 0.30 Bq/l and 0.19 Bq/l respectively.

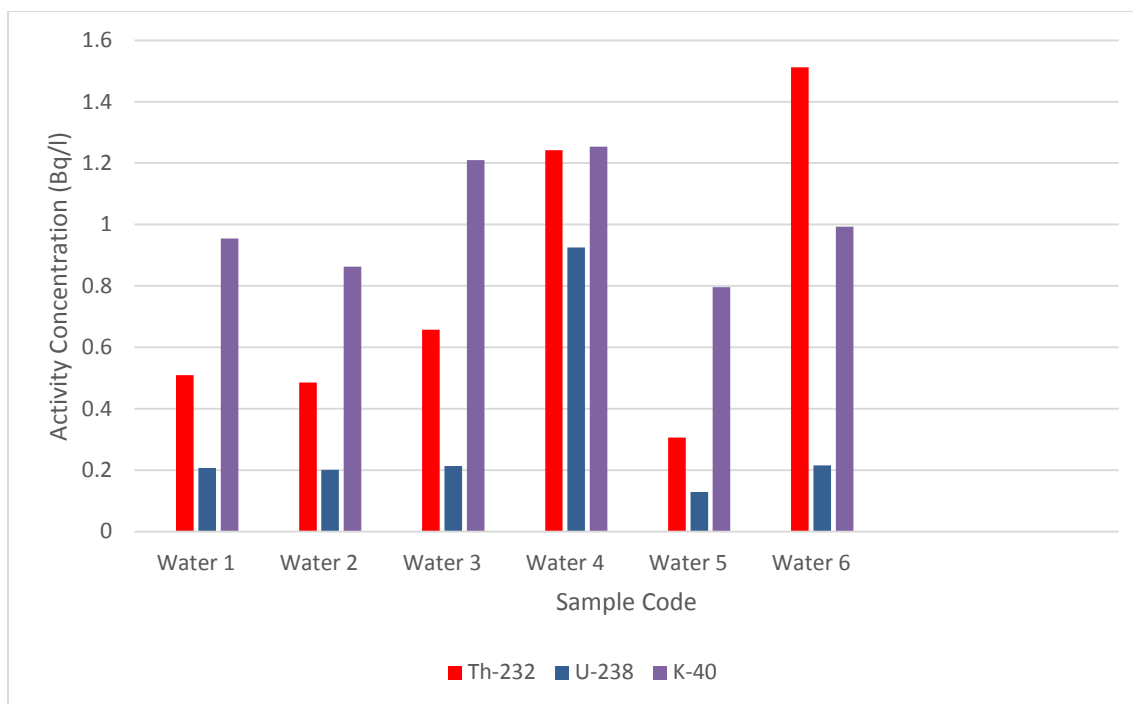


**Figure 4-6: Plot of activity concentration for natural radionuclides Th-232, U-238 and K-40 in water samples from the fly ash ponds**

As seen from Table 4-5, the mean gamma dose rate due to terrestrial gamma rays from Th-232, U-238 and K-40 activity concentrations was 0.66 nGy/h, with a range of 0.28-1.23 nGy/h and standard deviation of 0.39 nGy/h respectively. The mean gamma dose rate from this study is much lower than the worldwide average value of 60 nGy/h [UNSCEAR, 2000; Faanu, 2011]. It is also lower than the average annual external effective dose rate of 0.46 mSv/year [UNSCEAR, 1993; Pandit, Sahu and Puranik, 2011] from terrestrial radionuclides for areas with normal background radiation. The low average annual effective dose rate resulting from the water and fly ash mixture in the fly ash ponds could be attributed to variations in radionuclide concentrations per unit volume of water that is present in the fly ash pond at a particular time, depending on how dilute the fly ash slurry is [UNSCEAR, 2000]. As seen in Table 4-5, the mean annual effective dose value due to

natural radionuclides in the water samples was 3.00  $\mu\text{Sv}$ , with a range of 1.00-6.00  $\mu\text{Sv}$  and standard deviation of 2.00  $\mu\text{Sv}$ . This calculated mean annual effective dose (3.00  $\mu\text{Sv}$ ) falls within the public annual effective dose limit of 1 mSv [IAEA, 2003].

#### **4.4 COMPARISON OF ACTIVITY CONCENTRATION, GAMMA DOSE RATE AND ANNUAL EFFECTIVE DOSE TO SAMPLE TYPE**

Figures 4-7 to 4-9 below are graphical comparisons of the activity concentrations, dose rates and annual effective doses due to natural radionuclides in the samples from Sections 4.2.1 to 4.2.4 above. Figure 4-7 shows that the fly ash natural radionuclide content is greater than that of coal by a factor [UNSCEAR, 1982] greater than 2.3. This could be attributed to the fact that when coal is combusted, most of the non-combustible material, which includes the natural radionuclides, remains and concentrates in the fly ash [Penfold et al., 1998]. The non-uniform average K-40 activity concentrations, which is evidently clear for soil samples in Figure 4-7, could be attributed to variations in the geology and geochemical states of the various sampling sites [Faanu, 2011]. Figure 4-8 shows that contributions of samples to the gamma dose rates of the study area in ascending order for water, soil, coal and fly ash are 0.66 nGy/h, 14.15 nGy/h, 25.65 nGy/h and 65.27 nGy/h respectively. The same ascending order is maintained for contributions of samples to the annual effective dose due to the proportional relation for calculation of annual effective dose (Equation 3.7b) as shown in Figure 4-9.

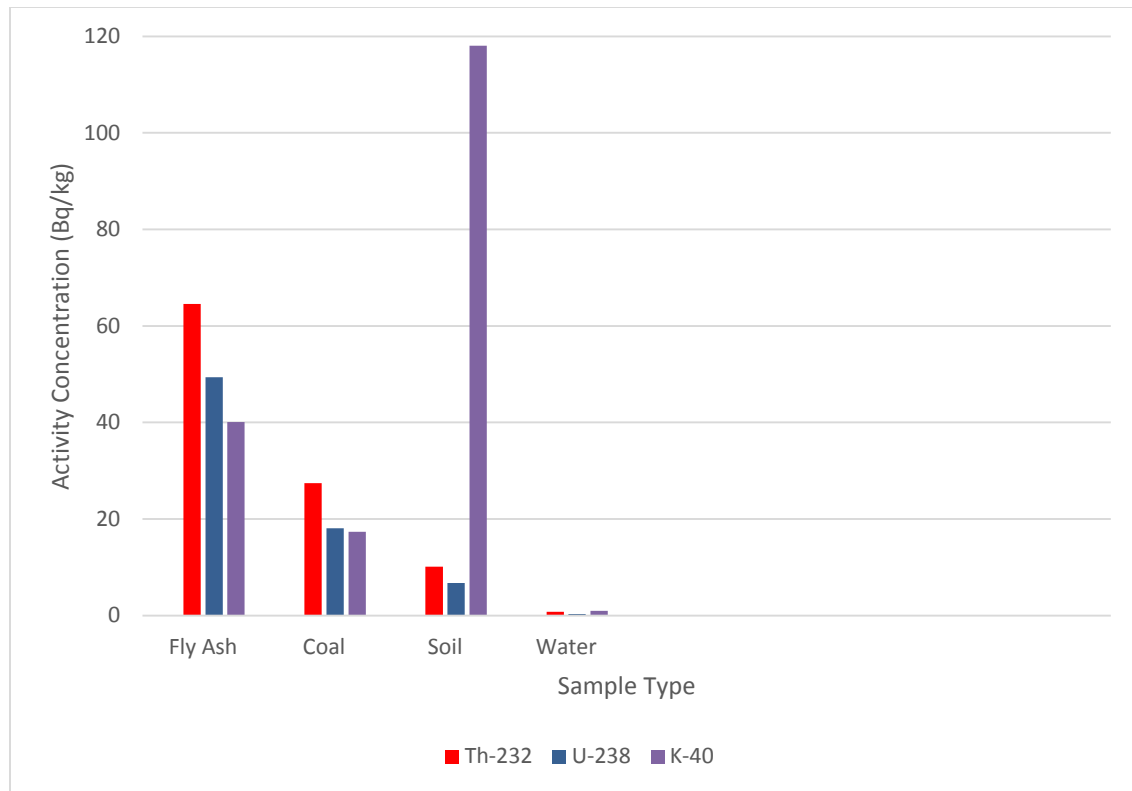


**Figure 4-7: Activity concentration comparison for samples in the study area**

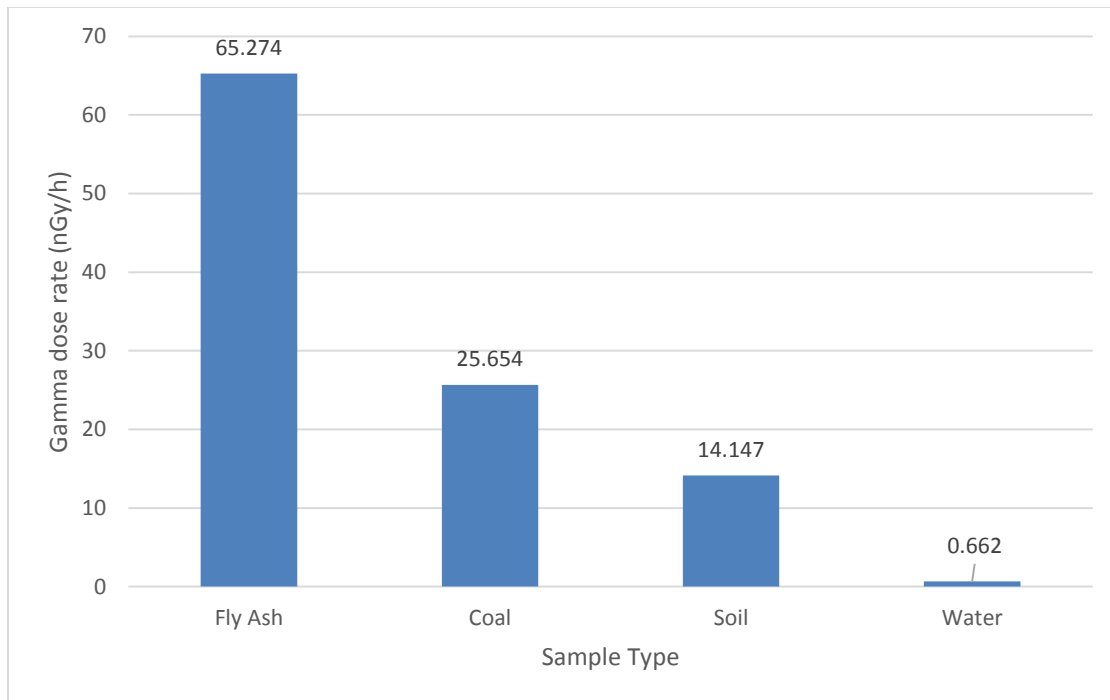


**Figure 4-8: Gamma dose rates comparison for samples in the study area**

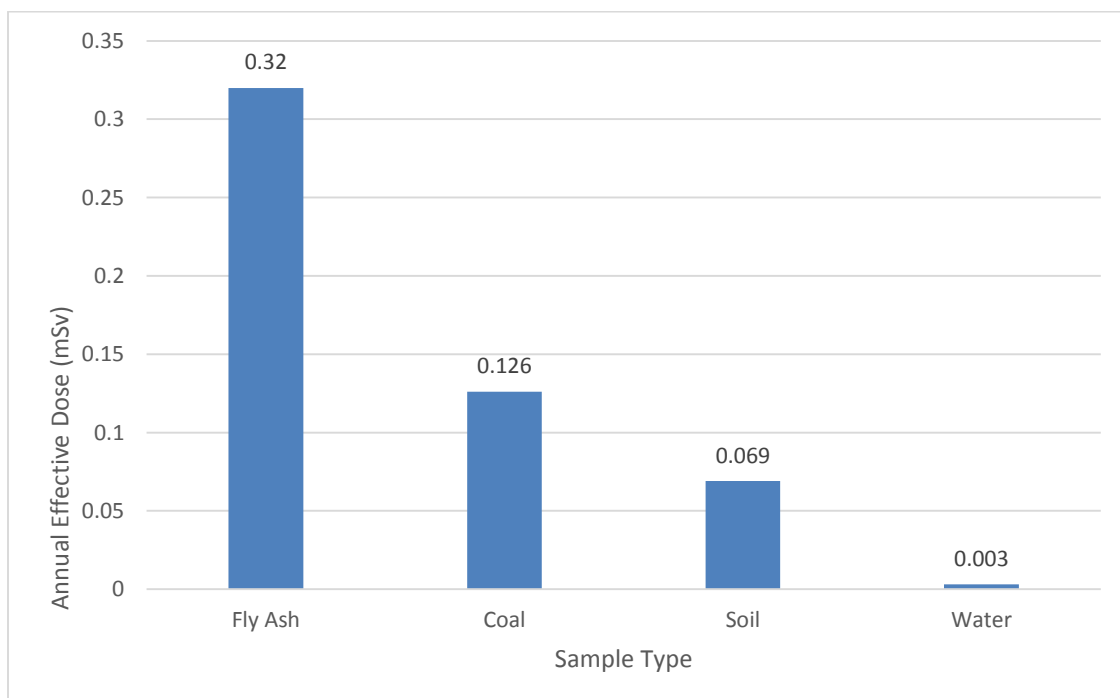


**Figure 4-9: Annual effective dose comparison for samples in the study area**



#### 4.5 RADIUM EQUIVALENT ACTIVITY, REPRESENTATIVE LEVEL INDEX, EXTERNAL AND INTERNAL HAZARD INDICES

Tables 4-6 to 4-9 clearly outline the dose rate, annual effective dose, representative level index ( $I_{\gamma r}$ ), radium equivalent activity ( $Ra_{eq}$ ), external hazard index ( $H_{ext}$ ) and internal hazard index ( $H_{int}$ ) associated with natural radionuclides in fly ash, coal, soil and water (from the fly ash ponds) samples respectively. It is important to assess the gamma radiation hazards on humans associated with the use of any of the above samples as building material by calculating the values of  $I_{\gamma r}$ ,  $Ra_{eq}$ ,  $H_{ext}$  and  $H_{int}$  for all samples in the study as shown in Tables 4-6 to 4-9 [Harb et al., 2008]. For example, fly ash is used in making cement or as a lightweight filler for concrete [Penfold et al., 1998]. The radium equivalent activity ( $Ra_{eq}$ ), external hazard index ( $H_{ext}$ ), internal hazard index ( $H_{int}$ ) and representative level index ( $I_{\gamma r}$ ) were computed by means of Equations 3.8, 3.9, 3.10 and 3.11 respectively.

As seen in Table 4-6, the average  $Ra_{eq}$ ,  $I_{\gamma r}$ ,  $H_{int}$  and  $H_{ext}$  values for fly ash samples are 149.038 Bq/kg, 1.031, 0.536 and 0.403 with ranges of 124.757-163.377 Bq/kg, 0.864-1.130, 0.445-0.588 and 0.337-0.441 respectively. From Table 4-7, the average  $Ra_{eq}$ ,  $I_{\gamma r}$ ,  $H_{int}$  and  $H_{ext}$  values for coal samples are 58.662 Bq/kg, 0.407, 0.207 and 0.158 with ranges of 45.075-85.974 Bq/kg, 0.312-0.596, 0.160-0.301 and 0.122-0.232 respectively. As per Table 4-8, the average  $Ra_{eq}$ ,  $I_{\gamma r}$ ,  $H_{int}$  and  $H_{ext}$  values for soil samples are 30.296 Bq/kg, 0.225, 0.100 and 0.082 with ranges of 21.628-39.451 Bq/kg, 0.164-0.299, 0.070-0.130 and 0.058-0.107 respectively. In Table 4-9, the average  $Ra_{eq}$ ,  $I_{\gamma r}$ ,  $H_{int}$  and  $H_{ext}$  values for water samples are 1.516 Bq/kg, 0.011, 0.005 and 0.004 with ranges of 0.628-2.798 Bq/kg, 0.004-0.019, 0.002-0.010 and 0.002-0.008 respectively.

The calculated values for  $R_{eq}$ ,  $I_{\gamma r}$ ,  $H_{int}$  and  $H_{ext}$  in this study are generally highest for fly ash, followed by coal, soil and water samples in descending order as shown in Figure 4-10. These relatively high fly ash values of  $R_{eq}$ ,  $I_{\gamma r}$ ,  $H_{int}$  and  $H_{ext}$  could be attributed to the fact that when coal is combusted, most of the non-combustible material, which includes the natural radionuclides, remains and concentrates in the fly ash thereby enhancing the  $R_{eq}$ ,  $I_{\gamma r}$ ,  $H_{int}$  and  $H_{ext}$  values [Penfold et al., 1998]. The average  $R_{eq}$  values for all the fly ash, coal, soil and water samples are below the internationally accepted value of 370 Bq/kg as seen in Tables 4-6 to 4-9. The average values of  $H_{ext}$  and  $H_{int}$  for all the fly ash, coal, soil and water samples are also below the internationally accepted value of unity [Ademola and Onyema, 2014]. The average values of  $I_{\gamma r}$  for all coal, soil and water samples are also below the internationally accepted value of unity [Harb et al., 2008]. The average value of  $I_{\gamma r}$  for the fly ash samples is approximately equal to the internationally accepted value of unity, with a calculated actual average value of 1.031 and a standard deviation of 0.088. All the calculated annual effective dose averages for all the fly ash, coal, soil and water samples are less than the acceptable value of 1.5 mSv/year [UNSCEAR, 2000; Xinwei et al., 2006] as seen in Tables 4-6 to 4-9. Based on these results, it is therefore safe to use these materials under study for construction purposes.

**Table 4-6: Dose rate, annual effective dose, representative level index ( $I_{yr}$ ), radium equivalent activity ( $Ra_{eq}$ ), external hazard index ( $H_{ext}$ ) and internal hazard index ( $H_{int}$ ) for fly ash samples**

Sample Code	Absorbed Dose Rate (nGy/h)	$Ra_{eq}$ (Bq/kg)	$I_{yr}$	$H_{int}$	$H_{ext}$	Annual Effective Dose (mSv)
ASH 1	70.24	160.41	1.11	0.58	0.43	0.35
ASH 2	71.55	163.38	1.13	0.59	0.44	0.35
ASH 3	69.24	158.09	1.09	0.57	0.43	0.34
ASH 4	63.79	145.65	1.01	0.52	0.39	0.31
ASH 5	66.52	151.86	1.05	0.55	0.41	0.33
ASH 6	65.40	149.27	1.03	0.54	0.40	0.32
ASH 7	54.59	124.76	0.86	0.45	0.34	0.27
ASH 8	60.87	138.89	0.96	0.50	0.38	0.30
Min.	54.59	124.76	0.86	0.45	0.34	0.27
Max.	71.55	163.38	1.13	0.59	0.44	0.35
Mean	65.27	149.04	1.03	0.54	0.40	0.32
Std Dev.	5.57	12.70	0.09	0.05	0.03	0.03

**Table 4-7: Dose rate, annual effective dose, representative level index ( $I_{yr}$ ), radium equivalent activity ( $Ra_{eq}$ ), external hazard index ( $H_{ext}$ ) and internal hazard index ( $H_{int}$ ) for coal samples**

Sample Code	Absorbed Dose Rate (nGy/h)	$Ra_{eq}$ (Bq/kg)	$I_{yr}$	$H_{int}$	$H_{ext}$	Annual Effective Dose (mSv)
Coal 1	21.61	49.43	0.34	0.18	0.13	0.11
Coal 2	22.76	52.00	0.36	0.19	0.14	0.11
Coal 3	37.57	85.97	0.60	0.30	0.23	0.18
Coal 4	35.85	82.05	0.57	0.29	0.22	0.18
Coal 5	20.61	47.07	0.33	0.17	0.13	0.10
Coal 6	21.48	49.04	0.34	0.18	0.13	0.11
Coal 7	19.71	45.08	0.31	0.16	0.12	0.10
Min.	19.71	45.08	0.31	0.16	0.12	0.10
Max.	37.57	85.97	0.60	0.30	0.23	0.18
Mean	25.65	58.66	0.41	0.21	0.16	0.13
Std Dev.	7.63	17.49	0.12	0.06	0.05	0.04

**Table 4-8: Dose rate, annual effective dose, representative level index ( $I_{yr}$ ), radium equivalent activity ( $Ra_{eq}$ ), external hazard index ( $H_{ext}$ ) and internal hazard index ( $H_{int}$ ) for soil samples**

Sample Code	Absorbed Dose Rate (nGy/h)	$Ra_{eq}$ (Bq/kg)	$I_{yr}$	$H_{int}$	$H_{ext}$	Annual Effective Dose (mSv)
Soil 1	12.41	26.57	0.20	0.09	0.07	0.06
Soil 2	13.73	29.45	0.22	0.10	0.08	0.07
Soil 3	12.03	25.73	0.19	0.08	0.07	0.06
Soil 4	15.26	33.90	0.24	0.12	0.09	0.08
Soil 5	13.01	28.09	0.21	0.09	0.08	0.06
Soil 6	10.34	21.63	0.16	0.07	0.06	0.05
Soil 7	17.73	38.56	0.28	0.13	0.10	0.09
Soil 8	18.77	39.45	0.30	0.13	0.11	0.09
Soil 9	14.05	29.29	0.22	0.09	0.08	0.07
Min.	10.34	21.63	0.16	0.07	0.06	0.05
Max.	18.77	39.45	0.30	0.13	0.11	0.09
Mean	14.15	30.30	0.23	0.10	0.08	0.07
Std Dev.	2.71	5.93	0.04	0.02	0.02	0.01

**Table 4-9: Dose rate, annual effective dose, representative level index ( $I_{yr}$ ), radium equivalent activity ( $Ra_{eq}$ ), external hazard index ( $H_{ext}$ ) and internal hazard index ( $H_{int}$ ) for water samples from the fly ash ponds**

Sample Code	Absorbed Dose Rate (nGy/h)	$Ra_{eq}$ (Bq/kg)	$I_{yr}$	$H_{int}$	$H_{ext}$	Annual Effective Dose (mSv)
Water 1	0.443	1.008	0.007	0.003	0.003	0.002
Water 2	0.422	0.962	0.007	0.003	0.003	0.002
Water 3	0.546	1.247	0.009	0.004	0.003	0.003
Water 4	1.230	2.798	0.019	0.010	0.008	0.006
Water 5	0.278	0.628	0.004	0.002	0.002	0.001
Water 6	1.054	2.455	0.017	0.007	0.007	0.005
Min.	0.278	0.628	0.004	0.002	0.002	0.001
Max.	1.230	2.798	0.019	0.010	0.008	0.006
Mean	0.662	1.516	0.011	0.005	0.004	0.003
Std Dev.	0.385	0.889	0.006	0.003	0.002	0.002

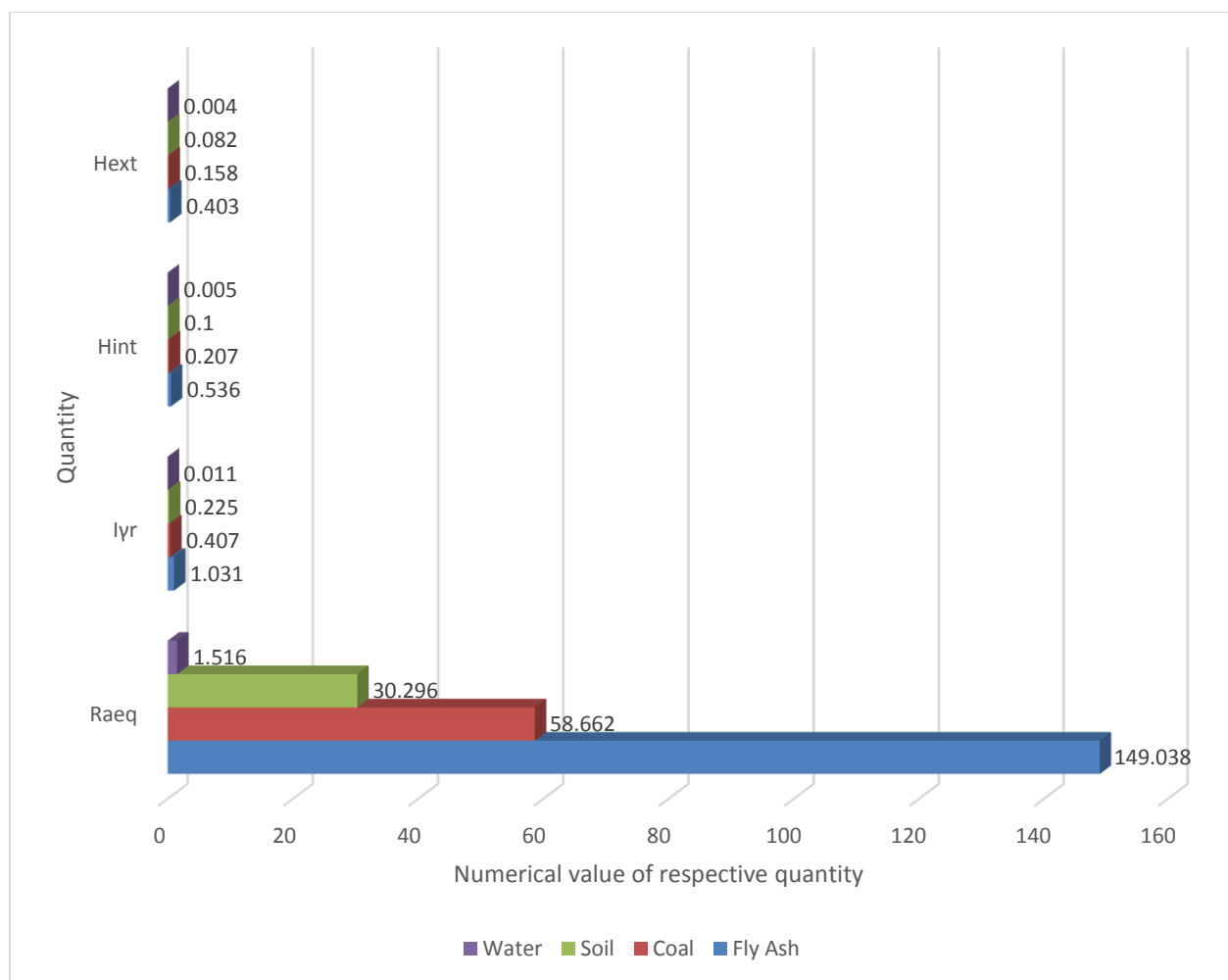


**Figure 4-10: Comparison of hazard indices and radium equivalent values for all samples**

#### 4.6 RECONSTRUCTED DOSES FROM THE STUDY AREA

Annual effective doses were reconstructed for all samples from the study area. Tables 4-10 to 4-13 shows the reconstructed annual effective doses due to fly ash, coal, soil and water (from the fly ash ponds) samples respectively. The graphical representation showing actual reconstructed annual effective doses for fly ash, coal, soil and water samples are shown in Figures 4-11, 4-12, 4-13 and 4-14 respectively.

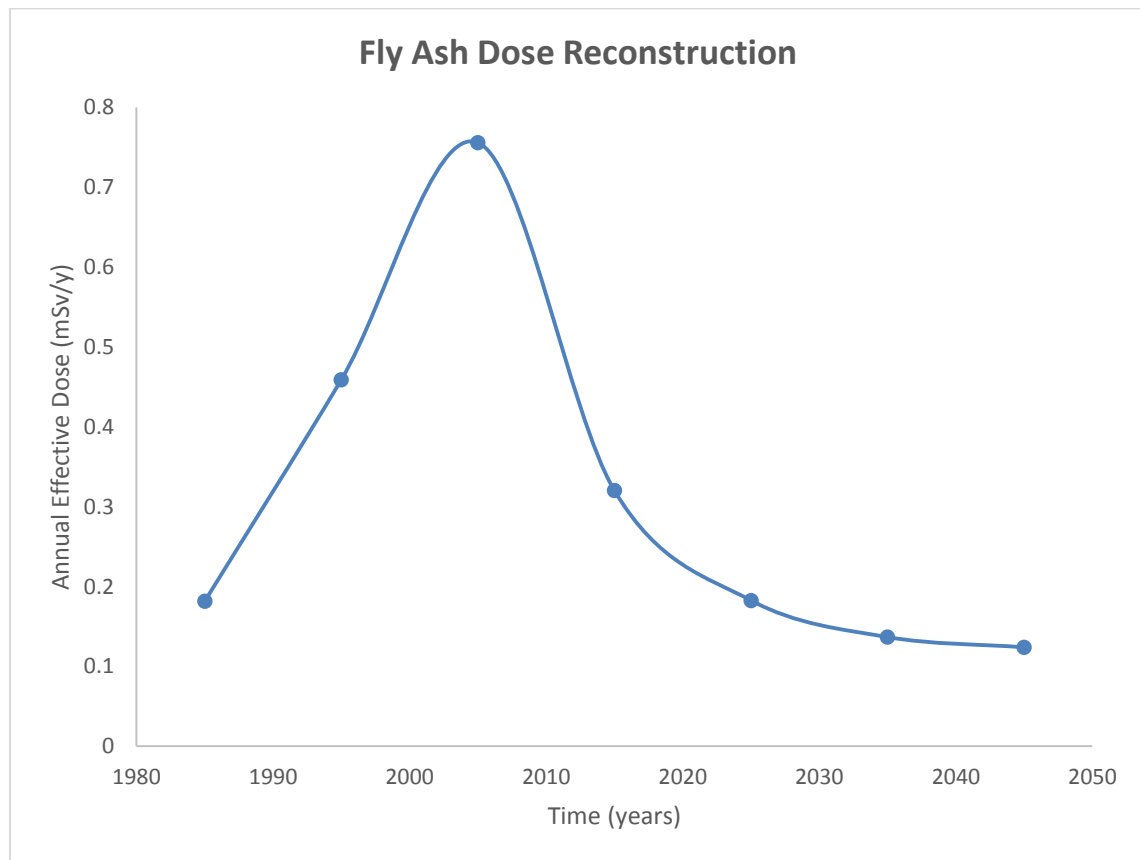


**Figure 4-11: Actual reconstructed annual effective dose for fly ash storage area**



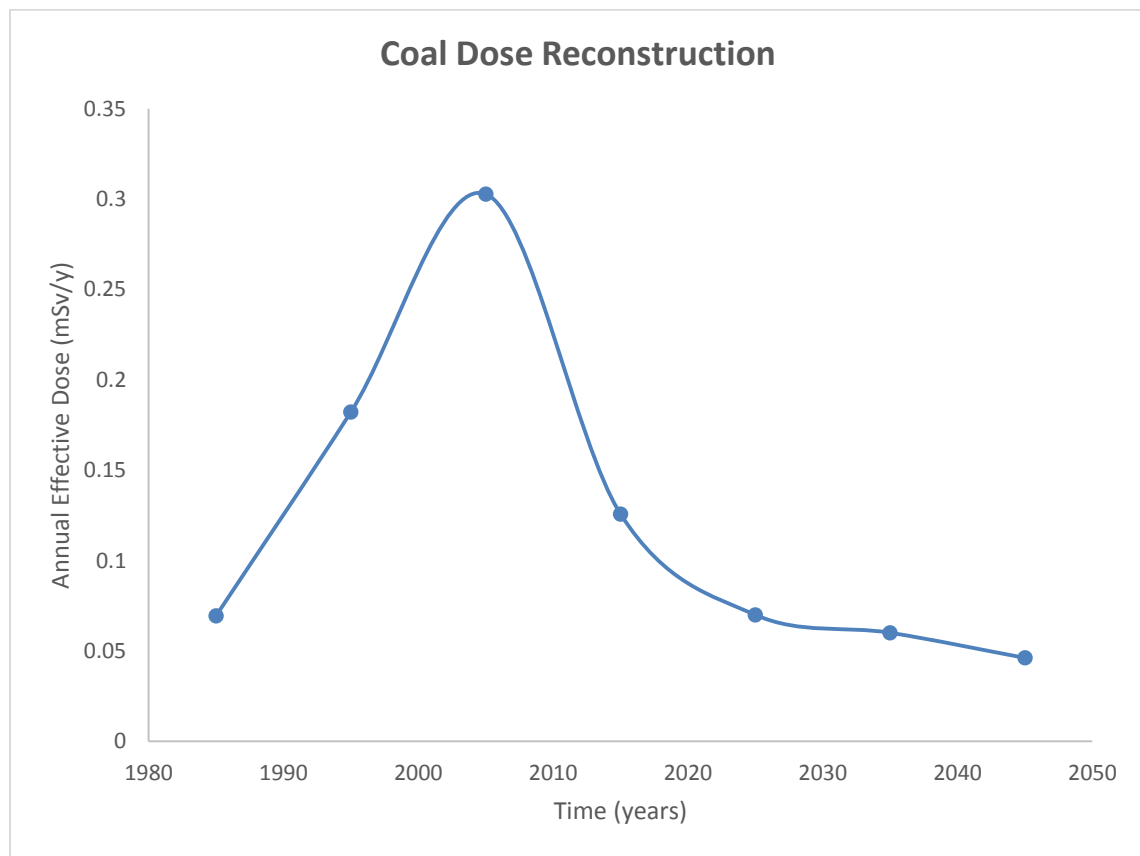


**Figure 4-12: Actual reconstructed annual effective dose for coal storage area**

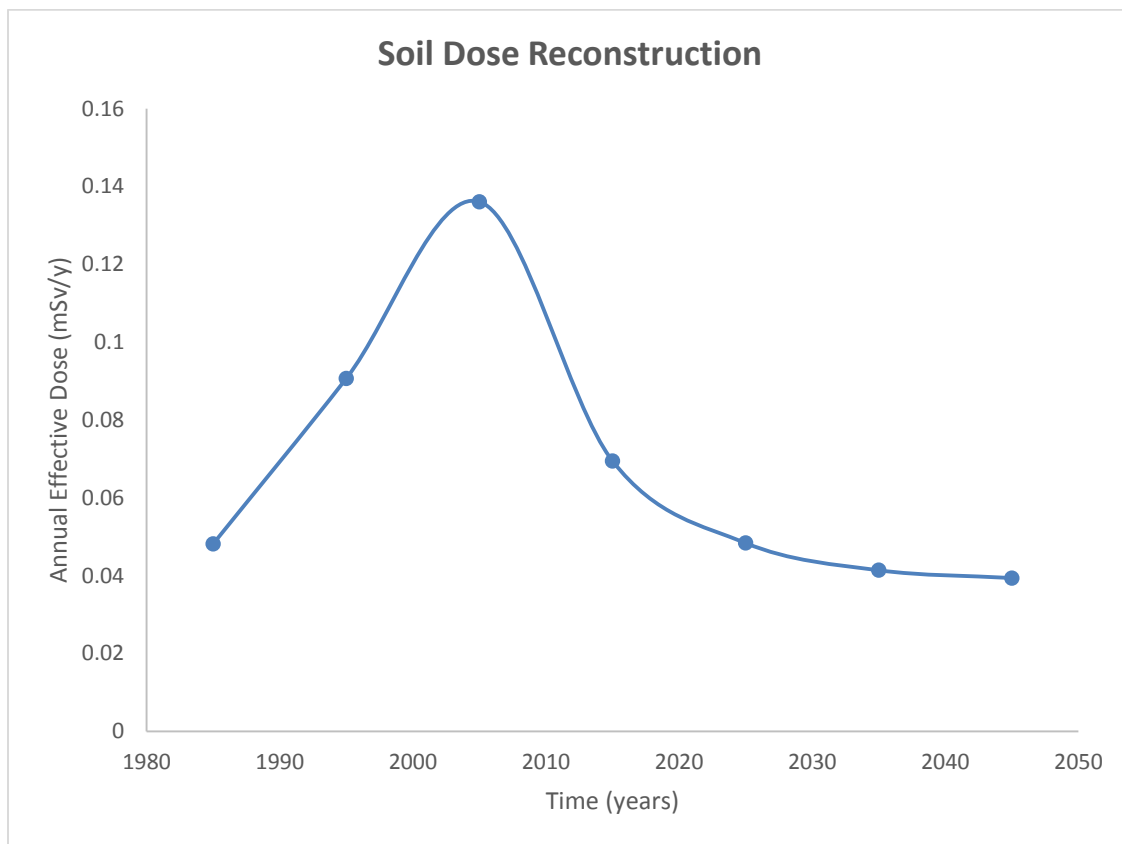


**Figure 4-13: Actual reconstructed annual effective dose for soil**

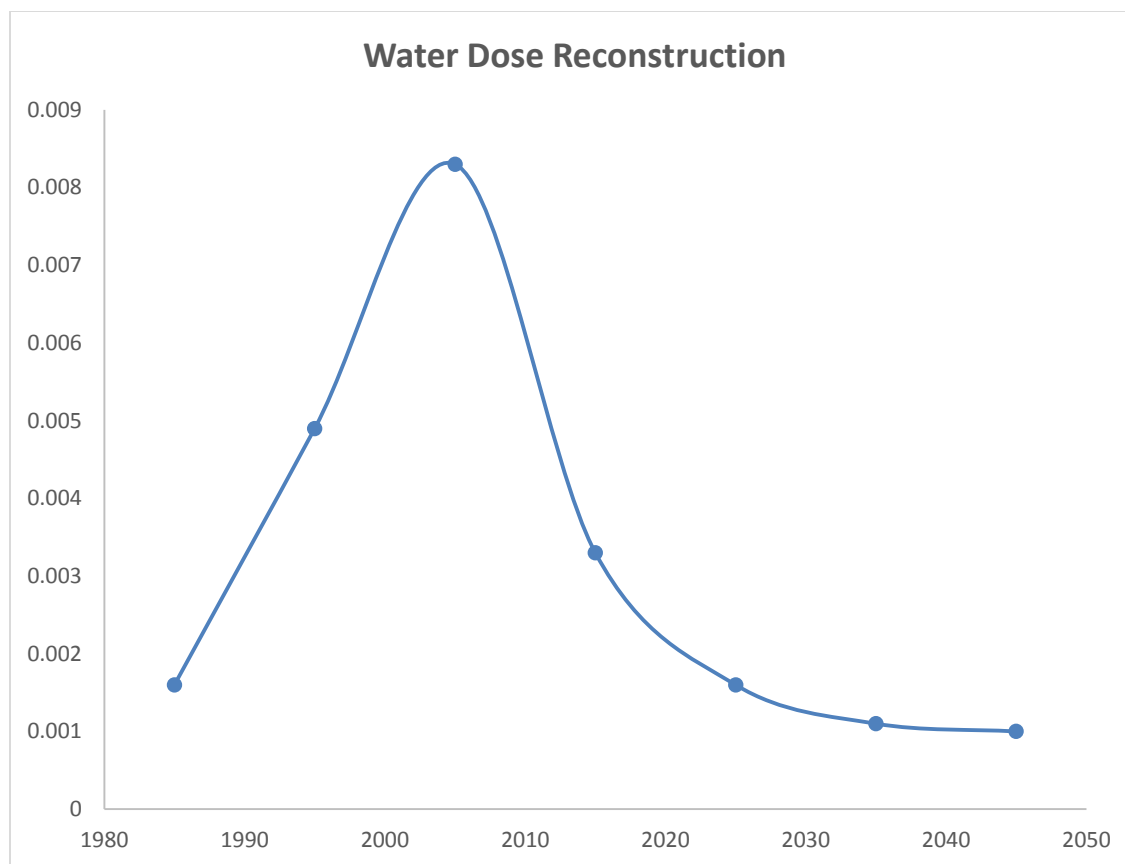


**Figure 4-14: Actual reconstructed annual effective dose for water**

Figures 4-15, 4-16, 4-17 and 4-18 show the dose reconstruction model graphs that represent the results from Tables 4-10, 4-11, 4-12 and 4-13 respectively. The mean annual effective doses from Tables 4-10 to 4-13 were used as inputs for these dose reconstruction models.

**Table 4-10: Reconstructed annual effective doses for fly ash samples**

RECONSTRUCTED ANNUAL EFFECTIVE DOSES FOR FLY ASH STORAGE AREA (mSv/y)							
	1985	1995	2005	2015	2025	2035	2045
ASH-1	0.1947	0.4946	0.8156	0.3445	0.1958	0.1462	0.1323
ASH-2	0.1993	0.5030	0.8279	0.3510	0.2005	0.1502	0.1361
ASH-3	0.1926	0.4869	0.8019	0.3397	0.1937	0.1450	0.1314
ASH-4	0.1772	0.4488	0.7395	0.3129	0.1783	0.1333	0.1208
ASH-5	0.1856	0.4673	0.7687	0.3263	0.1867	0.1401	0.1270
ASH-6	0.1827	0.4592	0.7551	0.3208	0.1837	0.1380	0.1252
ASH-7	0.1497	0.3860	0.6388	0.2678	0.1507	0.1116	0.1007
ASH-8	0.1707	0.4268	0.7008	0.2986	0.1716	0.1292	0.1174
Min.	0.1497	0.3860	0.6388	0.2678	0.1507	0.1116	0.1007
Max.	0.1993	0.5030	0.8279	0.3510	0.2005	0.1502	0.1361
Mean	0.1817	0.4591	0.7561	0.3202	0.1826	0.1367	0.1239
Std Dev.	0.0159	0.0388	0.0633	0.0273	0.0160	0.0122	0.0112

**Table 4-11: Reconstructed annual effective doses for coal samples**

RECONSTRUCTED ANNUAL EFFECTIVE DOSES FOR COAL STORAGE AREA (mSv/y)							
	1985	1995	2005	2015	2025	2035	2045
Coal 1	0.0585	0.1535	0.2550	0.1060	0.0589	0.0432	0.0389
Coal 2	0.0623	0.1610	0.2667	0.1116	0.0627	0.0464	0.0418
Coal 3	0.1004	0.2681	0.4476	0.1843	0.1012	0.1344	0.0657
Coal 4	0.0959	0.2558	0.4269	0.1759	0.0967	0.0702	0.0629
Coal 5	0.0565	0.1457	0.2410	0.1010	0.0569	0.0422	0.0381
Coal 6	0.0592	0.1516	0.2505	0.1054	0.0596	0.0443	0.0400
Coal 7	0.0536	0.1398	0.2320	0.0967	0.0540	0.0398	0.0358
Min.	0.0536	0.1398	0.2320	0.0967	0.0540	0.0398	0.0358
Max.	0.1004	0.2681	0.4476	0.1843	0.1012	0.1344	0.0657
Mean	0.0695	0.1822	0.3028	0.1258	0.0700	0.0601	0.0462
Std Dev.	0.0198	0.0550	0.0927	0.0374	0.0200	0.0343	0.0125

**Table 4-12: Reconstructed annual effective doses for soil samples**

RECONSTRUCTED ANNUAL EFFECTIVE DOSES FOR SOIL IN AND AROUND MORUPULE A COAL-FIRED POWER STATION (mSv/y)							
	1985	1995	2005	2015	2025	2035	2045
Soil 1	0.0424	0.0793	0.1188	0.0609	0.0426	0.0365	0.0348
Soil 2	0.0474	0.0874	0.1302	0.0674	0.0475	0.0409	0.0391
Soil 3	0.0413	0.0767	0.1145	0.0590	0.0415	0.0357	0.0340
Soil 4	0.0466	0.1031	0.1634	0.0748	0.0469	0.0375	0.0349
Soil 5	0.0431	0.0845	0.1288	0.0638	0.0433	0.0365	0.0346
Soil 6	0.0383	0.0632	0.0899	0.0507	0.0384	0.0342	0.0331
Soil 7	0.0581	0.1158	0.1777	0.0870	0.0583	0.0488	0.0461
Soil 8	0.0681	0.1161	0.1674	0.0921	0.0683	0.0604	0.0582
Soil 9	0.0486	0.0902	0.1346	0.0694	0.0488	0.0420	0.0400
Min.	0.0383	0.0632	0.0899	0.0507	0.0384	0.0342	0.0331
Max.	0.0681	0.1161	0.1777	0.0921	0.0683	0.0604	0.0582
Mean	0.0482	0.0907	0.1361	0.0695	0.0484	0.0413	0.0394
Std Dev.	0.0094	0.0179	0.028	0.0133	0.0094	0.0084	0.0082

**Table 4-13: Reconstructed annual effective doses for water samples**

RECONSTRUCTED ANNUAL EFFECTIVE DOSES FOR WATER SAMPLES FROM THE ASH PONDS (mSv/y)							
	1985	1995	2005	2015	2025	2035	2045
Water 1	0.0011	0.0032	0.0055	0.0022	0.0011	0.0008	0.0007
Water 2	0.0011	0.0031	0.0052	0.0021	0.0011	0.0008	0.0007
Water 3	0.0013	0.0040	0.0069	0.0027	0.0013	0.0009	0.0008
Water 4	0.0035	0.0086	0.0140	0.0060	0.0035	0.0027	0.0024
Water 5	0.0007	0.0020	0.0033	0.0014	0.0007	0.0005	0.0005
Water 6	0.0020	0.0083	0.0149	0.0052	0.0021	0.0011	0.0008
Min.	0.0007	0.0020	0.0033	0.0014	0.0007	0.0005	0.0005
Max.	0.0035	0.0086	0.0149	0.0060	0.0035	0.0027	0.0024
Mean	0.0016	0.0049	0.0083	0.0033	0.0016	0.0011	0.0010
Std Dev.	0.0010	0.0028	0.0049	0.0019	0.0010	0.0008	0.0007

#### 4.7 ANNUAL EFFECTIVE DOSE MODEL OF THE FLY ASH STORAGE AREA

The sixty (60) year interpolative and extrapolative annual effective dose model for the fly ash storage area is presented in Figure 4-15 and represented by the 4<sup>th</sup> order polynomial:

$$Y = -0.032z^4 + 0.23z^3 - 0.076z^2 - 0.46z + 0.42$$

The model is standardized by the z-score given below, which determines the number of standard deviations the x-axis value (time in years) is from the mean [Larsen and Marx, 2000]:

$$z = (x - 2000) / 22$$

Where, z is the z-score, 2000 is the average year, 22 is the standard deviation and x is the predictor data or year of interest. The model utilizes the least squares method which connects data points by means of a best fit line [Hastie, Tibshirani and Friedman, 2009].

This model is a reasonable predictor of the annual effective dose for the time range  $1985 \leq x \leq 2045$ . This model predicts a low mean annual effective dose of 0.1817 mSv/year which serves as the average baseline (reference) annual background radiation for 1985/86. This may be attributed to the fact that Morupule A Coal-Fired Power Station began operating in 1986 [UNSCEAR, 2008].

The average annual effective dose then gradually rose to a maximum value of 0.7561 mSv/y in 2005. This may be attributed to an increase in the activity of the coal-fired power station which led to an increase in fly ash production [Organo and Fenton, 2008]. The model further predicts a decrease in the average annual effective dose to a value of 0.1239 mSv/year in 2045. This decrease may be attributed to exponential decay according to the Radioactive Decay Law [Benedict, 2012]. The mean annual effective doses estimated by



the model are much lower than the public annual effective dose limit of 1 mSv [IAEA, 2003].

#### **4.8 ANNUAL EFFECTIVE DOSE MODEL OF THE COAL STORAGE AREA**

The eighty (80) year interpolative and extrapolative annual effective dose model for the coal storage area is presented in Figure 4-16 and represented by the 4<sup>th</sup> order polynomial:

$$Y = -0.018z^4 + 0.093z^3 - 0.02z^2 - 0.18z + 0.16$$

The model is standardized by the z-score given below, which determines the number of standard deviations the x-axis value (time in years) is from the mean [Larsen and Marx, 2000]:

$$z = (x - 2000) / 22$$

Where, z is the z-score, 2000 is the average year, 22 is the standard deviation and x is the predictor data or year of interest. The model utilizes the least squares method which connects data points by means of a best fit line [Hastie, Tibshirani and Friedman, 2009]. This model is a reasonable predictor of the annual effective dose for the time range  $1985 \leq x \leq 2065$ . This model predicts a low mean annual effective dose of 0.0695 mSv/year which serves as the average baseline (reference) annual background radiation for 1985/86. This may be attributed to the fact that Morupule A Coal-Fired Power Station began operating in 1986 [UNSCEAR, 2008].

The average annual effective dose then gradually rose to a maximum value of 0.3028 mSv/y in 2005. This may be attributed to an increase in the activity of the coal-fired power station which led to an increased accumulation of raw coal fuel in the coal storage area [Organo and Fenton, 2008]. The model further predicts a decrease in the average annual

effective dose to a value of 0.0269 mSv/year in 2069. This decrease may be attributed to exponential decay according to the Radioactive Decay Law [Benedict, 2012]. The mean annual effective doses estimated by the model are much lower than the public annual effective dose limit of 1 mSv [IAEA, 2003].

#### **4.9 ANNUAL EFFECTIVE DOSE MODEL FOR SOIL SAMPLES FROM THE STUDY AREA**

The sixty (60) year interpolative and extrapolative annual effective dose model for soil from the study area is presented in Figure 4-17 and represented by the 4<sup>th</sup> order polynomial:

$$Y = -0.005z^4 + 0.036z^3 - 0.012z^2 - 0.07z + 0.084$$

The model is standardized by the z-score given below, which determines the number of standard deviations the x-axis value (time in years) is from the mean [Larsen and Marx, 2000]:

$$z = (x - 2000) / 22$$

Where, z is the z-score, 2000 is the average year, 22 is the standard deviation and x is the predictor data or year of interest. The model utilizes the least squares method which connects data points by means of a best fit line [Hastie, Tibshirani and Friedman, 2009].

This model is a reasonable predictor of the annual effective dose for the time range  $1985 \leq x \leq 2045$ . This model predicts a low mean annual effective dose of 0.0482 mSv/year which serves as the average baseline (reference) annual background radiation for 1985/86. This may be attributed to the fact that Morupule A Coal-Fired Power Station began operating in 1986 [UNSCEAR, 2008].

The average annual effective dose then gradually rose to a maximum value of 0.1361 mSv/y in 2005. This may be due to an increased amount radionuclides in the chimney gases reaching the ground by either wet or dry deposition [Szefer and Nriagu, 2006]. The model further predicts a decrease in the average annual effective dose to a value of 0.0394 mSv/year in 2045. This decrease may be attributed to exponential decay according to the Radioactive Decay Law [Benedict, 2012]. The mean annual effective doses estimated by the model are much lower than the public annual effective dose limit of 1 mSv [IAEA, 2003].

#### **4.10 ANNUAL EFFECTIVE DOSE MODEL FOR WATER SAMPLES FROM THE FLY ASH PONDS**

The sixty five (65) year interpolative and extrapolative annual effective dose model for water from the ash ponds is presented in Figure 4-18 and represented by the 4<sup>th</sup> order polynomial:

$$Y = -0.00037z^4 + 0.0028z^3 - 0.0009z^2 - 0.0054z + 0.0044$$

The model is standardized by the z-score given below, which determines the number of standard deviations the x-axis value (time in years) is from the mean [Larsen and Marx, 2000]:

$$z = (x - 2000) / 22$$

Where, z is the z-score, 2000 is the average year, 22 is the standard deviation and x is the predictor data or year of interest. The model utilizes the least squares method which connects data points by means of a best fit line [Hastie, Tibshirani and Friedman, 2009]. This model is a reasonable predictor of the annual effective dose for the time range  $1985 \leq x \leq 2050$ . This model predicts a low mean annual effective dose of 0.0016 mSv/year which

serves as the average baseline (reference) annual background radiation for 1985/86. This may be attributed to the fact that Morupule A Coal-Fired Power Station began operating in 1986 [UNSCEAR, 2008].

The average annual effective dose then gradually rose to a maximum value of 0.0083 mSv/y in 2005. This may be due to an increased amount of radionuclides in the chimney gases reaching the ground and ash ponds by either wet or dry deposition [Szefer and Nriagu, 2006]. It could also be attributed to more of the fly ash produced being directly added to water in the ash ponds [Skodras et al., 2007]. The model further predicts a decrease in the average annual effective dose to a value of 0.0013 mSv/year in 2050. This decrease may be attributed to exponential decay according to the Radioactive Decay Law [Benedict, 2012]. The mean annual effective doses estimated by the model are much lower than the public annual effective dose limit of 1 mSv [IAEA, 2003].

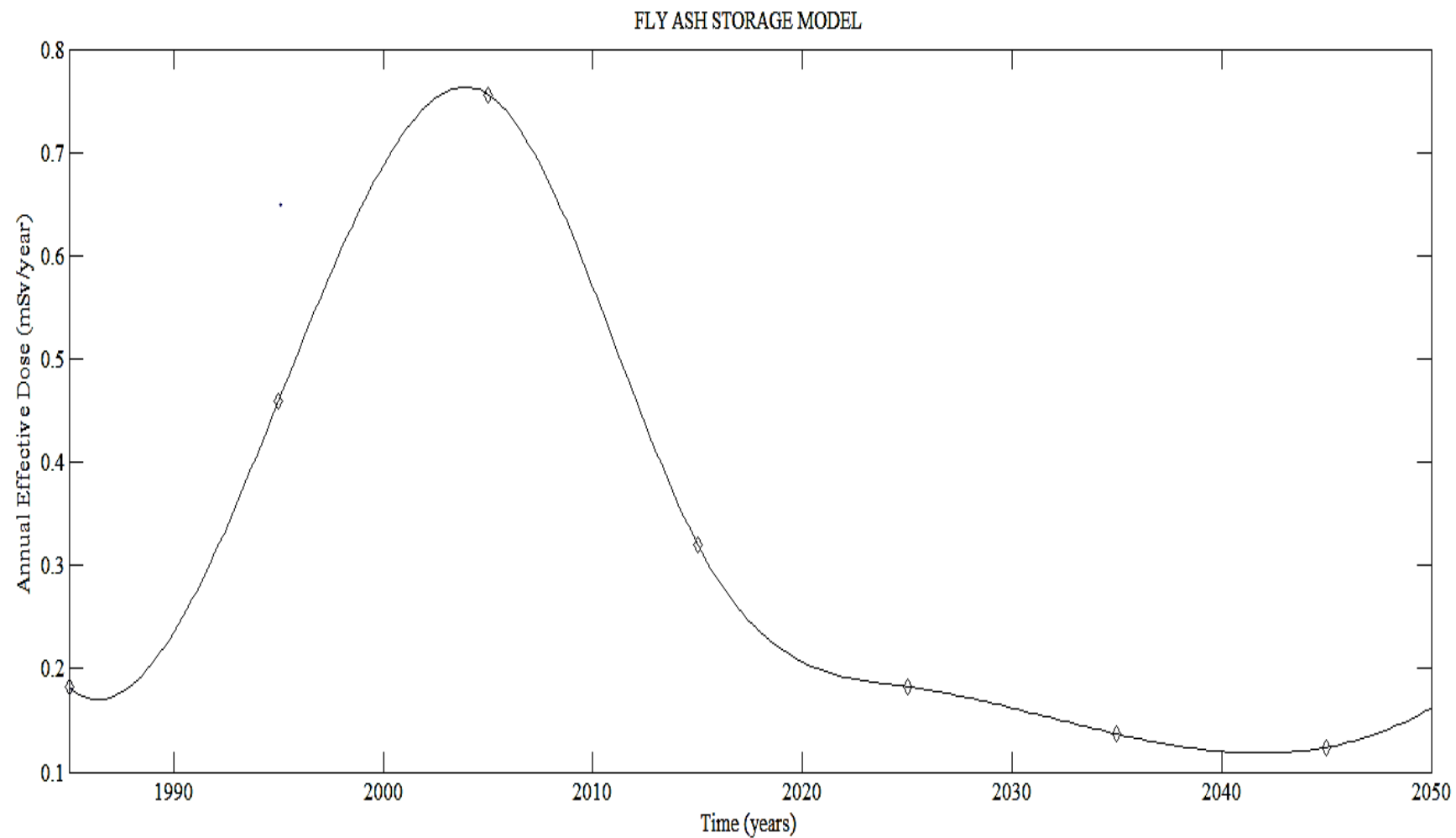


**Figure 4-15: Grapical representation of the fly ash storage area model**

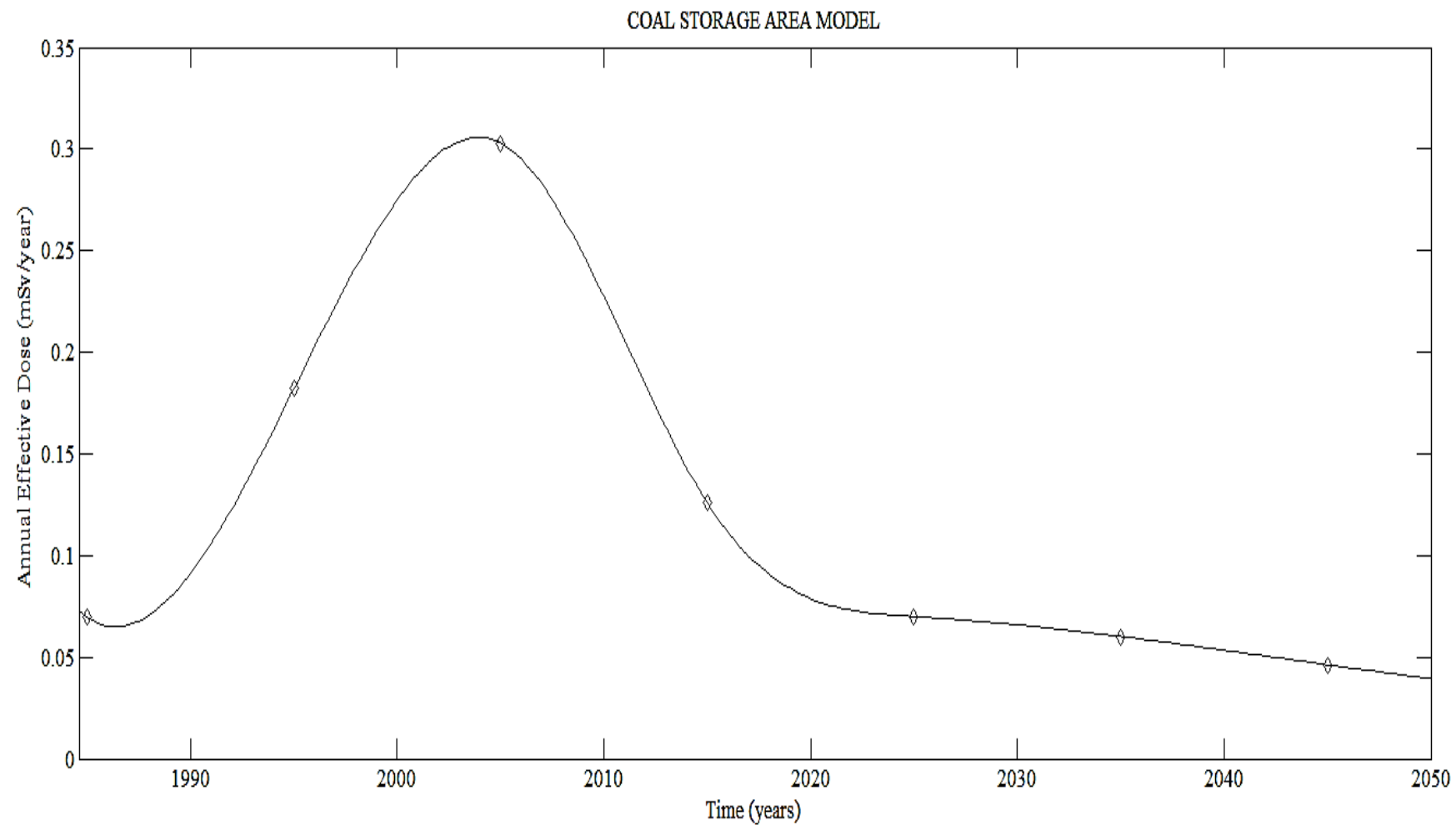


**Figure 4-16: Grapical representation of the coal storage area model**

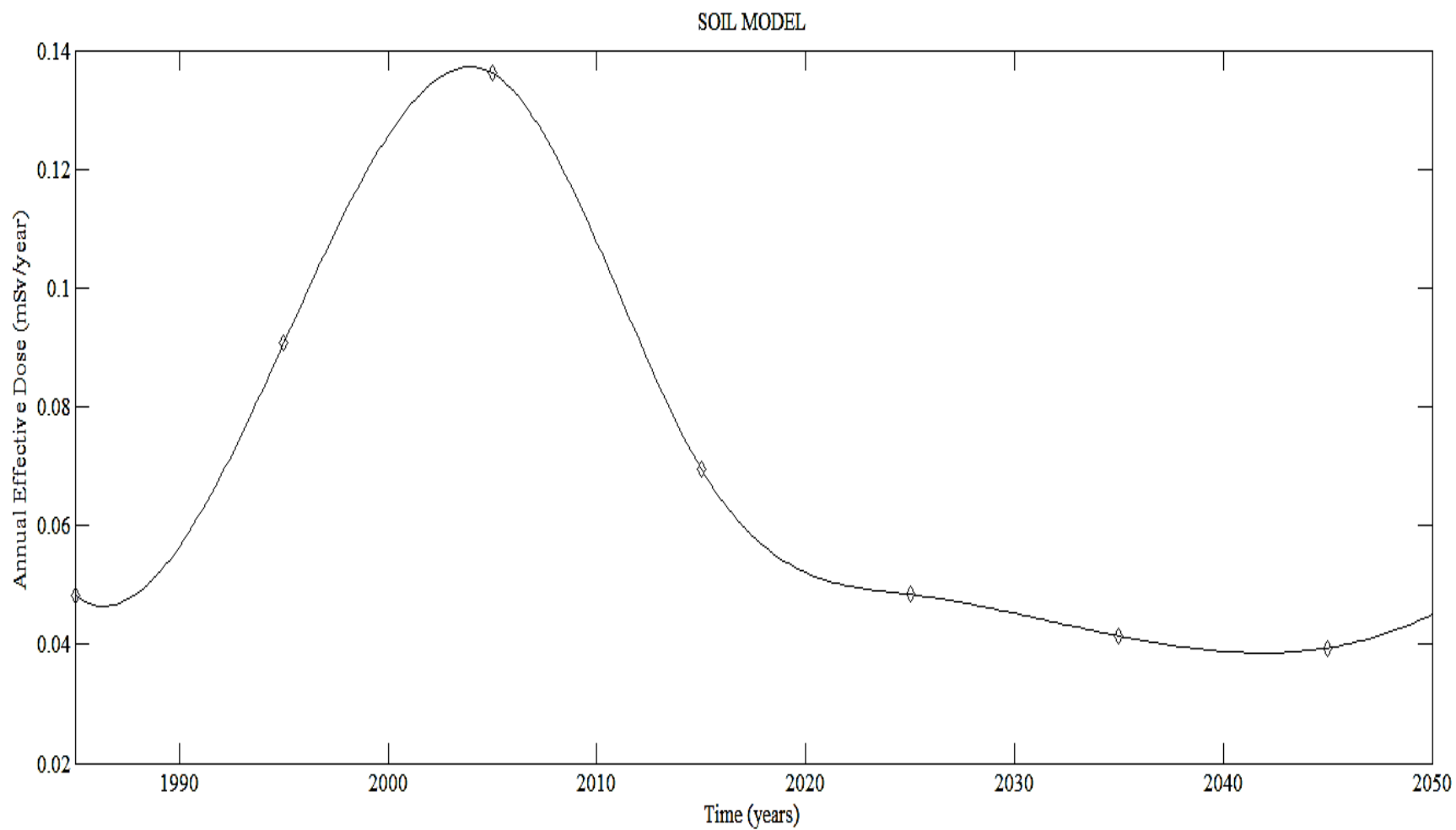


**Figure 4-17: Grapical representation of the soil model for the study area**

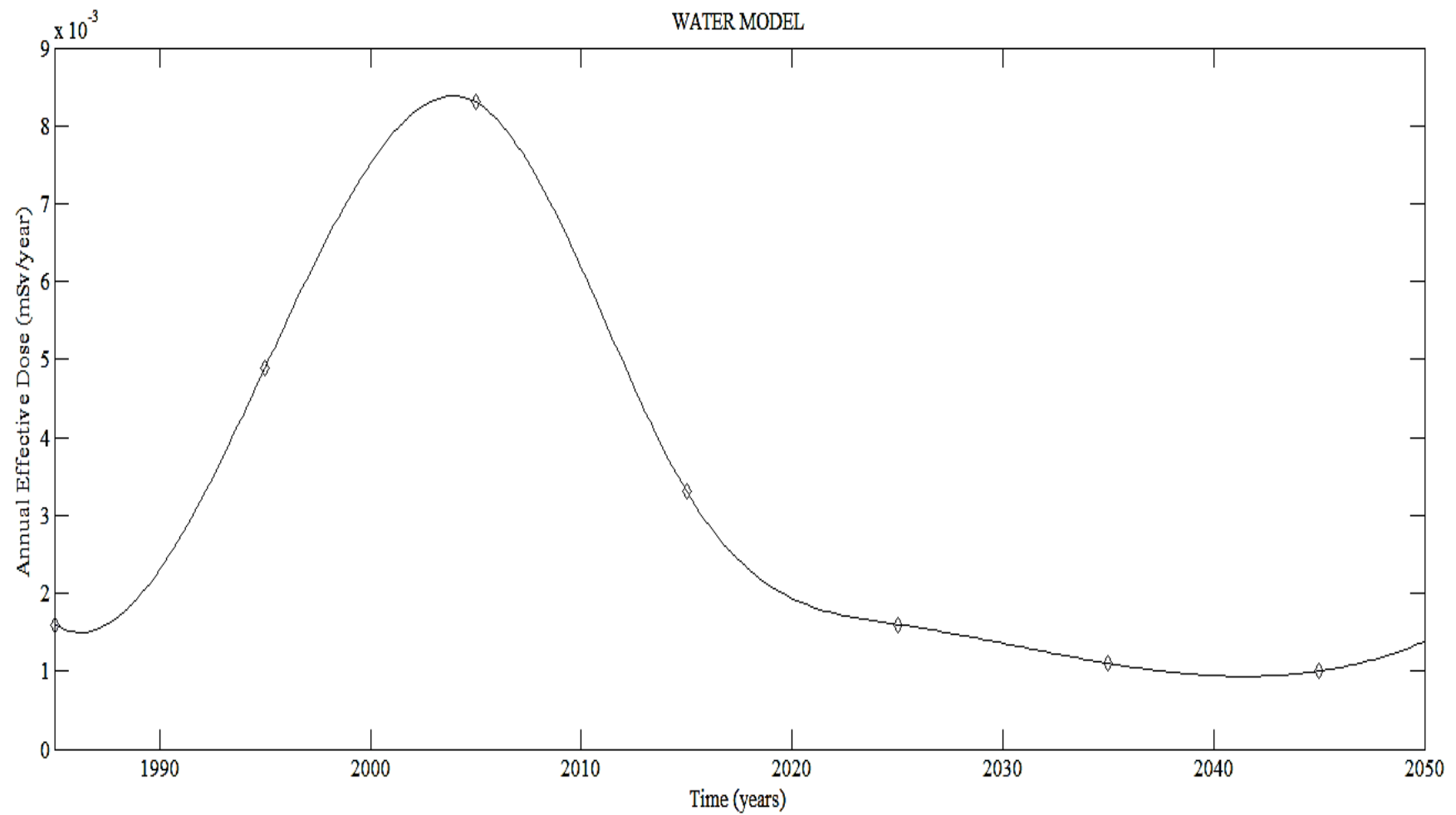


**Figure 4-18: Grapical representation of the water model for the fly ash ponds**



## **CHAPTER FIVE: CONCLUSION AND RECOMMENDATIONS**

This chapter gives insight to the main conclusions from the dose assessment of natural radioactivity in fly ash and environmental materials from Morupule A Coal-Fired Power Station in Botswana. It also focuses on recommendations addressed to the various stakeholders that were made based on results from this study.

### **5.1 CONCLUSION**

The aim of this study was to assess the natural radioactivity impact of Morupule A Coal-Fired Power Station to both workers and the public in the vicinity of the power station. The areas covered during this study include the soil, coal storage area and fly ash storage area within the power station. Areas outside the main power station include the fly ash ponds and soil from the vicinity of the power station. Soil from a ploughing field between Morupule and Palapye as well as from the New Palapye Bus Rank were instrumental to this work. The geology of the study area is similar to the *Striatopodocarpites fusus* Biozone in the Collie Basin of Western Australia and to the 3a Microfloral Biozone in the Northern Karoo Basin of South Africa.

Research on the activity concentrations due to the natural radionuclides U-238, Th-232 and K-40 from Morupule A Coal-Fired Power Station has never been carried out before. This study has established data on these natural radionuclides in the study area. The average activity concentration values of Th-232, U-238 and K-40 for the fly ash samples were estimated to be  $64.541 \pm 1.019$  Bq/kg,  $49.368 \pm 0.854$  Bq/kg and  $40.083 \pm 1.480$  Bq/kg respectively. They are generally lower than those from average world activity concentrations and French coal-fired power stations [UNSCEAR, 1982; Degrange and

Lepicard, 2004], but are also almost double in value to those estimated from Orji River Thermal Power Station in Nigeria [Ademola and Onyema, 2014]. The average activity concentrations of Th-232, U-238 and K-40 for the fly ash samples in this study were generally higher than other samples. The average activity concentrations of Th-232, U-238 and K-40 for the coal samples were estimated to be  $27.429 \pm 0.558$  Bq/kg,  $18.099 \pm 0.390$  Bq/kg and  $17.384 \pm 1.070$  Bq/kg respectively. They are generally comparable to the average world coal activity concentrations [UNSCEAR, 1982].

The average activity concentrations of Th-232, U-238 and K-40 for the soil samples were estimated to be  $10.106 \pm 0.322$  Bq/kg,  $6.757 \pm 0.193$  Bq/kg and  $118.026 \pm 2.621$  Bq/kg respectively. Those for the water samples are  $0.786 \pm 0.300$  Bq/l,  $0.315 \pm 0.055$  Bq/l and  $1.012 \pm 0.464$  Bq/l respectively. According to UNSCEAR, these low average activity concentrations resulting from the water and fly ash mixture in the fly ash ponds could be attributed to variations in the radionuclide concentrations per unit volume of water that is present in the fly ash pond at a particular time, depending on how dilute the fly ash slurry is [UNSCEAR, 2000].

The average annual effective doses from the study area for 2015 were estimated to be 0.320 mSv/year, 0.126 mSv/year, 0.069 mSv/year and 0.003 mSv/year for the fly ash, coal, soil and water samples respectively. All these values are much lower than the recommended annual effective dose limit for members of the public, whose value is 1 mSv/year [IAEA, 2003]. They are also much lower than the recommended annual effective dose limit for occupationally exposed workers, whose value is 20 mSv/year [IAEA, 2003]. These estimated average annual effective dose values show that the levels of natural radionuclides

in the study area are insignificant and do not pose significant radiological hazard to Morupule A Coal-Fired Power Station workers or to members of the public in the power station or its environs [Faanu, 2011].

The gamma radiation hazards associated with the use of any of the study samples as building materials were assessed by calculating the values of the representative level index ( $I_{\gamma r}$ ), radium equivalent activity ( $Ra_{eq}$ ), external hazard index ( $H_{ext}$ ) and internal hazard index ( $H_{int}$ ). The average  $Ra_{eq}$  values for all the samples were below the internationally accepted value of 370 Bq/kg. The average values of  $H_{ext}$  and  $H_{int}$  for all the samples were also below the internationally accepted value of unity. The average value of  $I_{\gamma r}$  for the fly ash samples was approximately equal to the internationally accepted value of unity, while values of  $I_{\gamma r}$  for all coal, soil and water samples were below the internationally accepted value of unity [Harb et al., 2008]. Based on these results, the materials under study could be used for construction purposes without posing any significant radiological hazards to humans.

Through this work, baseline data for the natural radionuclides U-238, Th-232 and K-40 has been estimated by means of a mathematical dose reconstruction modelling for all the study samples. The dose reconstruction model from this work was used to reconstruct radiation doses due to these natural radionuclides in the samples to include the period from 1985 to 2045. Across all samples, the model predicted a very low annual effective dose in 1985/86 and this corresponds to the time when Morupule A Coal-Fired Power Station started operating. The model shows that the annual effective dose gradually increased to a

maximum value in 2005 and then eventually decayed off to lower values for all samples. The model used utilized the least squares method which connects data points by means of a best fit line [Hastie, Tibshirani and Friedman, 2009]. For all samples, the mean annual effective doses estimated by the model are much lower than the public annual effective dose limit of 1 mSv [IAEA, 2003].

## **5.2 RECOMMENDATIONS**

Based on conclusions from this study, the following recommendations are made to the relevant stakeholders:

### **5.2.1 MANAGEMENT OF MORUPULE A COAL-FIRED POWER STATION**

The scrubbers/filters in the power station have so far been very effective in reducing the amount of radionuclides that are eventually emitted from the stack gas pipe into the atmosphere. This is partly reflected by the estimated values of the radium equivalent activity, hazard indices, annual effective doses and reconstructed annual effective doses that all fall within internationally accepted recommended limits. However, the power station management needs to ensure that there is proper planned maintenance and breakdown maintenance of the emission reduction equipment as a way of ensuring its continued efficiency and reliability. They should also ensure that personnel are trained on the latest technologies that are related to minimizing radiation exposures from coal-fired power stations.

### **5.2.2 WORKERS OF MORUPULE A COAL-FIRED POWER STATION**

The annual effective doses due to all samples from this study were all within the annual effective dose limit of 20 mSv for occupationally exposed workers, and all hazard indices

as well as the radium equivalent activity were within internationally accepted limits. Based on this and from a radiological point of view, it is concluded that all workers within Morupule A Coal-Fired Power Station are not prone to any significant radiological hazard. However, there is a need for constant and systematic monitoring of the environment in the study area.

### **5.2.3 MEMBERS OF THE PUBLIC**

The annual effective doses due to samples from this study were all within the annual effective dose limit of 1 mSv for members of the public, and all hazard indices as well as the radium equivalent activity were within internationally accepted limits. Based on this and from a radiological point of view, it is concluded that all public members within Morupule A Coal-Fired Power Station and its surroundings are not subjected to any significant radiological hazard. However, there is a need for constant and systematic monitoring of the environment in the study area.

### **5.2.4 THE REGULATORY AUTHORITY OF BOTSWANA**

The Regulatory Authority of Botswana should organize basic radiation protection training for the relevant coal-fired power station workers and public members. Results from this study and other similar research could aid in the development of NORM regulations for Botswana. In a joint venture with the management of the power station, the Regulatory Authority should consider performing area monitoring at certain locations within the study area. Two groups of people could be selected in this joint venture and be named the critical workers and critical public members respectively. The results from this venture would then be analysed and implemented if necessary.

### **5.2.5 RESEARCH SCIENTISTS**

In future, it is recommended that sampling should be done both during dry and rainy seasons, so as to cater for the seasonal variation of results. The study should gradually be implemented at all other coal-fired power stations in Botswana in order to obtain more comprehensive natural radioactivity baseline (reference) data for U-238, Th-232 and K-40. Careful study is recommended in order to improve upon the methods and come up with more enhanced related research in years to come. The study could be improved by including doses due to inhalation of the plume gases from the stack gas pipe of the coal-fired power station. The study could also be made more comprehensive by including more nearby communities and villages as possible sampling sites.

## REFERENCES

- Abdella, W. M. (2013). Optimization Method to Determine Gross Alpha-Beta in Water Samples Using Liquid Scintillation Counter, *Journal of Water Resource and Protection*, Cairo, Egypt, Vol. 5, pp. 900-905.
- Abhigyan, A. (2013). Resolution and Efficiency of High Purity Germanium Detector, *Academia online journals*, Downloaded from <http://www.academia.edu/4191151/> on 26 March, 2015.
- Abraham, A., Pelled O. and German, U. (2002). The effect of the detector thickness on the minimum detectable activity of lung counters, Israel.
- Ademola, J. A. and Onyema, U. C. (2014). Assessment of Natural Radionuclides in Fly Ash Produced at Orji River Thermal Power Station, Nigeria and the Associated Radiological Impact, *Natural Sciences Journal*, Vol. 6, pp. 752-759.
- Agalga R., Darko, E. O. and Schandorf, C. (2013). Preliminary study on the levels of natural radionuclides in sediments of the Tono irrigation dam, Navrongo, *International Journal of Science and Technology*, Vol. 2, pp. 770-776.
- Ahmed, S. N. (2007). *Physics and Engineering of Radiation Detection*, Academic Press Publishers, ISBN-13:978-0120455812, San Diego.
- Akkurt, I., Gunoglu, K. and Arda, S. S. (2014). Detection Efficiency of NaI (Tl) Detector in 511–1332 keV Energy Range, *Science and Technology of Nuclear Installations Journal*, Vol. 2014, Article ID 186798, DOI:10.1155/2014/186798.
- Allam, A., Ramadan, A. A. and Taha, A. (2014). Dose assessment for natural radioactivity resulting from tiling granite rocks, *Radiation Protection and Environment*, Vol. 36, pp. 99-105, DOI:10.4103/0972-0464.137471.
- Benedict, E. N. (2012). *Radiation from Oil Fields using High-Resolution Gamma-ray spectrometry* (MSc Thesis, September 2012).
- Cember, H. and Johnson, T. E. (2009). *Introduction to Health Physics*, 4<sup>th</sup> Edition, McGraw-Hill, New York, Clever, H. L., *Health Physics Instrumentation*, Volume 2, Pergamon Press.
- Choppin, G. R., Liljenzin, J. and Rydberg, J. (2002). *Radiochemistry and Nuclear Chemistry*, 3<sup>rd</sup> Edition, Butterworth-Heinemann Publications, Woburn MA.
- Conte, S. D. and de Boor, C. (1981). *Elementary Numerical Analysis: An Algorithmic Approach*, Third edition, McGraw-Hill, New York.

Cooper, M. B. (2005). Naturally Occurring Radioactive Materials (NORM) in Australian Industries - Review of Current Inventories and Future Generation, ERS-006, A Report prepared for the Radiation Health and Safety Advisory Council.

Cooper, J. R., Randle, K. and Sokhi, R. S. (2003). Radioactive Releases in the Environment: Impact and Assessment, John Wiley & Sons Ltd, Chichester UK.

Darko, E. O., Tetteh, G. K. and Akaho, E. H. K. (2005). Occupational Radiation Exposure to Norms in a Gold Mine, Journal of Radiation Protection.Dosimetry, Vol. 114, pp. 538–545.

Darko, E. O. and Faanu, A. (2007). Baseline radioactivity measurements in the vicinity of a Gold Treatment Plant, Journal of Applied Science and Technology, Vol. 10, Ghana.

Degrange, J. D. and Lepicard, S. (2004). Evaluation of Occupational Radiological Exposures Associated with Fly Ashes from French Coal Power Plants.

de Oliveira Loureiro, C. (1987). Simulation of the Steady-state Transport of Radon from Soil into Houses with Basements Under Constant Negative Pressure.

Ecosurv in association with GIBB Botswana for Botswana Power Corporation (2007). Morupule B Power Station Project ESIA, Development plan description, Section 4.

Ecosurv Environmental Consultants (2008). Morupule Colliery Expansion Project Draft Environmental Impact Statement, Vol. 1.

Ecosurv (2009). Morupule B Power Station Groundwater Investigation Final.

El-Taher, A. and Al-Zahrani, J. H. (2013). Radioactivity measurements and radiation dose assessments in soil of Al-Qassim region, Saudi Arabia, Indian Journal of Pure and Applied Physics, Vol. 52, pp. 147-154.

European Commission (2003). Effluent and dose control from European Union NORM industries: Assessment of current situation and proposal for a Harmonized Community Approach, Issue No. 135, Vol. 1.

European Commission (2001). Practical use of the concepts of clearance and exemption – Part II – Application of the concepts of exemption and clearance to natural radiation sources, Radiation Protection Report No. 122, Luxembourg.

Faanu, A., Ephraim J. H. and Darko, E. O. (2010). Assessment of public exposure to naturally occurring radioactive materials from mining and mineral processing activities of Tarkwa Goldmine in Ghana, Environmental Monitoring and Assessment, Vol. 180, pp. 15-29.



Faanu, A. (2011). Assessment of Public Exposure to Naturally Occurring Radioactive Materials from Mining and Mineral Processing Activities of Tarkwa Goldmine in Ghana (PhD Dissertation, February, 2011).

Faanu, A., Kpeglo, D. O., Sackey, M., Darko, E. O., Emi-Reynolds, G., Lawluvi, H., Awudu, R., Adukpo, O. K., Kansaana, C., Ali, I. D., Agyeman, B., Agyeman L. and Kpodzro, R. (2013). Natural and artificial radioactivity distribution in soil, rock and water of the Central Ashanti Gold Mine, Ghana. Environmental Earth Sciences, DOI 10.1007/s12665-013-2244-z.

Harb, S., El-Kamel, A. H., El-Mageed, A. I. A., Abbady, A. and Rashed, W. (2008). Concentration of U-238, U-235, Ra-226, Th-232 and K-40 for some granite samples in eastern desert of Egypt.

Hasan, M. M., Ali, M. I., Paul, D., Haydar, M. A. and Islam, S. M. A. (2014). Natural Radioactivity and Assessment of Associated Radiation Hazards in Soil and Water Samples Collected from in and around of the Barapukuria 2×125 MW Coal Fired Thermal Power Plant, Dinajpur, Bangladesh, Journal of Nuclear and Particle Physics, Vol. 4, pp. 17-24, DOI: 10.5923/j.jnpp.20140401.03.

Hastie, T., Tibshirani, R. and Friedman, J. H. (2009). The Elements of Statistical Learning, Second Edition, Springer-Verlag, New York, ISBN 978-0-387-84858-7.

Hossain, I., Sharip, N. and Viswanathan, K. K. (2011). Efficiency and resolution of HPGe and NaI (TI) detectors using gamma-ray spectroscopy, Academic Journals, Vol. 7, pp. 86-89, ISSN: 1992-2248.

IAEA (1989). Measurement of Radionuclides in Food and the Environment, A Guidebook, Technical Reports Series No. 295, STI/DOC/10/295, Vienna

IAEA (1998). Characterization of Radioactively Contaminated Sites for Remediation Purposes, IAEA-Tecd-1017, Vienna.

IAEA (1999). Occupational Radiation Protection: Safety Guide, Safety Standards Series RS-G-1.1, IAEA, Vienna.

IAEA (2000). Regulatory control of radioactive discharges to the environment: Safety Guide, Safety Standards Series No. WS-G-2.3, IAEA, Vienna.

IAEA (2001). Generic Models for use in Assessing the Impact of Discharges of Radioactive Substances to the Environment, Safety Reports Series No. 19, Vienna.

IAEA (2003). Derivation of activity limit for disposal of radioactive waste in near surface disposal facilities, IAEA-TECDOC-1380, Vienna.

IAEA (2003). Radiation Protection and the Management of Radioactive Waste in the Oil and Gas Industry, Safety Report Series No. 419, STI/PUB/1171 (ISBN: 9201140037), Vienna.

IAEA (2004). Attributing Radiation-Linked Disease to Occupational Exposure, IAEA, Vienna.

IAEA (2005). Naturally occurring radioactive materials (NORM IV) - Proceedings of an international conference held in Szczyrk, Poland, 17-21 May 2004, IAEA TECDOC Series No. 1472, Vienna.

IAEA (2007). Modelling the Transfer of Radionuclides from Naturally Occurring Radioactive Material (NORM), Report of the NORM working group of EMRAS, Theme 3, Environmental Modelling for Radiation Safety (EMRAS) Programme.

IAEA (2007). Radiation Protection Programmes for the Transport of Radioactive Material, Safety Guide, Safety Standards Series No. TS-G-1.3, Vienna.

IAEA (2011). Radiation Protection and Safety of Radiation Sources: International Basic Safety Standards Interim Edition General Safety Requirements, Vienna.

ICRP (1993). Protection from Potential Exposure - A Conceptual Framework. ICRP Publication 64, Ann. ICRP 23 (1).

ICRP (1997). Protection from Potential Exposures: Application to Selected Radiation Sources, Publication 76, Pergamon Press, Oxford and New York.

Khandaker, M. U., Latif, A., Karim, A. N. M. R., Uddin, N., Murad, H. and Jojo, P. J. (2012). Characterization of HPGE-Detector for Gamma-Ray Spectrometry and its Application for Analyzing Natural Samples.

Larsen, R. J. and Marx, M. L. (2000). An Introduction to Mathematical Statistics and Its Applications, Third Edition, ISBN 0-13-922303-7, pp. 282.

Martin, P. and Hancock, G. (1992). Routine Analysis of Naturally Occuring Radionuclides in Environmental Samples by Alpha-Particle Spectroscopy, Australian Government Publishing Service, ISBN: 0644256672.

Mayin, S. (2014). Characterization of Mine Waste and Radiation Dose Reconstruction of a Historical Mine Site at Konongo-Odumase, Ashanti Region, Ghana (Unpublished MPhil Thesis, July, 2014). University of Ghana, Legon.

McNaught, A. D. and Wilkinson, A. (1997). IUPAC. Compendium of Chemical Terminology, Second Edition, Blackwell Scientific Publications, Oxford, ISBN 0-86542-6848.

Miletics, E. and Moln'arka, G. (2014). Taylor Series Method with Numerical Derivatives for Numerical Solution of ODE Initial Value Problems.

Napier, B. A., Kennedy Jr., W. E. and Soldat, J. K. (1980). Assessment of Effectiveness of Geologic Isolation Systems: PABLM-A Computer program to calculate accumulated radiation doses from radionuclides in the environment, Downloaded from [https://openlibrary.org/works/OL11282083W/PABLM\\_a\\_computer\\_program\\_to\\_calculate\\_accumulated\\_radiation\\_doses\\_from\\_radionuclides\\_in\\_the\\_environment](https://openlibrary.org/works/OL11282083W/PABLM_a_computer_program_to_calculate_accumulated_radiation_doses_from_radionuclides_in_the_environment) on 20 February 2015.

NEA-OECD (Nuclear Energy Agency). (1979). Exposure to radiation from natural radioactivity in building materials, OECD, Paris.

Organo, C. and Fenton, D. (2008). Radiological assessment of NORM Industries in Ireland – Radiation doses to workers and members of the public, Dublin.

Özgan Çetiner, N. (2008). Specifications and performance of the compton suppression spectrometer at the Pennsylvania State University by Nesrin (MSc Thesis, May 2008).

Pandit, G. G., Sahu, S. K. and Puranik, V. D. (2011). Natural radionuclides from coal fired thermal power plants – estimation of atmospheric release and inhalation risk. Radioprotection Vol. 46: pp.173-179, DOI: <http://dx.doi.org/10.1051/radiopro/20116982s>.

Paschoa, A. S. and Steinhausler, F. (2010). TENR - Technologically Enhanced Natural Radiation (Radioactivity in the Environment) Elsevier, pp. 244.

Penfold, J. S. S., Smith, K. R., Harvey, M. P. and Mobbs, S. F. (1998). Assessment of the radiological impact of coal-fired power stations in the United Kingdom, Didcot, Oxfordshire, pp. 67-71.

Rahman, M. M., Naher, N., Ghosh, S. and Islam, M. M. (2014). Efficiency Calibration of Gamma Spectrometry for Powdered Milk Sample Using Cylindrical Geometry, Journal of Nuclear and Particle Physics, Vol. 4, pp. 171-175.

Reguigui, N. (2006). Gamma Ray Spectrometry – Practical Information, A compilation, International Journal of Science and Technology, Vol. 3, No. 10.

Reitz, G. (1993). Radiation Environment in the Stratosphere, Health Physics 48, pp. 5.

Saha, G. B. (2006). Physics and Radiobiology of Nuclear Medicine, Third Edition, Wiley, New York.

Shamshad, A., Fulekar, M. H. and Bhawana, P. (2012). Impact of Coal Based Thermal Power Plant on Environment and its Mitigation Measure, International Research Journal of Environmental Sciences, Vol. 1, pp. 60-64, India.

Shultis, J. K. and Faw, R. E. (2007). *Fundamentals of Nuclear Science and Engineering*, Second Edition, CRC Press, ISBN-10: 1420051350.

Skodras, G., Grammelis, P., Kakaras, E., Karangelos, D., Anagnostakis, M. and Hiniş, E. (2007). Quality characteristics of Greek fly ashes and potential uses, *Science Direct Journal*, Vol. 88, Issue 1, pp. 77–85.

Smyth, G. K. (1998). *Polynomial Approximation in Encyclopedia of Biostatistics*, Edited by Armitage, P. and Colton, T., John Wiley & Sons Ltd, Chichester, ISBN 0471 975761.

Stephenson, M. H. and McLean, D. (2004). International Correlation of Early Permian Palynofloras from the Karoo sediments of Morupule, Botswana, *South African Journal of Geology*, Vol. 102, pp. 3-14.

Stroud, K. A. (2003). *Advanced Engineering Mathematics*, Fourth Edition, Palgrave Macmillan Publishers, New York.

Szefer, P. and Nriagu, J. O. (2006). *Mineral Components in Foods*, CRC Press-Technology & Engineering.

UNSCEAR (1982). *Sources and Biological Effects*, 1982 Report to the General Assembly, with annexes, United Nations, New York.

UNSCEAR (1993). *Exposure from natural sources of radiation*, 1993 Report to General Assembly, United Nations, New York.

UNSCEAR (2000). *Sources and Effects of Ionizing Radiation*, Report to General Assembly, with Scientific Annexes, Vol. 1, United Nations, New York.

UNSCEAR (2006). *Sources-to-effects assessment for radon in homes and workplaces*, Annex E to Volume II of the Report to the General Assembly, *Effects of Ionizing Radiation*, available on the UNSCEAR 2006 Report Vol. II, United Nations, New York.

UNSCEAR (2008). *Sources and effects of ionizing radiation*, Report to the General Assembly with Scientific Annexes Vol. 1, United Nations, New York.

USEIA (2010). *U.S. Coal Supply and Demand 2009 Review*, DOE/EIA-0121, Washington DC.

USEPA (2006). *Coal-Fired Power Plant Emissions*, EPA 402-F-06-028, Washington DC.

USGS (1997). *Radioactive Elements in Coal and Fly Ash: Abundance, Forms, and Environmental Significance*, U.S. Geological Survey Fact Sheet FS-163-97.

Uslu, I. and Gökmeşe, F. (2010). Coal an Impure Fuel Source: Radiation Effects of Coal-fired Power Plants in Turkey, pp. 259-268.

Xhixha, G. (2012). Advanced gamma-ray spectrometry for environmental radioactivity monitoring.

Xinwei L., Lingquig W., Xiaodan J., Leipeng Y. and Gelian D. (2006). Specific activity and hazards of Archeozoic-Cambrian rock samples collected from the Weibei area of Xhaanxi, China. Radiation Protection Dosimetry Vol. 118, pp. 352–359.

Zeevaert, T., Sweeck, L. and Vanmarcke, H. (2005). The radiological impact from airborne routine discharges of a modern coal-fired power plant, Journal of Environmental Radioactivity, Vol. 85, pp. 1-22.

Zhang, Y. (2011). Groundwater Flow and Solute Transport Modeling, Ye Zhang

Zheng, C. and Bennet, G. D. (2002). Applied Contaminant Transport Modeling, Wiley-Interscience, pp. 656.

[http://www.eia.gov/KIDS/energy.cfm?page=coal\\_home-basics](http://www.eia.gov/KIDS/energy.cfm?page=coal_home-basics), United States Environmental Information Administration, Accessed 17 December 2014.

<http://pubs.usgs.gov/fs/1997/fs163-97/FS-163-97.htm>, Accessed October 23, 2014.

<http://www.world-nuclear.org/info/Safety-and-Security/Radiation-and-Health/Naturally-Occurring-Radioactive-Materials-NORM/>, Accessed December 17, 2014.

## APPENDICES

### APPENDIX 1

#### CALIBRATION

The reliability and quality of an analytical instrument is dependent upon how it calibrated using standard materials [IAEA, 2003; Faanu, 2011]. The HPGe system that was used in this study was calibrated with respect to energy and efficiency, using mixed standard radionuclides in 1L Marinelli beaker geometry. The system was calibrated for the fly ash, coal, soil and water samples. Efficiency calibration depends on geometry and is necessary for the quantification of K-40, Th-232 and U-238 radionuclides [Rahman, Naher, Ghosh and Islam, 2014]. Figures 4-1 and 4-2 show the HPGe detector energy and efficiency calibration curves respectively, using mixed standard radionuclides in 1L Marinelli beaker.

The correlations of the energy and efficiency calibrations are  $R^2 = 1$  and  $R^2 = 0.999$  respectively. The energy calibration plot is linear, while the efficiency calibration curve is an exponential as seen in Figures 4-1 and 4-2 respectively. The efficiency calibration curve is a smooth plot of the Efficiency vs. Energy. The energy calibration curve shows the linear relationship between the radionuclide energy and the corresponding centroid channel number of a full energy peak.

The mixed radionuclide standard that was used in the energy and efficiency calibration of the HPGe detector has the specifications below:

**MIXED RADIONUCLIDE STANDARD SPECIFICATIONS**


---

Certificate Number: 9031 – OL – 146 / 14

Type: MBSS 2

Production Number: 050214 – 1425039

Mass: 0.980 kg

Density: 0.980 g/cm<sup>3</sup>

Volume: 1000 cm<sup>3</sup>

Reference Date: 20 March 2014

---

Radionuclide	Gamma Energy (keV)	Activity (Bq)	Emission Rate
Americium-241	60	4.694E03	0.359
Cadmium-109	88	1.454E+04	0.036
Cerium-139	166	1.355E+03	0.800
Cobalt-57	122	1.156E+03	0.856
Cobalt-57	136	1.156E+03	0.107
Cobalt-60	1173	2.697E+03	0.999
Cobalt-60	1332	2.697E+03	0.999
Caesium-137	662	2.689E+03	0.851
Tin-113	255	4.000E+03	0.018
Tin-113	392	4.000E+03	0.640
Strontium-85	514	4.570E+03	0.960
Yttrium-88	1836	5.323E+03	0.992

---

**DESCRIPTION**

The homogeneity of the mixed radionuclide standard is better than 1%, while its radionuclide impurities contribute less than 0.1% gamma radiation. The radioactive material used in the standard is homogeneously dispersed in a silicone resin such that composition mass ratios are 0.324, 0.0816, 0.216 and 0.379 for Carbon, Hydrogen, Oxygen and Silicon respectively.

**MEASURING METHOD**

An HPGe detector was used to determine the radionuclides qualitatively and quantitatively. To ensure homogeneity of the standard, an element standard deviation of 1 cm<sup>3</sup> was chosen. Mass and density were used to calculate the required volume.

**QUALITY ASSURANCE AND QUALITY CONTROL**

The mixed radionuclide standard certificate was issued by the Czech Metrology Institute Inspectorate for Ionizing Radiation on the 25<sup>th</sup> February, 2014 and has a validity of 3 (three) years.



**APPENDIX 2****DETECTOR SPECIFICATIONS AND PERFORMANCE DATA**

Detector Model:	GX4020
Cryostat Model:	7500SL
Pre Amplifier Model:	2002 CSL
Serial Number:	b14130
Relative Efficiency:	40%
Resolution:	2.00 keV (FWHM) @ 1.33MeV 1.10 keV (FWHM) @ 122keV
Peak/ Compton:	56:1
Cryostat description or drawing number if special:	7500SL

**PHYSICAL CHARACTERISTICS**

Geometry:	Coaxial one open end, closed end faces window
Length:	61.5 mm
Diameter:	60.5mm
Outside distance from window:	6mm

**ELECTRICAL CHARACTERISTICS**

Depletion voltage:	+4000V dc
Bias voltage that is recommended:	+4500V dc
Leakage current @ recommended bias voltage:	0.01nA
Preamplifier test point voltage @ recommended bias voltage:	-0.8V dc

**RESOLUTION AND EFFICIENCY**

The amplitude time constant value is 4 $\mu$ s

<b>ISOTOPE</b>	<b>COBALT - 57</b>	<b>COBALT – 60</b>
<b>ENERGY (keV)</b>	122	1332
<b>FWHM (keV)</b>	0.878	1.92
<b>FWTM (keV)</b>	-	3.51
<b>PEAK/ COMPTON</b>	-	63.4:1
<b>RELATIVE EFFICIENCY</b>	-	44.2%

- Tests were carried out in line with IEEE standard test ANSI/IEEE std325-1996
- Standard Canberra electronics were used as per Section 7 of Germanium detector manual
- Calibration was performed by Canberra
- Calibration date is 29 January, 2014

**APPENDIX 3****Soil sampling points within Morupule A Coal-Fired Power Station and its surroundings**

LOCATION	SAMPLE ID	GPS COORDINATES	DESCRIPTION OF SAMPLING LOCATION
MORUPULE	Soil 1	22°31'19.18"S, 27°02'04.76"E	Soil sample within the power station
MORUPULE	Soil 2	22°31'09.63"S, 27°02'03.15"E	Soil sample within the power station
MORUPULE	Soil 3	22°31'13.89"S, 27°02'01.11"E	Soil sample within the power station
MORUPULE	Soil 4	22°31'16.22"S, 27°02'12.42"E	Soil within the power station near the turbines
MORUPULE	Soil 5	22°31'50.55"S, 27°02'17.93"E	Soil sample at Kgaswe Primary School
MORUPULE	Soil 6	22°31'06.97"S, 27°02'12.62"E	Soil sample near the two fly ash storage tanks
MORUPULE	Soil 7	22°31'26.63"S, 27°02'10.02"E	Soil just outside main power station entrance
PALAPYE	Soil 8	22°32'25.23"S, 27°05'10.51"E	Soil sample at the new Palapye Bus Rank
MORUPULE/ PALAPYE	Soil 9	22°32'10.00"S, 27°03'12.01"E	Soil at ploughing field between Morupule and just outside of Palapye

**APPENDIX 4****Fly ash sampling points within Morupule A Coal-Fired Power Station**

<b>LOCATION</b>	<b>SAMPLE ID</b>	<b>GPS COORDINATES</b>	<b>DESCRIPTION OF SAMPLING LOCATION</b>
MORUPULE	ASH 1	22°31'07.38"S, 27°02'12.80"E	Fly ash storage tank within the power station
MORUPULE	ASH 2	22°31'07.24"S, 27°02'12.90"E	Fly ash storage tank within the power station
MORUPULE	ASH 3	22°31'07.37"S, 27°02'13.02"E	Fly ash storage tank within the power station
MORUPULE	ASH 4	22°31'07.48"S, 27°02'12.90"E	Fly ash storage tank within the power station
MORUPULE	ASH 5	22°31'07.34"S, 27°02'13.12"E	Fly ash storage tank within the power station
MORUPULE	ASH 6	22°31'07.23"S, 27°02'13.20"E	Fly ash storage tank within the power station
MORUPULE	ASH 7	22°31'07.34"S, 27°02'13.31"E	Fly ash storage tank within the power station
MORUPULE	ASH 8	22°31'07.43"S, 27°02'13.22"E	Fly ash storage tank within the power station

**APPENDIX 5****Bituminous coal sampling points within Morupule A Coal-Fired Power Station**

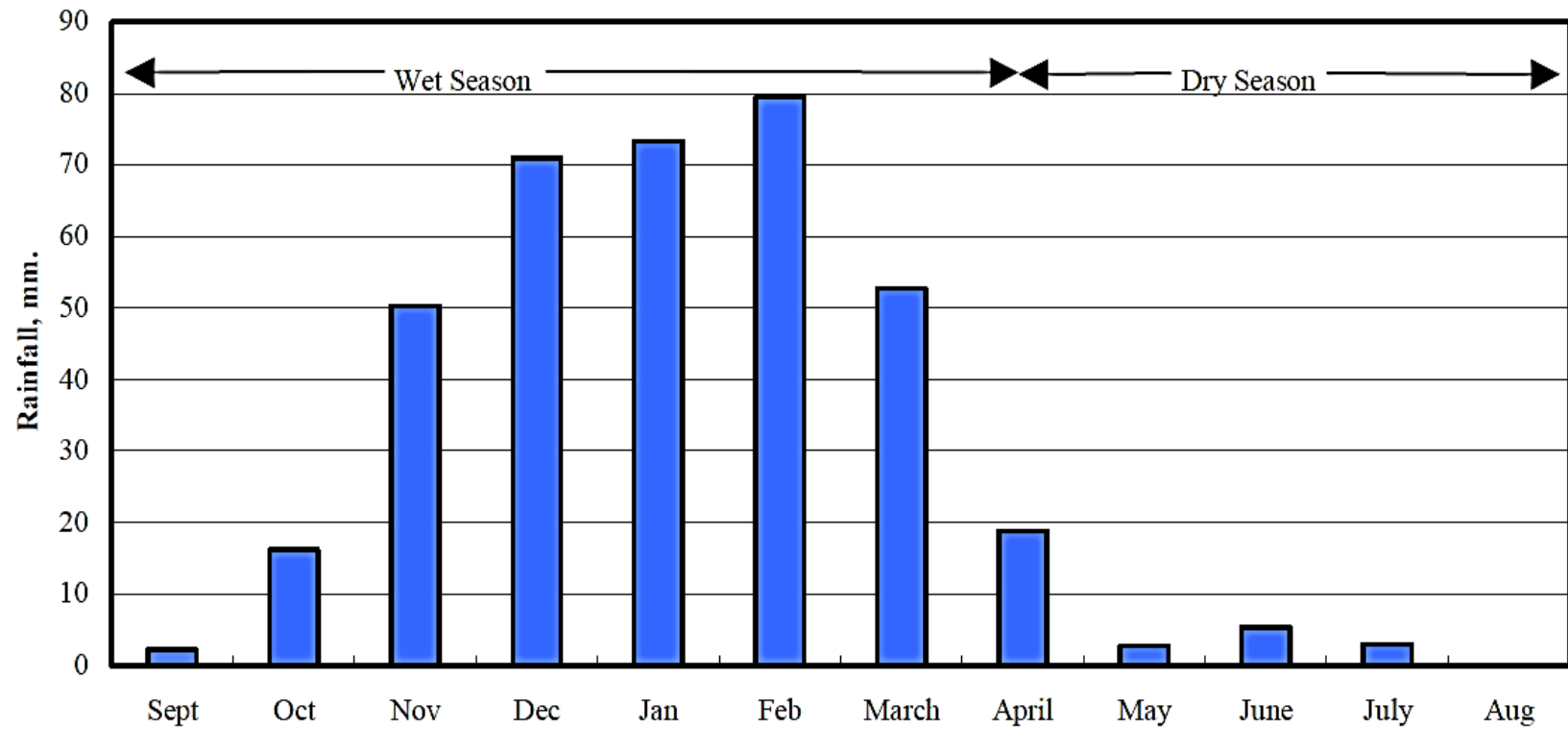
<b>LOCATION</b>	<b>SAMPLE ID</b>	<b>GPS COORDINATES</b>	<b>DESCRIPTION OF SAMPLING LOCATION</b>
MORUPULE	Coal 1	22°31'14.20"S, 27°02'01.49"E	Bituminous coal storage area
MORUPULE	Coal 2	22°31'15.57"S, 27°02'01.74"E	Bituminous coal storage area
MORUPULE	Coal 3	22°31'18.62"S, 27°02'01.51"E	Bituminous coal storage area
MORUPULE	Coal 4	22°31'21.20"S, 27°02'04.40"E	Bituminous coal storage area
MORUPULE	Coal 5	22°31'13.54"S, 27°02'04.17"E	Bituminous coal storage area
MORUPULE	Coal 6	22°31'15.80"S, 27°02'03.64"E	Bituminous coal storage area
MORUPULE	Coal 7	22°31'15.80"S, 27°02'03.64"E	Bituminous coal storage area

**APPENDIX 6****Water sampling points from the fly ash ponds**

<b>LOCATION</b>	<b>SAMPLE ID</b>	<b>GPS COORDINATES</b>	<b>DESCRIPTION OF SAMPLING LOCATION</b>
MORUPULE	Water 1	22°31'01.91"S, 27°02'24.08"E	Fly ash ponds containing slurry
MORUPULE	Water 2	22°31'05.70"S, 27°02'30.56"E	Fly ash ponds containing slurry
MORUPULE	Water 3	22°31'02.67"S, 27°02'36.03"E	Fly ash ponds containing slurry
MORUPULE	Water 4	22°30'58.56"S, 27°02'31.82"E	Fly ash ponds containing slurry
MORUPULE	Water 5	22°30'57.50"S, 27°02'26.39"E	Fly ash ponds containing slurry
MORUPULE	Water 6	22°30'54.71"S, 27°02'24.97"E	Fly ash ponds containing slurry

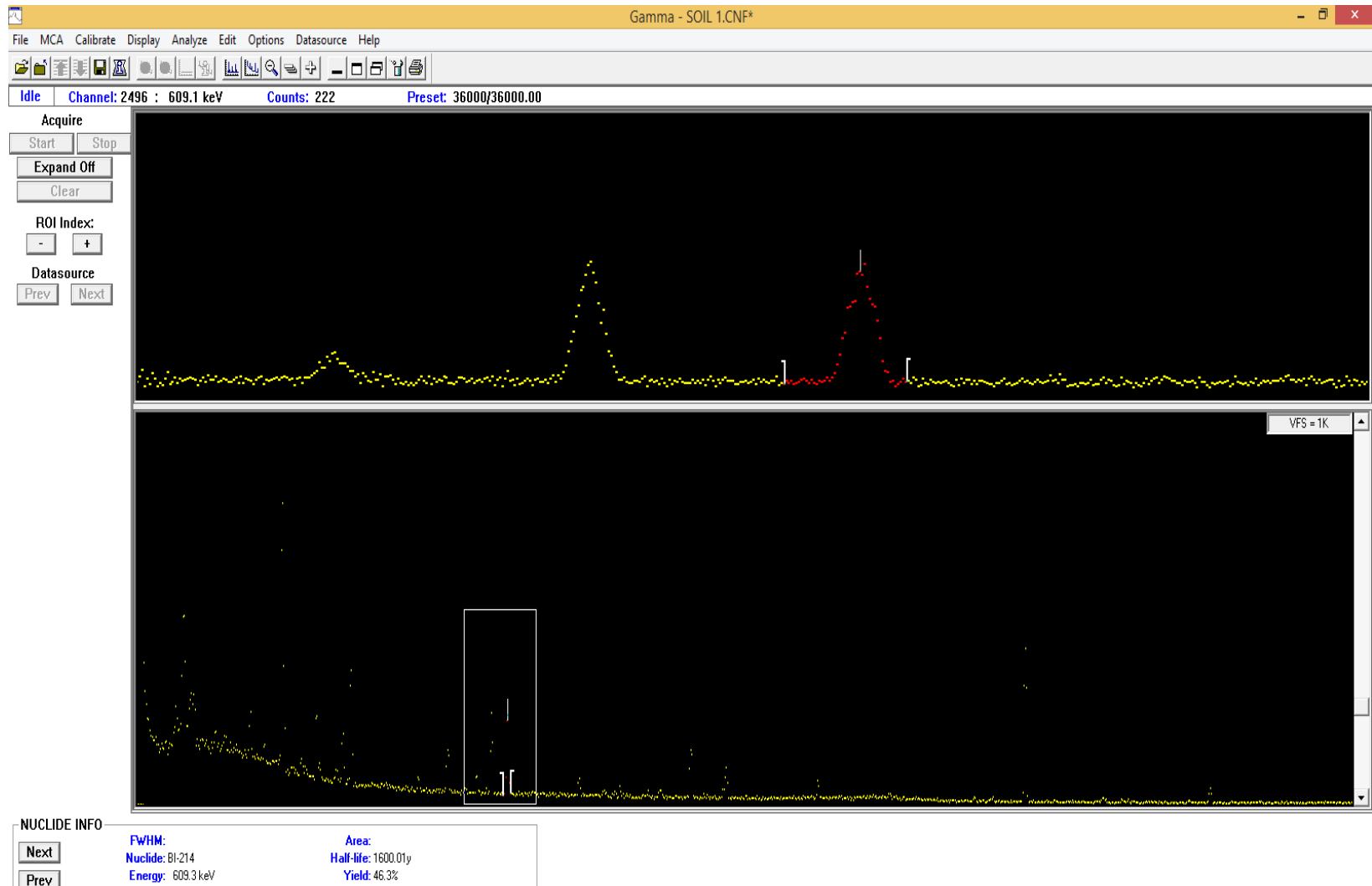
**APPENDIX 7**

**Mean monthly rainfall at Morupule A Coal-Fired Power Station area from 1989 to 2006 [Ecosurv, 2009]**



## APPENDIX 8

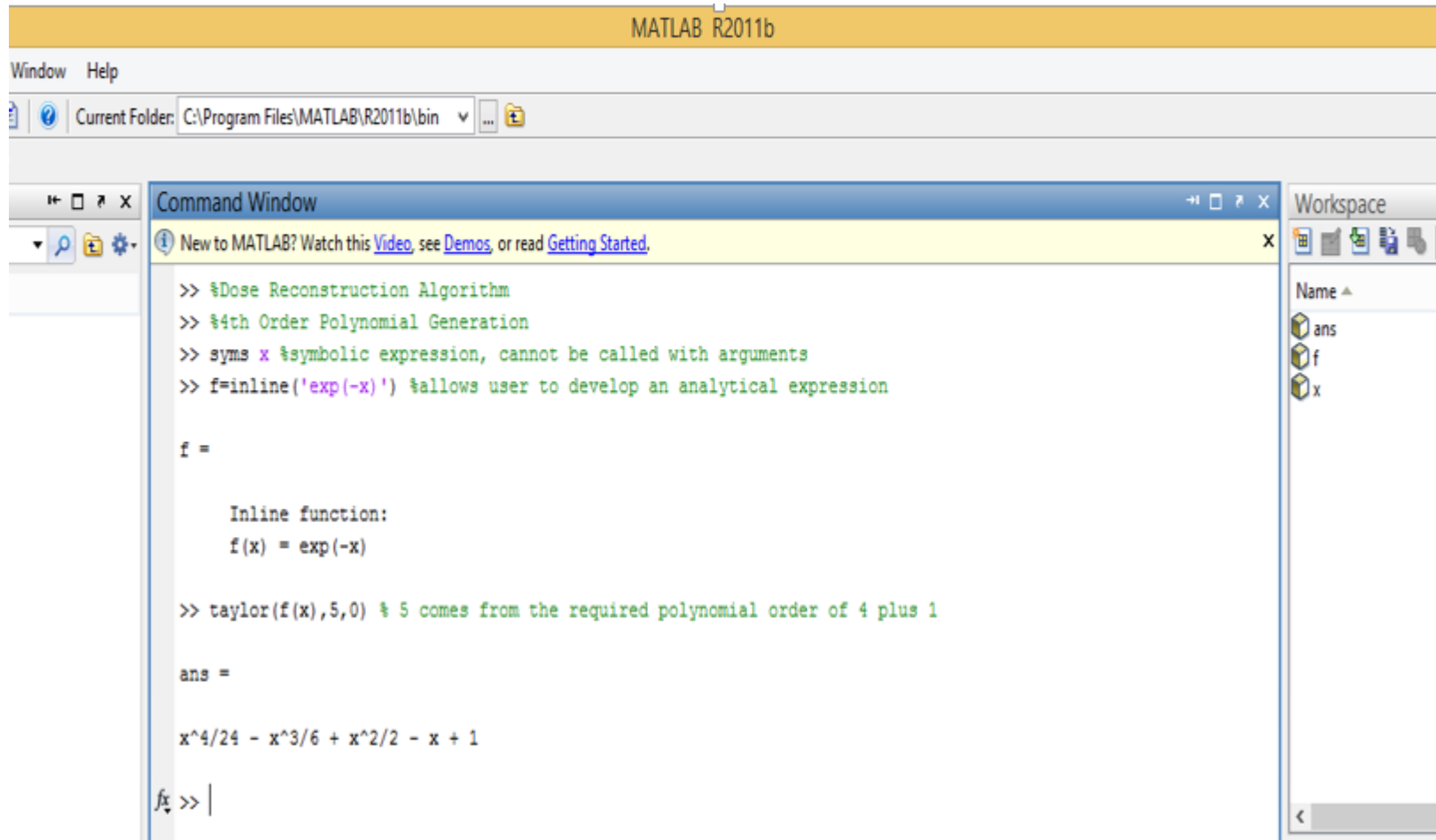
### Screenshot of Genie 2000 user interface for one of the analysed samples i.e. Sample Soil 1





## APPENDIX 9

**MATLAB algorithm used to generate dose reconstruction Taylor series polynomial for  $e^{-\lambda t} = e^{-x}$**



The image shows a screenshot of the MATLAB R2011b Command Window. The title bar reads "MATLAB R2011b". Below the title bar is a menu bar with "Window" and "Help". A toolbar shows icons for file operations and a "Current Folder" dropdown set to "C:\Program Files\MATLAB\R2011b\bin". The Command Window itself has a toolbar with navigation and editing icons. A yellow information banner at the top of the Command Window reads: "New to MATLAB? Watch this [Video](#), see [Demos](#), or read [Getting Started](#)." The Command Window contains the following text:

```
>> %Dose Reconstruction Algorithm
>> %4th Order Polynomial Generation
>> syms x %symbolic expression, cannot be called with arguments
>> f=inline('exp(-x)') %allows user to develop an analytical expression

f =

    Inline function:
    f(x) = exp(-x)

>> taylor(f(x),5,0) % 5 comes from the required polynomial order of 4 plus 1

ans =

x^4/24 - x^3/6 + x^2/2 - x + 1

fx >> |
```

The Workspace panel on the right side of the Command Window shows three variables: "ans", "f", and "x".

**APPENDIX 10****MATLAB code for development of all sample dose reconstruction models for fly ash, coal, soil and water samples**

```

function createfigure(X1, Y1)
%CREATEFIGURE(X1,Y1)
% X1: vector of x data
% Y1: vector of y data
% Create figure
figure1 = figure;
% Create axes
axes1 = axes('Parent',figure1);
box(axes1,'on');
hold(axes1,'all');
% Create plot
plot1 = plot(X1,Y1,'Parent',axes1,'Marker','x','LineStyle','none',...
'DisplayName','data 1');
% Create xlabel
xlabel('Time(years)');
% Create ylabel
ylabel('Annual Effective Dose (mSv/year)');
% Get xdata from plot
xdata1 = get(plot1, 'xdata');
% Get ydata from plot
ydata1 = get(plot1, 'ydata');
% Make sure data are column vectors
xdata1 = xdata1(:);
ydata1 = ydata1(:);
% Remove NaN values and warn
nanMask1 = isnan(xdata1(:)) | isnan(ydata1(:));
if any(nanMask1)
    warning('GenerateMFile:IgnoringNaNs', ...
'Data points with NaN coordinates will be ignored. ');
    xdata1(nanMask1) = [];
    ydata1(nanMask1) = [];
end
% Find x values for plotting the fit based on xlim
axesLimits1 = xlim(axes1);
xplot1 = linspace(axesLimits1(1), axesLimits1(2));
% Preallocate for "Show equations" coefficients
coeffs1 = cell(1,1);
% Find coefficients for polynomial (order = 4)
[fitResults1, ignoreArg1, mu1] = polyfit(xdata1, ydata1, 4);
% Evaluate polynomial
yplot1 = polyval(fitResults1, xplot1, [], mu1);

```

```

% Save type of fit for "Show equations"
fittypesArray1(1) = 5;
% Save coefficients for "Show Equation"
coeffs1{1} = fitResults1;
% Plot the fit
fitLine1 = plot(xplot1,yplot1,'DisplayName',' 4th degree','Parent',axes1,...
    'Tag','4th degree',...
    'Color',[0.75 0.75 0]);
% Set new line in proper position
setLineOrder(axes1, fitLine1, plot1);
% "Show equations" was selected
showEquations(fittypesArray1, coeffs1, 2, axes1, xdata1);
% Create legend
legend(axes1,'show');
%-----%
function setLineOrder(axesh1, newLine1, associatedLine1)
%SETLINEORDER(AXESH1,NEWLINE1,ASSOCIATEDLINE1)
% Set line order
% AXESH1: axes
% NEWLINE1: new line
% ASSOCIATEDLINE1: associated line
% Get the axes children
hChildren = get(axesh1,'Children');
% Remove the new line
hChildren(hChildren==newLine1) = [];
% Get the index to the associatedLine
lineIndex = find(hChildren==associatedLine1);
% Reorder lines so the new line appears with associated data
hNewChildren = [hChildren(1:lineIndex-1);newLine1;hChildren(lineIndex:end)];
% Set the children:
set(axesh1,'Children',hNewChildren);
%-----%
function showEquations(fittypes1, coeffs1, digits1, axesh1, xdata1)
%SHOWEQUATIONS(FITTPES1,COEFFS1,DIGITS1,AXESH1,XDATA1)
% Show equations
% FITTPES1: types of fits
% COEFFS1: coefficients
% DIGITS1: number of significant digits
% AXESH1: axes
% XDATA1: x data
n = length(fittypes1);
txt = cell(length(n + 2),1);
txt{1,:} = '';
for i = 1:n
    txt{i + 1,:} = getEquationString(fittypes1(i),coeffs1{i},digits1,axesh1);
end

```

```

meanx = mean(xdata1);
stdx = std(xdata1);
format = ['where z = (x - %0.', num2str(digits1), 'g)/%0.', num2str(digits1), 'g'];
txt{n + 2,:} = sprintf(format, meanx, stdx);
text(.05,.95,txt,'parent',axesh1, ...
    'verticalalignment','top','units','normalized');
%-----%
function [s1] = getEquationString(fittype1, coeffs1, digits1, axesh1)
%GETEQUATIONSTRING(FITTYPE1,COEFFS1,DIGITS1,AXESH1)
% Get show equation string
% FITTYPE1: type of fit
% COEFFS1: coefficients
% DIGITS1: number of significant digits
% AXESH1: axes
if isequal(fittype1, 0)
    s1 = 'Cubic spline interpolant';
elseif isequal(fittype1, 1)
    s1 = 'Shape-preserving interpolant';
else
    op = '+-';
    format1 = ['%s %0.',num2str(digits1),'g*z^{ %s } %s'];
    format2 = ['%s %0.',num2str(digits1),'g'];
    xl = get(axesh1, 'xlim');
    fit = fittype1 - 1;
    s1 = sprintf('y =');
    th = text(xl* [.95;.05],1,s1,'parent',axesh1, 'vis','off');
    if abs(coeffs1(1) < 0)
        s1 = [s1 '-'];
    end
    for i = 1:fit
        sl = length(s1);
        if ~isequal(coeffs1(i),0) % if exactly zero, skip it
            s1 = sprintf(format1,s1,abs(coeffs1(i)),num2str(fit+1-i), op((coeffs1(i+1)<0)+1));
        end
        if (i==fit) && ~isequal(coeffs1(i),0)
            s1(end-5:end-2) = []; % change x^1 to x.
        end
        set(th,'string',s1);
        et = get(th,'extent');
        if et(1)+et(3) > xl(2)
            s1 = [s1(1:sl) sprintf('\n    ') s1(sl+1:end)];
        end
    end
    if ~isequal(coeffs1(fit+1),0)
        sl = length(s1);
        s1 = sprintf(format2,s1,abs(coeffs1(fit+1)));
    end
end

```

```
set(th,'string',s1);
et = get(th,'extent');
if et(1)+et(3) > xl(2)
    s1 = [s1(1:sl) sprintf("\n    ") s1(sl+1:end)];
end
end
delete(th);
% Delete last "+"
if isequal(s1(end),'+')
    s1(end-1:end) = []; % There is always a space before the +.
end
if length(s1) == 3
    s1 = sprintf(format2,s1,0);
end
end
```